

Characterization of the Munc13-Calmodulin Interaction

PhD Thesis

in partial fulfillment of the requirements
for the degree “Doctor of Philosophy (PhD)”
in the Molecular Biology Program
at the Georg August University Göttingen,
Faculty of Biology

Submitted by

Kalina Dimova

born in
Assenovgrad, Bulgaria

2009

Declaration

This dissertation has been written independently and with no other sources and aids than quoted.

Kalina Dimova

Göttingen, March 28th, 2009

List of Publications

Dimova, K., Kawabe, H., Betz, A., Brose, N., and Jahn, O. (2006). Characterization of the Munc13-calmodulin interaction by photoaffinity labeling. *Biochimica et Biophysica Acta - Molecular Cell Research* 1763, 1256-1265.

Werner, H. B., Kuhlmann, K., Shen, S., Uecker, M., Schardt, A., Dimova, K., Orfaniotou, F., Dhaunchak, A., Brinkmann, B. G., Mobius, W., *et al.* (2007). Proteolipid protein is required for transport of sirtuin 2 into CNS myelin. *J Neurosci* 27, 7717-7730.

Dimova, K., Kalkhof, S., Pottratz, I., Ihling, C., Rodriguez-Castaneda, F., Liepold, T., Griesinger, C., Brose, N., Sinz, A., and Jahn, O. (2009). Structural insights into the calmodulin - Munc13 interaction obtained by cross-linking and mass spectrometry. Manuscript in revision.

TABLE OF CONTENTS

ACKNOWLEDGEMENTS	iii
ABSTRACT	iv
ABBREVIATIONS	v
LIST OF FIGURES	vii
1. INTRODUCTION.....	9
1.1. Basics of synaptic transmission	9
1.2. The synaptic vesicle cycle	9
1.3. The Munc13 protein family	11
1.4. Munc13 proteins and short-term synaptic plasticity	14
1.5. Ca ²⁺ and calmodulin in the brain	16
1.6. Photoaffinity labeling	20
1.6.1. General principles of photoaffinity labeling for structural analysis	20
1.6.2. Requirements of the photoreactive group	21
1.7. Principles and applications of MALDI-TOF mass spectrometry	23
1.8. Aims of this study	26
2. MATERIALS AND METHODS.....	27
2.1. Photoaffinity Labeling and Mass Spectrometry	27
2.1.1. Prediction of CaM binding sites	27
2.1.2. Peptide synthesis	27
2.1.3. Photoaffinity labelling (PAL)	29
2.1.4. Detection of photoadducts by mass spectrometry	29
2.1.5. PAL-based Ca ²⁺ titration assay	30
2.1.6. Documentation and quantification of SDS-PAGE gels	31
2.1.7. Determination of trace calcium	31
2.2. Structural analysis of photoadducts by LC-MALDI-MS	31
2.2.1. Calmodulin	31
2.2.2. PAL	32
2.2.3. HPLC/MALDI-TOF-MS for analysis of photoreaction mixtures	32
2.2.4. Secondary proteolytic cleavage of exceptionally large cross-linked peptides with endoproteinase Asp-N	33
2.2.5. On-target CNBr cleavage of PAL-cross-linked peptides	33
2.3. Molecular Biology	34
2.3.1. Materials	34
2.3.1.1. Bacterial strains	34
2.3.1.2. Vectors	34
2.3.1.3. Plasmids	34
2.3.1.4. Oligonucleotides	35
2.3.2. Methods	36
2.3.2.1. Electroporation of plasmid DNA into competent bacteria	36
2.3.2.2. Small scale plasmid-DNA preparation	36
2.3.2.3. Medium scale plasmid DNA preparation	37
2.3.2.4. Determination of DNA concentration	37
2.3.2.5. Sequencing of DNA	37
2.3.2.6. DNA digest with restriction endonucleases	37
2.3.2.7. Dephosphorylation of 5' DNA-ends	37

2.3.2.8. Refilling of cohesive 5'DNA fragment ends	38
2.3.2.9. DNA Ligation	38
2.3.2.10. Ethanol precipitation of DNA	38
2.3.2.11. Phenolchloroform extraction	38
2.3.2.12. Agarose gel electrophoresis	39
2.3.2.13. Agarose gel extraction of DNA fragments	39
2.3.2.14. Polymerase Chain Reaction (PCR)	39
2.3.2.15. Subcloning in TOPO pCR ® 2.1 vectors	40
2.3.2.16. Cloning strategies for constructs generated and used in this study	40
2.3.2.17. Site-directed mutagenesis	41
2.4. Co-sedimentation assays	42
2.4.1 Expression of GST-fusion proteins	42
2.4.2. CaM co-sedimentation assay	42
3. RESULTS.....	44
3.1. Characterization of the CaM interactions of bMunc13-2 and Munc13-3	44
3.1.1. Screening for CaM binding sites in bMunc13-2 and Munc13-3	44
3.1.2. Peptide design	45
3.1.3. Detection of the photoadducts	46
3.1.4. Specificity of photoadduct formation	49
3.1.5. Ca ²⁺ sensitivity of photoadduct formation	50
3.1.6. Stoichiometry of the interaction of CaM with bMunc13-2 and Munc13-3	56
3.1.7. Co-sedimentation assays with GST-fusion proteins of bMunc13-2(366-780) and Munc13-3(711-1063)	57
3.2. Structural characterization of the Munc13/CaM interaction by PAL	61
3.2.1. Analytical strategy	61
3.2.2. Detection of intact CaM complexes	63
3.2.3. Identification of cross-linked peptides	64
3.2.4. Identification of contact sites between Munc13 and CaM by PAL	67
3.3. PAL and structural characterization of the CaM interaction of C-terminally elongated Munc13-1- and ubMunc13-2-derived peptides	72
4. DISCUSSION.....	78
4.1. Munc13 proteins interact with CaM via structurally distinct non-conserved binding sites	78
4.2. Munc13/CaM complex formation is triggered at Ca ²⁺ concentrations in the lower nanomolar range	80
4.3. Structural characterization of the Munc13/CaM interaction	81
4.3.1. A novel PAL- based strategy for interaction site mapping	81
4.3.2. CaM interacts with Munc13 through key Met residues	82
4.3.3. Integration of PAL and chemical cross-linking constraints for molecular modeling of the CaM/Munc13 complex	84
4.3.4. The high-resolution structure of the CaM/Munc13 complex reveals a novel 1-26 CaM recognition motif	87
5. CONCLUSIONS AND OUTLOOK.....	89
6. REFERENCES.....	90
7. CURRICULUM VITAE.....	96

ACKNOWLEDGEMENTS

First and foremost, I would like to thank my supervisor Dr. Olaf Jahn – for his willingness to embark upon this journey with me, to share his knowledge and enthusiasm for science, and for the commitment, support and encouragement he offered, always.

I am indebted to Prof. Nils Brose for letting me be part of his exceptional lab, for his trust and support for my work, and for his critical input as head of my thesis committee.

I would like to thank Prof. Frauke Melchior and Prof. Christian Griesinger for the time, expertise, and guidance they offered as members of my thesis committee.

I am grateful to Dr. Steffen Burkhardt and his team at the Coordination office of the Graduate Program in Molecular Biology for providing outstanding help with all things administrative and organizational surrounding life and graduate work in Göttingen.

I would like to express my sincere gratitude to the Proteomics group at the Max Planck Institute of Experimental medicine – Dr. Hartmut Kratzin, Dörte Hesse, Thomas Liepold, Gabi Paetzold, Lars Piepkorn, Marina Uecker and Lars van Werven – for welcoming me in their keratin-free world and for the patience and readiness with which they shared their know-how and offered their help through my first 2D-PAGE challenges and MALDI spectra.

For the laughter, the comfort and the friendship, both in and outside the lab, I am indebted to Noa Lipstein, Alexandros Poulopolous, Tolga Soykan and Benjamin Cooper.

Cristina Suarez I thank for experimentally proving that temporal and spatial distance is relative, while other feelings “naturally” aren’t.

For keeping me sane, helping me smile and making me proud, I would like to thank my sister, Assya Dimova.

I dedicate this work to my parents, Rossitza Dimova and Peter Dimov, who have stood by me and supported every choice I made, through unconditional love and confidence in my abilities.

ABSTRACT

The Munc13 proteins are the key mediators of synaptic vesicle priming, an essential step in Ca^{2+} -regulated neurotransmitter release that renders docked vesicles fusion-competent prior to exocytosis. They have emerged as important regulators of adaptive synaptic mechanisms such as presynaptic short-term plasticity, a process by which the release of neurotransmitter is dynamically adapted to a changing demand. Indeed, Munc13-1 and ubMunc13-2 contain a conserved calmodulin (CaM) binding site and the Ca^{2+} -dependent interaction of these Munc13 isoforms with CaM constitutes a molecular mechanism that transduces residual Ca^{2+} signaling to the synaptic exocytotic machinery. This study aimed to (i) establish whether such regulation through CaM exists in the other Munc13 isoforms, bMunc13-2 and Munc13-3, and (ii) provide structural insights into the Munc13-CaM interaction.

Bioinformatic tools were used to identify potential CaM recognition motifs in the non-conserved sequences of bMunc13-2 and Munc13-3. Munc13-derived model peptides covering the potential CaM binding sites were used in photoaffinity labeling (PAL) experiments with CaM, followed by mass spectrometric characterization of the covalent photoadducts. Analysis of these peptide-protein interactions demonstrated that all four Munc13 isoforms bind CaM in a stoichiometric and Ca^{2+} -dependent manner and that only slightly elevated intracellular Ca^{2+} concentrations are sufficient to trigger these interactions. These results support the conclusion that convergent evolution has generated structurally distinct but functionally similar Ca^{2+} /CaM binding sites in Munc13-1/ubMunc13-2, bMunc13-2, and Munc13-3, all of which can contribute to presynaptic short-term plasticity.

A novel PAL-based analytical strategy using isotopically labeled CaM and mass spectrometry was established for the structural characterization of the covalent Munc13-CaM photoadducts. It revealed that, in the bound state, the hydrophobic anchor residue of the CaM-binding motif in Munc13 contacts two distinct Met residues in the C-terminal domain of CaM. These contact sites provided a valuable basis for molecular modeling of the Munc13-CaM complex through integration with constraints obtained by chemical cross-linking methods. The PAL analysis, carried out under physiological solvent and concentration conditions, also emerged as an important complement to high-resolution NMR studies on the Munc13/CaM interaction, as it yielded biochemical support for a novel 1-26 CaM binding motif in Munc13-1 and ubMunc13-2. The structural data on the Munc13-CaM complex offer new options for future studies towards a deeper understanding of the role of Munc13 proteins in synaptic vesicle priming and short-term synaptic plasticity.

ABBREVIATIONS

Bis-Tris	bis(2-hydroxyethyl)amino-tris(hydroxymethyl)methane
b	brain-specific
CaM	Calmodulin
CaMK	Ca ²⁺ /calmodulin-dependent protein kinase
cAMP	cyclic adenosine monophosphate
cDNA	Complementary DNA
ce, <i>C. elegans</i>	<i>Caenorhabditis elegans</i>
CNS	central nervous system
DAG	diacylglycerol
DKO	double knockout
DNA	deoxyribonucleic acid
dNTPs	deoxynucleosides triphosphates
dr, <i>D. melanogaster</i>	<i>Drosophila melanogaster</i>
DTT	1,4-dithiothreitol
<i>E. coli</i>	<i>Escherichia coli</i>
EF hands	helix-loop-helix Ca ²⁺ binding motifs
EGFP	enhanced green fluorescent protein
EGTA	ethylene glycol tetraacetic acid
EPSCs	excitatory postsynaptic currents
ESI	electrospray ionization
Fmoc	fluorenylmethoxycarbonyl
GST	Glutathione S-transferase
HCCA	α -cyano-4-hydroxycinnamic acid
HEPES	4-(2-hydroxyethyl)-1-piperazineethanesulfonic acid
HPLC	high-pressure liquid chromatography
ICP-MS	inductively coupled plasma mass spectrometry
IPTG	isopropyl β -D-1-thiogalactopyranoside
KO	knockout
LB	Luria-Bertani
LC	liquid chromatography
m/z	mass-to-charge ratio
MALDI	matrix-assisted laser desorption/ionization
MHD	Munc13 homology domain
MLCK	Myosin Light Chain Kinase
MOPS	3-(N-morpholino) propanesulfonic acid
MS	mass spectrometry
Munc13	mammalian Unc13
NMR	nuclear magnetic resonance
n	neuronal
NOS	Nitric Oxide Synthase
NT	neurotransmitter
OD	optical density
PAL	photoaffinity labeling
pBpa	p-Benzoyl-Phe
PCR	Polymerase chain reaction

pdb	Protein Data Base
<i>Pfu</i>	<i>Pyrococcus furiosus</i>
PKC	Protein Kinase C
PMF	peptide-mass fingerprinting
PMSF	phenylmethanesulphonylfluoride
ppm	parts per million
PTP	posttetanic potentiation
<i>r</i>	<i>Rattus norvegicus</i>
rpHPLC	reverse phase high pressure liquid chromatography
RRP	readily releasable pool
SDS-PAGE	sodium dodecyl sulfate polyacrylamide gel electrophoresis
SNARE	Soluble N-ethylmaleimide-sensitive Factor Attachment Protein Receptor
STP	short-term plasticity
TFA	trifluoroacetic acid
TOF	time-of-flight
ub	ubiquitously expressed
Unc	uncoordinated
UV	ultraviolet
WT	wild type

LIST OF FIGURES

Figure 1	The synaptic vesicle cycle	10
Figure 2	Domain structure of the Munc13 protein family	11
Figure 3	Electrophysiological characterization of Munc13-defficient mice	13
Figure 4	Altered short-term plasticity in glutamatergic autaptic Munc13-1/2 DKO neurons rescued with wild type or CaM-insensitive Munc13 variants	16
Figure 5	CaM structure and CaM-binding motifs	17
Figure 6	Helical wheel projections of the CaM binding site in Munc13-1 and ubMunc13-2 and evolutionary conservation	19
Figure 7	Schematic representation of the main principles of a photoaffinity labeling (PAL) experiment	20
Figure 8	Photochemistry of the p-Benzoyl-phenylalanine photophore	22
Figure 9	MALDI-TOF-MS	24
Figure 10	Mechanism of CNBr-induced ligand release of p-benzoyl-L-phenylalanine-labeled photoadducts cross linked at a Met residue	34
Figure 11	Established and potential CaM binding sites in the Munc13 proteins	44
Figure 12	(A) Amino acid sequences of the model peptides covering the CaM binding sites of the different Munc13 isoforms	46
Figure 13	Detection of CaM and its photoadducts by SDS PAGE and mass spectrometry	48
Figure 14	Competition experiments	50
Figure 15	PAL-based Ca^{2+} titration assay	53
Figure 16	PAL-based heterotrimer formation assay	56
Figure 17	Co-sedimentation assays with GST-fusion proteins of bMunc13-2(366-780) and Munc13-3(711-1063)	57
Figure 18	Co-sedimentation assays with GST-bMunc13-2(366-780) and its mutant variants	59
Figure 19	Co-sedimentation assays with GST-Munc13-3(711-1063) and its mutant variants	60
Figure 20	Analytical strategy for mapping the sites of photoincorporation into CaM	62
Figure 21	Detection of intact photoadducts by SDS-PAGE and MS	63
Figure 22	Peptide mapping of recombinant CaM by mass spectrometry	64
Figure 23	Identification of cross-linked peptides by HPLC/MALDI-MS	65
Figure 24	Characterization of the photoadducts at the amino acid level	67
Figure 25	On-target CNBr cleavage of the cross-linked peptide Bpa ⁴⁶⁴ -13-1(5-9)-CaM(127-148)	69
Figure 26	Fragment ion mass spectra of the photoprobe fragment Bpa ⁴⁶⁴ -13-1(5-9) and its methylthiocyanate derivative	70
Figure 27	Amino acid sequences of the model peptides covering the extended CaM binding sites in Munc13-1 and ubMunc13-2	72
Figure 28	Photoaffinity labeling of CaM with Munc13-1(458-492)-derived photoprobes	73
Figure 29	PAL-based Ca^{2+} titration assay	74
Figure 30	Characterization of the photoadduct of Bpa ^{464,489} -13-1 ⁴⁸⁷⁻⁴⁹² and CaM at the amino acid level	75
Figure 31	Photoaffinity labeling of CaM with ubMunc13-2(382-415)-derived photoprobes	76

Figure 32	Characterization of the photoadduct of Bpa ^{387,412} -ub13-1 ³⁸²⁻⁴¹⁵ and CaM at the amino acid level	77
Figure 33	Molecular modeling of the Munc13-1/CaM complex	85
Figure 34	High-resolution structure of the Munc13-1 ⁴⁵⁸⁻⁴⁹² /4Ca ²⁺ -CaM complex	87

1. INTRODUCTION

1.1. Basics of synaptic transmission

The human brain is in all likelihood the most complex known biological system. It comprises a sophisticated network of many billions of neurons, the highly differentiated electrically excitable cells dedicated to the conduction, computation, storage and modulation of electrical information. Neuronal connectivity is the indispensable prerequisite for such complex tasks. It is achieved through an overwhelming number of synapses, the specialized regions of chemical contact between neurons.

Chemical synapses are asymmetric transcellular junctions capable of converting the electrical activity of the presynaptic neuron into an extracellular chemical signal to be received by the postsynaptic neuron, a process termed synaptic transmission. Synaptic transmission is initiated by membrane depolarization waves that reach the presynapse in the form of action potentials. They induce the opening of voltage-gated calcium ion (Ca^{2+}) channels which triggers the Ca^{2+} -dependent exocytosis of synaptic vesicles filled with chemical compounds - the neurotransmitters - into the intercellular cleft defined by the synapse. The neurotransmitters bind receptors at the postsynaptic membrane leading to a translation of this chemical signal back into an electrical signal within the postsynaptic neuron.

Ca^{2+} -dependent vesicular neurotransmitter release at neuronal synapses involves a specialized and tightly regulated form of Ca^{2+} -triggered membrane fusion of exceptionally high spatial and temporal precision and speed. Transduction of the electric activity invading the synapse into synaptic vesicle fusion events takes place in less than 1 ms (Sabatini and Regehr, 1999), and is spatially restricted to the active zone, a defined electron-dense presynaptic membrane region equipped with a unique protein machinery mediating regulated exocytosis (Rosenmund et al., 2003).

1.2. The synaptic vesicle cycle

Synaptic vesicles pass through a complex cycle of membrane fusion and fission reactions in order to execute regulated neurotransmitter release. They bud from early endosomes, get loaded with neurotransmitter and are recruited to the plasma membrane, where they dock to the active zone. Once docked at the active zone, synaptic vesicles undergo maturation to a fusion-competent state (priming) that is responsive to action-potential-induced elevation in intracellular Ca^{2+} concentrations,

leading to their fusion with the plasma membrane and secretion of neurotransmitter into the postsynaptic cleft. Following fusion the protein and membrane constituents of the synaptic vesicles are endocytosed and recycled (Fig. 1; Sudhof, 2004).

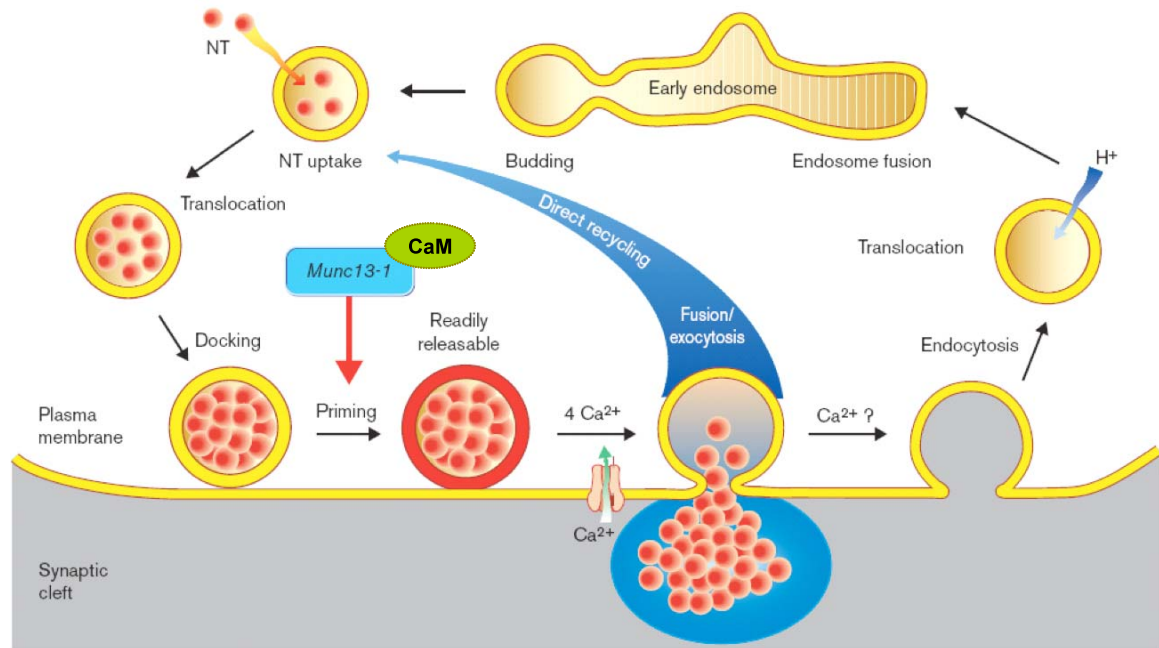


Figure 1. The synaptic vesicle cycle. Synaptic vesicles get loaded with neurotransmitter by active transport and are translocated to the presynaptic plasma membrane and dock at the active zone. A priming/maturation step involving the Munc13 proteins (see text for details) renders them fusion-competent. Munc13s are modulated by calmodulin (CaM) in processes of short-term plasticity (Junge et al., 2004). Ca^{2+} -triggered exocytosis leads to neurotransmitter release into the synaptic cleft. Synaptic vesicles are recycled via clathrin-mediated endocytosis or through a direct step bypassing endosomal intermediates. NT, neurotransmitter. Adapted from Brose et al., 2000.

Synaptic vesicle priming emerged as a concept from electrophysiological and morphological observations that repetitive stimulation can functionally exhaust synapses (i.e. leading to decelerated exocytosis) before causing a decrease in the number of docked vesicles (Sudhof, 1995). The need for such a vesicle maturation step is supported by the fact that neurotransmitter release takes place only 200 μs following Ca^{2+} influx (Llinás et al., 1981). Such fast coupling between excitation and secretion is only feasible when the essential parts of the protein machinery required for Ca^{2+} -induced membrane fusion are already assembled (Sudhof, 1995; Sudhof, 2004; Wojcik and Brose, 2007). In the past decade the Munc13 proteins have been established as the major molecular presynaptic priming factors.

1.3. The Munc13 protein family

The Munc13 proteins were identified as mammalian homologues of the *Caenorhabditis elegans* Unc-13 proteins, initially discovered in a genetic screen for mutations leading to an uncoordinated (unc) phenotype in worms. The *unc-13* mutant worms were paralyzed, suffered irregular pharyngeal movements, and were characterized by an abnormal accumulation of acetylcholine and resistance to acetyltransferase inhibitors, features suggestive of compromised neurotransmitter release (Brenner, 1974). At least two splice variants of a single *unc-13* gene are expressed in *C. elegans* and three splice variants have been identified in *D. melanogaster* (Aravamudan et al., 1999; Maruyama and Brenner, 1991; Richmond et al., 1999; Xu et al., 1998). Mammals have three different Munc13 genes (Munc13-1, Munc13-2 and Munc13-3; (Augustin et al., 1999a; Brose et al., 1995b) and two more distantly related Munc13-like genes, Munc13-4 and Baiap3 (Koch et al., 2000). Expression of Munc13-1 and Munc13-3 is restricted to neurons and neuroendocrine cells, while Munc13-2 is present as a brain-specific (bMunc13-2) and a ubiquitously expressed (ubMunc13-2) splice variant (Betz et al., 2001; Song et al., 1998).

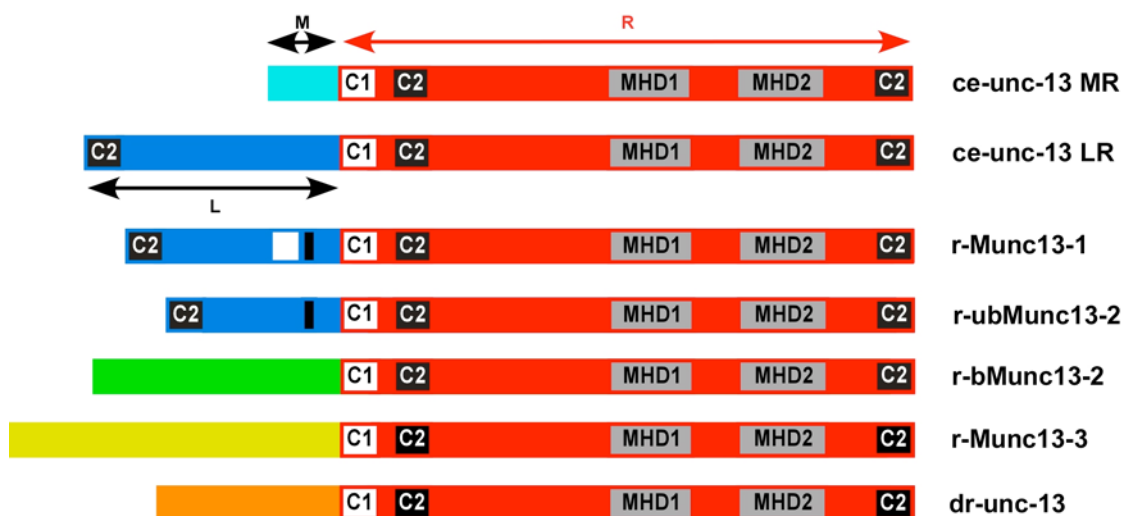


Figure 2. Domain structure of the Munc13 protein family. All Munc13 proteins share a highly homologous C-terminus (R-region, red) containing two Munc13 homology domains (MHDs), one diacylglycerol/phorbol ester binding C1 domain, and two C2 domains. *C. elegans* Unc-13 (ce-unc-13) is expressed as two splice variants (MR and LR). Only the mammalian homologs Munc13-1 and ubMunc13-2 share homology with the ce-Unc-13 LR protein N-terminally of the C1 domain (L-region, blue). The N-termini of bMunc13-2 (green) and Munc13-3 (yellow) and the *D. melanogaster* isoform dr-unc-13 (orange) are unrelated. A highly acidic stretch in the N-terminus of Munc13-1 (white) is not conserved in ubMunc13-2. The established conserved CaM binding sites in Munc13-1 and ubMunc13-2 are represented by black bars. Adapted from Koch et al., 2000.

Structurally, Munc13 proteins are characterized by their highly conserved C-terminal parts, which contain a C1 domain, two C2 domains, and two Munc13 homology domains (MHDs) (Fig. 2). A combination of ultrastructural, biochemical, cell biological and electrophysiological methods have established the C1 domain of Munc13-1 as a functional target of the DAG second messenger pathway, where Munc13-1 acts as a presynaptic phorbol ester/DAG receptor and can translocate to the membrane in a PKC-independent manner to enhance neurotransmitter release (Ashery et al., 2000; Betz et al., 1998). C2 domains are found in many proteins as modules for Ca^{2+} -dependent phospholipid or protein interactions (Brose et al., 1995a) but such functions of the C2 domains in the Munc13 proteins have not been established so far. The MHD regions present in the conserved C-termini of all Munc13 isoforms convey the priming function to these proteins as they are sufficient to rescue neurotransmitter release in hippocampal neurons of Munc13-1/2 knockout mice (Basu et al., 2005; Stevens et al., 2005).

In contrast to the evolutionarily conserved C-termini across the Munc13 family, the N-terminal parts of the proteins are largely unrelated and only Munc13-1 and ubMunc13-2 share homology with the amino-terminus of the longer Unc-13 splice variant in *C. elegans*. The N-terminal sequences of bMunc13-2 and Munc13-3 are not homologous to each other or to other known proteins. Such structural distinction between conserved and variable modules in the Munc13 protein family indicates that while all isoforms are capable of promoting synaptic vesicle priming (through interactions taking place in the C-terminus of the proteins) they may be subject to differential regulation (defined by their variable N-termini).

Munc13-1 is highly expressed throughout the rodent brain, while Munc13-2 and Munc13-3 exhibit complementary expression patterns. Munc13-2 is only present in rostral brain regions, including cerebral cortex and 'cornu ammonis' regions of the hippocampus, and Munc13-3 expression is restricted to the cerebellum in regions of high synaptic density (Augustin et al., 1999a).

Genetic studies have established the significance of Munc13-1 in both spontaneous and evoked neurotransmitter release. Morphological and electrophysiological analysis of individual primary neurons of mice lacking Munc13-1 showed its essential role as a molecular factor in the priming of synaptic vesicles. Loss of Munc13-1 leads to a 90% reduction of the pool of readily-releasable vesicles and thus to a significant decrease in neurotransmitter release (Fig. 3A) (Augustin et al., 1999b). In *C. elegans* and *D. melanogaster*, loss of function mutations in the unc-13

gene abolished neurotransmitter release at the neuromuscular junction. Unc13 appeared essential to the fusion competence of GABAergic and cholinergic synaptic vesicles (Aravamudan et al., 1999; Richmond et al., 1999). Ablations of Munc13-2 or Munc13-3 in mice do not cause significant anatomical, morphological or ultrastructural changes in the brain or a severe behavioral phenotype, indicating a compensatory role for the Munc13-1 isoform. Hippocampal neurons from animals lacking both Munc13-1 and Munc13-2 are completely deficient in transmitter release underscoring the indispensable role of the Munc13 proteins for proper neuronal function (Fig. 3B; Varoqueaux et al., 2002).

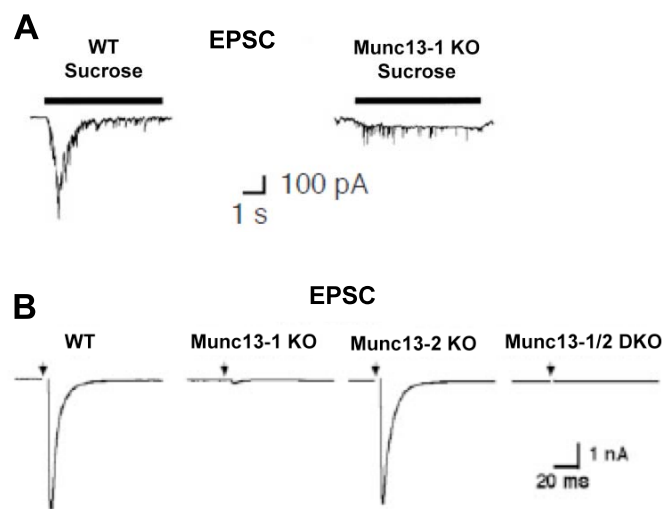


Figure 3. Electrophysiological characterization of Munc13-deficient mice. (A) Excitatory postsynaptic currents (EPSCs) recorded from primary autaptic wild type (WT) and Munc13-1 knockout (KO) hippocampal neurons by application of hypertonic sucrose solution showing a 90 % decrease in the size of readily releasable vesicle pool at glutamatergic synapses lacking Munc13-1. **(B)** Evoked EPSCs from Munc13-2 KO neurons were similar to WT, while Munc13-1 deletion led to a 90% reduction of evoked transmitter release. Hippocampal neurons lacking both Munc13-1 and Munc13-2 show neither evoked nor spontaneous release events. Adapted from Augustin et al., 1999b (A) and Varoqueaux et al., 2002 (B).

The syntaxin binding properties of Munc13 proteins have been considered essential for their role in synaptic vesicle priming (Brose et al., 2000). Syntaxin is a presynaptic membrane protein constituent of the fusogenic SNARE (soluble N-ethylmaleimide-sensitive factor attachment protein receptor) complex that is required for the Ca^{2+} -triggered synaptic vesicle fusion (Jahn and Südhof, 1999). The observation that a constitutively open syntaxin mutant can partially restore neurotransmitter release in *unc-13* knockout nematodes indicated that *unc-13*/Munc13s may play a role in the conformational transition of syntaxin-1 (Richmond et al., 2001). Although this role was originally attributed to a direct

interaction between Munc13 and the N-terminal region of syntaxin-1 (Betz et al., 1997), it was later found that purified Munc13-1 does not bind to isolated syntaxin-1 (Basu et al., 2005), suggesting that additional factors or proteins, such as tomosyn may be mediating this interaction (Gracheva et al., 2006; McEwen et al., 2006; Wojcik and Brose, 2007).

1.4. Munc13 proteins and short-term synaptic plasticity

Due to their essential function in synaptic vesicle priming and in the modulation of synaptic strength, Munc13 proteins have emerged as key regulators of adaptive synaptic mechanisms such as presynaptic short-term plasticity (STP). Short-term synaptic plasticity encompasses processes of activity-dependent modulation of neural networks and information processing in the CNS that occur on a timescale of milliseconds to minutes and typically reflect a rapid change in presynaptic transmitter release characteristics in response to acute changes in activity (Katz and Miledi, 1968; Zucker and Regehr, 2002). STP can result in either synaptic enhancement or synaptic depression, responses that are strongly dependent on the initial efficiency with which synapses transduce action potentials into synaptic transmitter release. Synaptic enhancement is manifested in three possible ways depending on its duration — facilitation, augmentation, or posttetanic potentiation (PTP). STP can also reduce neurotransmission, resulting in synaptic depression (Zucker and Regehr, 2002). The molecular mechanisms underlying the various forms of short-term plasticity are not completely understood, but it is generally accepted that most of them are Ca^{2+} dependent (Katz and Miledi, 1968; Zucker and Regehr, 2002).

The initial hypothesis that residual Ca^{2+} build-up in the synapse after an action potential is responsible for the enhanced synaptic transmission has been supported by more recent experiments in which a slow Ca^{2+} chelator, EGTA, was introduced into the presynaptic terminal and caused reduction in synaptic enhancement (Korogod et al., 2005). Originally it was believed that residual Ca^{2+} from prior activity simply summates with subsequent presynaptic Ca^{2+} transients in order to increase the efficacy of release probability (Katz and Miledi, 1968). It is now generally accepted, however, that residual Ca^{2+} also acts specifically on Ca^{2+} -binding proteins other than the sensor for neurotransmitter release, in order to alter release efficacy (Zucker and Regehr, 2002).

Ca^{2+} could interfere with every step of the synaptic vesicle cycle to promote short-term changes of synaptic release probability. Thus, adaptations in synaptic efficacy

may be caused by a direct effect of Ca^{2+} on molecular factors that regulate synaptic vesicle recruitment, docking, priming, fusion, and even endocytosis. Furthermore, elevation of presynaptic Ca^{2+} concentrations may regulate cytoskeletal elements and kinases/phosphatases that in turn modulate components of the synaptic release machinery (Rosenmund et al., 2002). In the search of molecular mechanisms underlying short-term plasticity events, the Munc13 proteins emerged as presynaptic factors to confer differential, isoform-specific presynaptic STP characteristics (Rosenmund et al., 2002). Functional studies on Munc13 knock-out neurons showed that Munc13-2 dependent synapses facilitate during trains of action potentials and show augmentation following high-frequency stimulation while Munc13-1-dependent synapses are characterized by short-term depression and no augmentation under the same stimulation conditions (Rosenmund et al., 2002). These results indicated a direct involvement of the Munc13 proteins in the mechanisms of STP.

STP characteristics are mainly determined by the transient increase in the residual presynaptic Ca^{2+} levels (see section 1.4.). There is, however, no known direct Ca^{2+} -dependent regulation of the Munc13 proteins suggesting that an additional molecular link is needed to confer Ca^{2+} sensitivity upon Munc13s for STP. Such molecular link was recognized in calmodulin (CaM), as Junge and colleagues identified a CaM binding site in Munc13-1 and ubMunc13-2, and demonstrated that the Ca^{2+} -dependent CaM binding of Munc13-1 and ubMunc13-2 generates a Ca^{2+} sensor/effector complex linking residual Ca^{2+} signaling to the synaptic exocytotic machinery (Fig. 4) (Junge et al., 2004). Using synaptic depression, frequency facilitation and augmentation protocols in autaptic hippocampal neurons they showed that CaM binding to Munc13 proteins enhances priming activity and increases the size of the readily releasable pool (RRP) of synaptic vesicles.

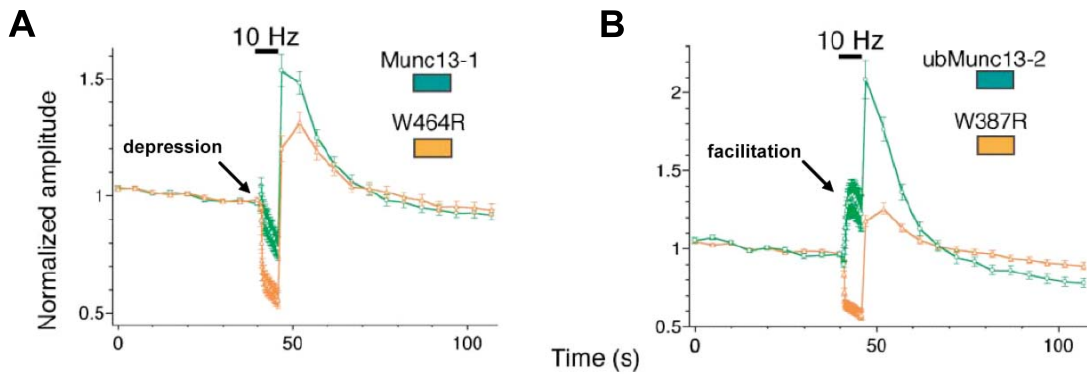


Figure 4. Altered short-term plasticity in glutamatergic autaptic Munc13-1/2 DKO neurons rescued with wild type or CaM-insensitive Munc13 variants. (A) Short-term plasticity of autaptic Munc13-1/2 DKO neurons rescued with wild type (WT) Munc13-1 or CaM-insensitive Munc13-1W464R mutant. Cells rescued with Munc13-1W464R showed a stronger depression and lack of augmentation following high-frequency stimulation. (B) Short-term plasticity of autaptic Munc13-1/2 DKO neurons rescued with WT ubMunc13-2 or CaM-insensitive ubMunc13-2W387R mutant. Cells rescued with WT ubMunc13-2 exhibited frequency facilitation and augmentation, while cells rescued with ubMunc13-2W387R showed depression and hardly any augmentation under the same conditions. Adapted from Junge et al., 2004.

1.5. Ca^{2+} and calmodulin in the brain

Tight regulation of the cytosolic concentration of calcium ions is essential for the control of a wide range of biological processes, including muscle contraction, cell proliferation, apoptosis, fertilization, and neurotransmitter release. Many proteins involved in Ca^{2+} signal transduction alter their activity in response to changes in free Ca^{2+} levels, but are themselves unable to bind Ca^{2+} ions. In many of these cases, a modulatory function is carried out by calmodulin (CaM), an intracellular Ca^{2+} sensor with a multitude of known interactors (Ikura and Ames, 2006).

Calmodulin (16.7 kDa) has one of the most conserved amino acid sequences across eukaryotes (Copley et al., 1999). It is a highly acidic protein (pI ~4.6), further characterized by an unusual abundance of Met residues (6.1% Met frequency in sequence). Structurally CaM contains N- and C-terminal globular domains connected by a flexible central linker. Each of the two globular lobes is made out of a pair of helix-loop-helix Ca^{2+} binding motifs (EF hands) accommodating a total of 4 Ca^{2+} ions. The two EF hand pairs share a high degree of sequence homology. However, the subtle differences in sequence are sufficient to relay different Ca^{2+} binding affinities to the N- and C-terminal lobes of CaM: the C-terminus binds Ca^{2+} with a $K_d \approx 2 \times 10^{-7}$ M, while the N-terminal lobe has a 10 times lower Ca^{2+} affinity ($K_d \approx 2 \times 10^{-6}$ M) (Falke et al., 1994). The two domains of CaM adopt different

conformations in the absence and presence of Ca^{2+} (Fig. 5). In apo-CaM, the N-terminal domain adopts a closed arrangement in which the helices of both EF hands are packed tightly together while the C-terminus remains in a partially open conformation allowing some solvent access to its Met-rich hydrophobic binding patch (Swindells and Ikura, 1996). Binding of Ca^{2+} to the EF hands of CaM induces significant structural rearrangements in the relative orientation of the helices in each lobe, prompting the exposure of the several Met residues to the solvent that take part in interactions with CaM targets (Crivici and Ikura, 1995; Ikura, 1996). This property, in addition to the flexibility of the linker joining the two domains, confers upon CaM an extraordinary versatility in macromolecular interactions and the resulting regulatory mechanisms (Hoeftlich and Ikura, 2002; Vetter and Leclerc, 2003).

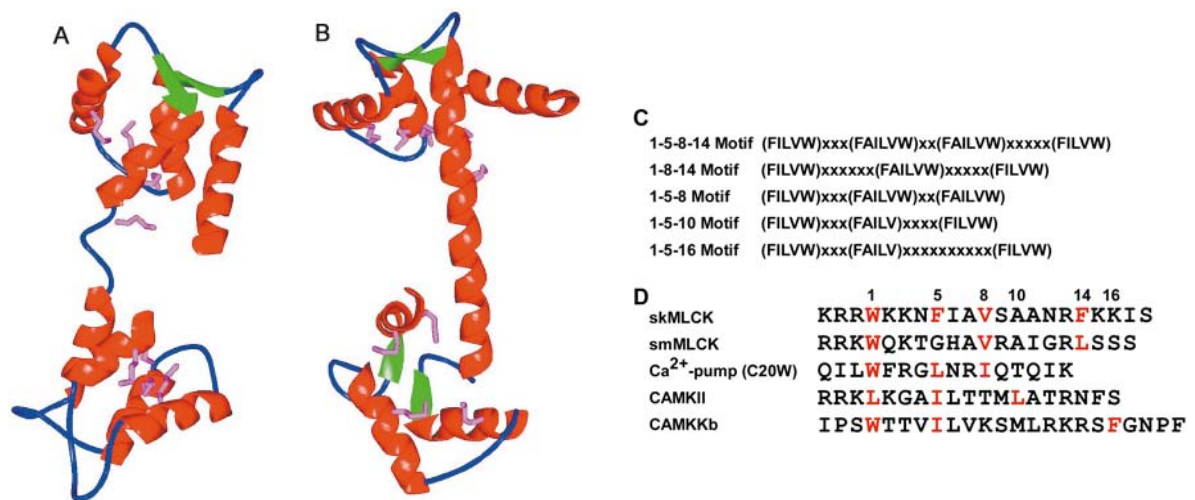


Figure 5. CaM structure and CaM-binding motifs. (A, B) Ribbon representation of CaM structure in Ca^{2+} -free state (apo CaM, A) and with all 4 Ca^{2+} -binding sites occupied (Ca^{2+} /CaM, B). N-terminal lobe is oriented to the top. Met side chains (purple) define potential hydrophobic pockets in each of the two domains. Ca^{2+} binding to CaM induces conformational changes that lead to exposure of hydrophobic surfaces that take part in interactions with target proteins. **(C)** Different Ca^{2+} -dependent CaM binding motifs with characteristic distribution of hydrophobic amino acids **(D)** Aligned sequences of known CaM binding motifs. Hydrophobic residues are shown in red and are numbered relative to the anchor residue in position one of the motif. Adapted from Chin and Means, 2000 (A, B); Rhoads and Friedberg, 1997 (C, D).

Considering the extraordinarily high concentrations of CaM in the brain (10-100 μ M; Xia and Storm, 2005), it is not surprising that many of the known Ca^{2+} -dependent CaM binding partners are neuronal proteins. However, the Ca^{2+} receptor essential for vesicle fusion is not calmodulin. Synaptotagmin, a low- Ca^{2+} -affinity, C2-domain-containing protein, is now well established as the Ca^{2+} sensor for fast neurotransmission (Geppert et al., 1994; Sudhof and Rizo, 1996). Calmodulin is involved, however, in controlling synaptic vesicle recruitment via activation of Ca^{2+} /calmodulin-dependent protein kinases (CaMKs) I and II and the phosphorylation of the synapsins on the synaptic vesicle. Phosphorylated synapsins dissociate from the vesicle, which leads to release of synaptic vesicles from cytoskeletal attachment and their recruitment to the presynaptic plasma membrane (Benfenati et al., 1992; Hilfiker et al., 1999; Valtorta et al., 1992). Calmodulin is important in many other aspects of Ca^{2+} -dependent modulation of neuronal function. These include post-synaptic changes during synaptic plasticity via the interaction of calmodulin with CaMKII (Malenka et al., 1989; Pettit et al., 1994), regulation of gene expression (Deisseroth et al., 1998), Ca^{2+} -dependent inactivation of voltage-gated Ca^{2+} channels (Lee et al., 1999; Peterson et al., 1999; Zuhlke et al., 1999), or activation of Ca^{2+} -dependent K^{+} channels (Keen et al., 1999; Xia et al., 1998).

Prominent examples of neuronal CaM targets include the Munc13 proteins, the key mediators of synaptic vesicle priming. Through extensive biochemical analysis the CaM binding sites of Munc13-1 and ubMunc13-2 were narrowed down to a highly homologous 21 amino acid stretch in the N-termini of the proteins. These CaM binding sites are defined by a conserved bulky hydrophobic anchor residue (Trp-464 in Munc13-1 and Trp-387 in ubMunc13-2) and a high propensity to form a basic amphiphilic α -helix – minimal requirements shared by most of the otherwise rather diverse Ca^{2+} -dependent CaM binding partners (Fig. 6, Junge et al., 2004).

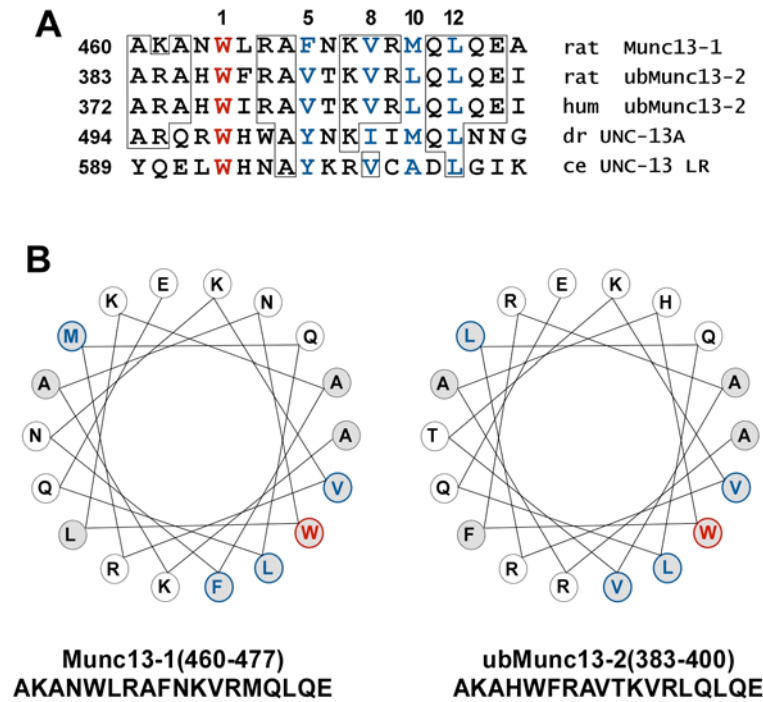


Figure 6. Helical wheel projections of the CaM binding site in Munc13-1 and ubMunc13-2 and evolutionary conservation (A) Sequence alignment of CaM binding sites in Munc13/Unc-13 homologs. Identical amino acids are boxed in black. Proposed hydrophobic anchor residues are shown in red, further hydrophobic residues with conserved distribution for CaM binding are shown in blue. **(B)** Amphipathic helices predicted in the CaM binding regions of Munc13-1 and ubMunc13-2 expose clusters of hydrophobic (gray circles) and hydrophilic (open circles) amino acids. Color coding from A applies. Adapted from Junge et al., 2004.

Despite the extensive functional characterization of the Munc13/CaM interactions in STP phenomena, little is known about the actual mechanism of regulation of Munc13 proteins by CaM. More detailed insights into the structure of the CaM/Munc13 complex could provide a platform for the design of Munc13 variants with altered affinity to CaM which would be useful for the comprehensive analysis of the role of Munc13 proteins in synaptic transmission and plasticity. A major obstacle in obtaining such structural information is the size of the Munc13 proteins (200 - 250 kDa) - a challenge for recombinant production and thus for NMR and crystallography approaches. In such cases, methodologies employing model peptides mimicking the binding site of the ligand, such as photoaffinity labeling, may provide useful initial structural information.

1.6. Photoaffinity labeling

1.6.1. General principles of photoaffinity labeling for structural analysis

Photoaffinity labeling (PAL) emerged as a technique for the characterization of protein/ligand interactions more than four decades ago (Singh et al., 1962), but recent developments of more efficient photophores, new high resolution separation methods and detection techniques with higher sensitivity have led to renewed appreciation and applications of this methodology. The basic principles of PAL have remained essentially unchanged: ligands carrying photoreactive (but chemically inert) moieties are introduced into a system that includes a target protein interactor and are allowed to form ligand-protein complexes. UV light irradiation results in the formation of activated ligand intermediates that react with amino acids within the binding pocket of the target protein to form covalent photoadducts. These can be isolated and analyzed at the protein level, oligopeptide level, and amino acid level, the latter providing the most comprehensive structural information (Fig. 7).

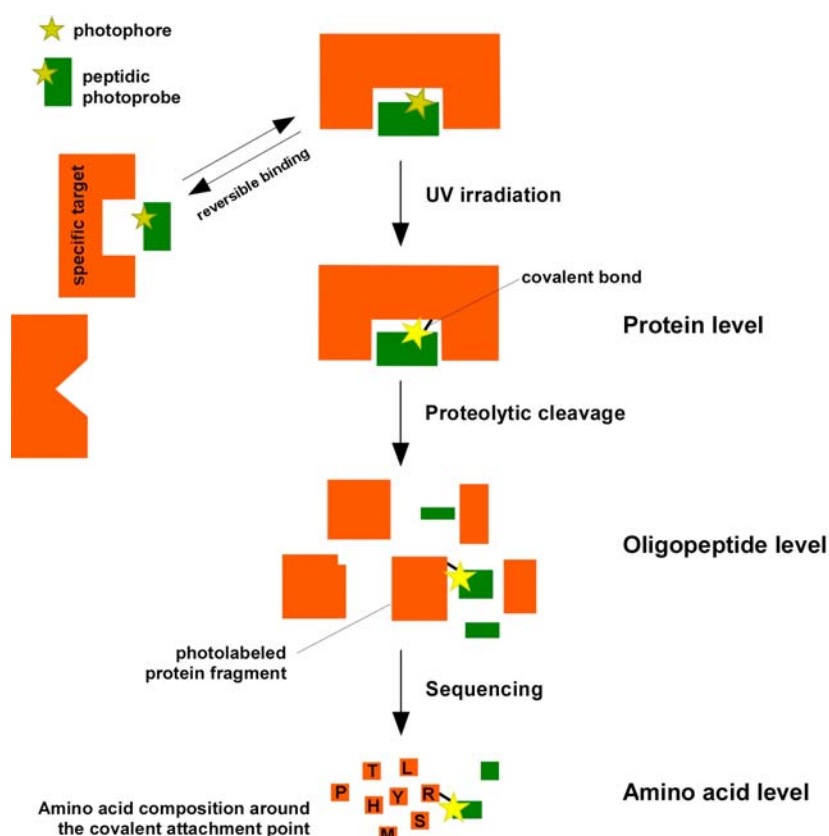


Figure 7. Schematic representation of the main principles of a photoaffinity labeling (PAL) experiment. Photoactivation leads to the covalent attachment of a peptidic photoprobe carrying a photoreactive group (photophore) to a specific target protein. Thereby, a reversible non-covalent interaction is converted into a covalent complex, making it accessible for standard protein analytical techniques. Several levels of analysis can yield information about the structure of the complex. See text for details, adapted from Dorman and Prestwich, 2000.

At the protein level, detection of the intact photoadducts by gel electrophoresis - or more accurately by mass spectrometry - reveals the molecular weight of the complex and thereby information on its stoichiometry. Proteolytic digestion of the complex and subsequent chromatographic and mass spectrometric methods allows narrowing down the protein sequences that have participated in photoadduct formation and are thus part of the binding site of the protein. Sequencing of a photolabeled protein fragment (i.e. a cross-linked peptide) can ultimately lead to the identification of the exact site of photoincorporation at the amino acid level. For this purpose, mass spectrometry – rather than Edman degradation – is the method of choice, as it is very sensitive and, most importantly, allows sequencing from peptide mixtures. Thus, a single PAL experiment can provide valuable information about the stoichiometry of a peptide-protein interaction, and the location and architecture of the binding interface.

1.6.2. Requirements of the photoreactive group

An efficient photoreactive group should meet several requirements. The photophore should be sufficiently small so that, once incorporated into the ligand, it does not create any steric interference that may compromise the biopotency of the photoprobe. It is important to establish that the incorporated photoreactive group does not significantly alter the binding affinity and functionality of the photoprobe, compared to the nonderivatized ligand. The photophore should demonstrate reasonable chemical stability under ambient light. Its photochemically generated excited state should have a lifetime shorter than that of the ligand-target protein complex but sufficiently long for the photophore to remain in close proximity to the binding site and form a covalent bond within it. The photoreactive group should undergo unambiguous photochemistry that leads to the generation of a single covalent photoadduct. Finally, the photophore should preferentially attack C–H and nucleophilic X–H bonds at an activation wavelength longer than the UV absorption of most proteins (300 nm), in order to avoid photolytic damage. Under these conditions stable covalent complexes are formed that can survive more rigorous downstream structural analysis, such as electrophoresis, chromatography and mass spectrometry.

The most common photophores currently employed in photoaffinity labeling studies belong to the families of aryl azides, aryl diazirines and benzophenones (Brunner,

1993; Vodovozova, 2007). The aryl azide and diazirine photoreactive groups are precursors of nitrene and carbene reactive species, while the benzophenone-based compounds rely on the photochemistry of aryl ketone intermediates (Dorman and Prestwich, 2000). Benzophenone photophores offer several advantages compared to their azide and diazirine counterparts in studies of protein complex structures and interactions. Benzophenone derivatives are generally more stable and may be manipulated in ambient light without significant degradation. Their activation takes place at 350 nm, a wavelength sufficiently high to avoid protein photolysis (Dorman and Prestwich, 1994). Furthermore, benzophenones retain stability in many common protic solvents and preferentially react with C–H bonds, even in the presence of water (Fig. 8; Brunner, 1993; Dorman and Prestwich, 1994).

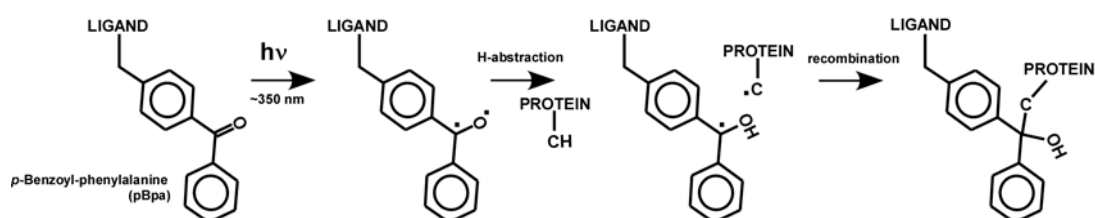


Figure 8. Photochemistry of the p-Benzoyl-Phe photophore. Adapted from Dorman and Prestwich, 1994.

The utility of p-Benzoyl-Phe (pBpa) was first demonstrated in the lab of William DeGrado where they incorporated this amino acid into a designed 17-residue peptide that interacted with, and efficiently labeled calmodulin (Kauer et al., 1986). In extension of this work they used fragmentation of the labeled protein, separation of the fragments by reverse-phase HPLC, and Edman degradation, and were able to identify the site of photolabel incorporation in calmodulin, which, depending on the position of the photoprobe within the peptide, was either Met71 or Met144 (O'Neil et al., 1989). In another early study, Miller and Kaiser used a pBpa-modified analogue of kemptide in similar interaction studies with cAMP-dependent protein kinase to identify Gly125 and Met127 of the enzyme as the sites of photoincorporation (Miller and Kaiser, 1988; see Dorman and Prestwich, 1994, for review of examples of site-directed photoaffinity labeling with pBpa containing ligands).

More recently, PAL techniques have been interfaced with modern mass spectrometry (MS) to yield greater efficiency and speed in providing additional structural and mechanistic information regarding protein complexes, such as the ligand–receptor stoichiometry, a map of the binding pocket, and even the exact

identification of the amino acid residues, which are involved in the ligand–receptor interaction (Girault et al., 1996; Jahn et al., 2002; Jahn et al., 2003; Mills et al., 1998). This capacity to provide insights into the primary structure of interaction sites makes the integration of PAL and MS tools a powerful strategy for structure-based drug design (Dorman and Prestwich, 2000).

PAL in combination with mass spectrometric characterization of the covalent photoadducts was used in the initial characterization of the conserved CaM binding sites in Munc13-1 and ubMunc13-2 (Junge et al., 2004). Using peptidic photoprobes covering the proposed CaM binding domains in Munc13-1 and ubMunc13-2 Junge and colleagues showed the specific, stoichiometric, and Ca^{2+} -dependent binding of these Munc13 isoforms to CaM.

1.7. Principles and applications of MALDI-TOF mass spectrometry

Mass spectrometry (MS) is an analytical technique that measures the mass-to-charge ratio (m/z) of ionized molecules in the gas phase as a function of their motility in an electric or magnetic field. Measurements are performed on a mass spectrometer, an instrument that consists of three main components: an ion source where the gas phase ions are produced from the sample molecules, a mass analyzer that measures the m/z of the ionized analytes, and a detector that registers the number of ions at each m/z value.

Electrospray ionization (ESI) (Fenn et al., 1989) and matrix-assisted laser desorption/ionization (MALDI) (Karas and Hillenkamp, 1988) are by far the most important ionization techniques in bioanalytical MS. By ESI, the analytes are transferred from the liquid phase into the high-vacuum of the mass analyzer, leading mainly to multiply charged ions. It is therefore well suited for a direct on-line coupling with liquid-based chromatographic separation methods, most commonly reversed-phase HPLC. By MALDI, in contrast, the analytes are transferred from the solid phase into the high-vacuum of the mass analyzer, leading mainly to singly charged ions. As a prerequisite, the analyte needs to be embedded into a crystalline UV light-absorbing matrix, from which it can be desorbed via laser pulses. Due to the pulsed nature of MALDI, it has been predominantly coupled with the time-of-flight (TOF) analyzer - a pulsed analyzer that measures m/z ratios on the basis of the flight time of an ion, which, at a constant accelerating voltage, is proportional to the square root of its m/z ratio.

Two technical developments have contributed greatly to the high resolution and mass accuracy of the MALDI-TOF instruments. First, the delayed extraction of ions from the source ensured that a much tighter packet of ions arrives at the detector. Second, the incorporation of a reflector unit meant an increase in the effective length of the analyzer tube and thus the path of the ions, while it led to a reduction in the kinetic energy distribution of ions of the same mass, thereby causing their improved, time-focused arrival at the detector (Fig. 9) (see (Hillenkamp and Peter-Katalinic, 2007) for technical details).

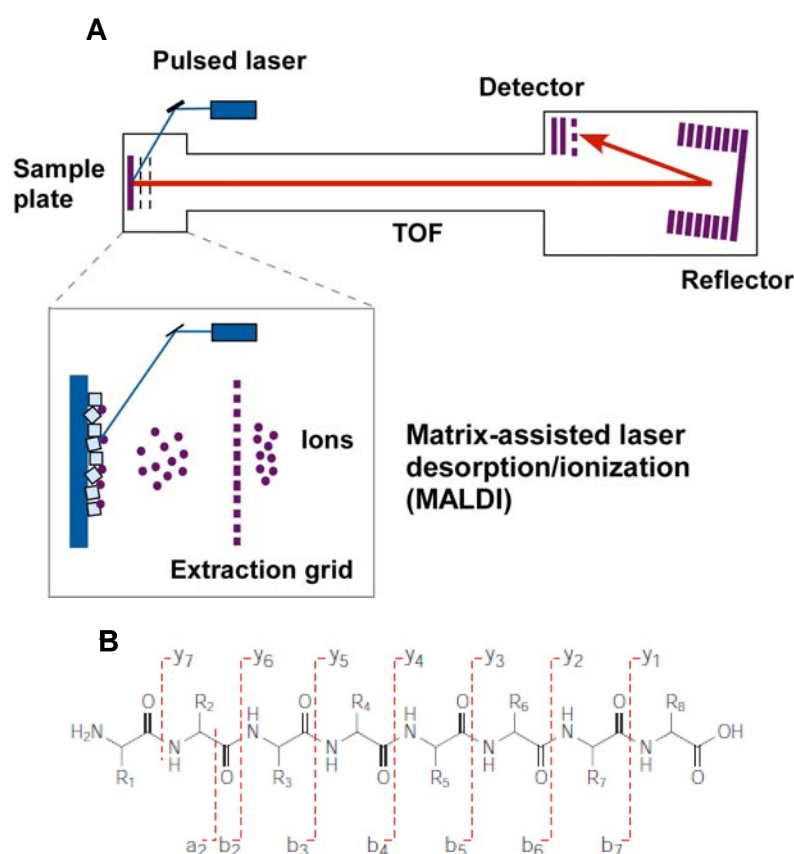


Figure. 9 MALDI-TOF-MS. (A) Schematic of a reflector MALDI-TOF mass spectrometer. In a MALDI time-of-flight (TOF) instrument, analytes are desorbed and ionized by a laser pulse. Following a delayed extraction (magnified inset), ions get accelerated to high kinetic energy and separated along a flight tube as a result of their different velocities. The ions are turned around in a reflector to compensate for slight differences in kinetic energy, and reach a detector that amplifies and counts arriving ions. **(B)** Chemical structure of a polypeptide showing the nomenclature for fragment ions (after Roepstorff–Fohlmann–Biemann) resulting from peptide fragmentation by collision-induced dissociation. Bond breakage occurs predominantly through the lowest energy pathways, i.e. cleavage of the amide bonds. This generates b-ions when the charge is retained by the amino-terminal fragment and y-ions when it is retained by the carboxyl-terminal fragment. The major fragment ions of tryptic peptides observed in MALDI-TOF-MS are $y > b \gg a$, and so only these are shown for the sake of clarity. Adapted from Aebersold and Mann, 2003 (A); Steen and Mann, 2004 (B).

MALDI-TOF-MS provides high resolution, mass accuracy and sensitivity, while being robust, fast, and easy to automate, features making it well suited for the analysis of peptides in general. One of its most prominent applications is the identification of proteins by peptide-mass fingerprinting (PMF), a method based on the matching of a list of experimentally determined peptide masses with the calculated list of all peptide masses of each entry in a comprehensive protein database (Thiede et al., 2005). More recently, straightforward peptide sequencing capabilities have been implemented into MALDI-TOF-MS, technically realized with the advent of TOF/TOF tandem mass analyzers (Suckau et al., 2003). In MALDI-TOF-MS-based sequencing, a particular peptide ion is isolated, and its fragmentation is induced through high-energy collisions with residual gas molecules or an inert collision gas. The resulting fragment ion mass spectra (commonly referred to as MS/MS spectra) represent amino acid sequence-specific fragment ions as products of randomized breakages at different bonds within the precursor peptide. The most abundant (and thus often most informative ions) are generated by fragmentation at the peptide backbone. They are called b-ions if the charge is retained by the N-terminal part of the peptide and y-ions if the charge is retained by the C-terminal part (Fig. 9) (Steen and Mann, 2004). These sequencing capabilities have not only added another level of confidence to protein identification by MALDI-TOF MS, but also allow for the detection and localization of post-translational and chemical modifications as well as cross-linking sites.

Traditionally, MALDI-TOF MS has been preferred for the analysis of relatively simple peptide mixtures. However, it can be interfaced to an off-line liquid chromatography (LC) separation step to assay more complex samples. In such an LC-MALDI configuration peptides are eluted from an LC-column and directly spotted onto a MALDI target plate. In this way samples are available for comprehensive data acquisition and can even be archived for reconsideration, independent from the temporal constraints imposed by an on-line LC configuration. The chromatographic separation leads to a reduction in spectral complexity and circumvents the effects of ion suppression, promoting increased coverage of complex peptide mixtures.

1.8. Aims of this study

Using the initial biochemical and functional annotation of the Munc13/CaM interactions (Junge et al., 2004) as a starting point, the work presented here was motivated by the following goals:

- Establishment and biochemical characterization of non-conserved CaM domains in bMunc13-2 and Munc13-3 and generation of tools for elucidating the physiological features of these interactions.
- Definition of the Ca^{2+} sensitivity of formation of the Munc13/CaM complex,
- Establishment of a PAL-based analytical workflow for the structural characterization of peptide/protein interactions,
- Implementation of this workflow for the structural analysis of the Munc13/CaM interaction,

2. MATERIALS AND METHODS

2.1. Photoaffinity Labeling and Mass Spectrometry

2.1.1. Prediction of CaM binding sites

Due to the lack of a single consensus sequence for CaM binding sites across all Munc13 isoforms, the N-terminal sequences of bMunc13-2 (GenBank accession number U24071) and Munc13-3 (GenBank accession number U75361) were surveyed for similarities with a web-based CaM target database (<http://calcium.uhnres.utoronto.ca/ctdb>) (Yap et al., 2000). As these searches returned no hits, a bioinformatic prediction tool available on the same server was used to screen the Munc13 sequences for the presence of potential CaM recognition motifs. This program employs biophysical and structural criteria such as hydropathy, α -helical propensity, residue size, residue charge, hydrophobic residue content, helical class, and occurrence of particular residues to determine putative CaM binding sites (Yap et al., 2000). Scores indicating the propensity of a residue to be part of a CaM binding site are evaluated for a sliding twenty-residue window and normalized to the entire sequence.

2.1.2. Peptide synthesis

All peptides and peptidic photoprobes (Table 1) were synthesized by solid phase peptide synthesis using standard fluorenylmethoxycarbonyl (Fmoc) chemistry as described (Jahn et al., 2002). The shorter peptides were N-terminally elongated by an artificial Cys residue to enable a selective coupling chemistry via the sulfhydryl group, an option for future experiments that was not used in the present study. Three types of peptides were synthesized: unmodified, 'wild type' peptides covering the predicted CaM binding sequences in each Munc13 isoform; CaM-insensitive peptides in which the proposed hydrophobic anchor residue (Trp or Phe) was substituted for Arg; and peptides carrying a p-Benzoyl-Phe photophore. Instead of modifying the Munc13-derived peptides N-terminally by a benzophenone group as performed previously (Junge et al., 2004), the photophore was directly introduced into the polypeptide chain by using the photoreactive amino acid derivative Fmoc-p-Benzoyl-Phe (Bachem). Purified peptides were characterized by analytical reversed-phase HPLC and mass spectrometry. Amino acid analysis was used to determine the exact concentrations of peptide stock solutions.

Table 1. Synthetic peptides used in this study. Numbering of amino acids refers to the rat sequences (GenBank accession numbers: Munc13-1, U24070; ubMunc13-2, AF159706; bMunc13-2, U24071; Munc13-3, U75361). Bp, benzophenone; f, p-Benzoyl-Phe.

Nomenclature	Sequence	Origin
13-1	CRAKANWLRAF NKVRMQLQEAR	Munc13-1 (459-479)
Bp ^N -13-1	Bp-CRAKANWLRAF NKVRMQLQEAR	
Bpa ⁴⁶⁴ -13-1	CRAKANfLRAF NKVRMQLQEAR	
R ⁴⁶⁴ -13-1	CRAKANRLRAF NKVRMQLQEAR	
13-1 ⁴⁵⁹⁻⁴⁹²	RAKANWLRAF NKVRMQLQEARGE GEMSKSLWFKG	Munc13-1 (459-492)
Bpa ⁴⁶⁴ -13-1 ⁴⁵⁹⁻⁴⁹²	RAKANfLRAF NKVRMQLQEARGE GEMSKSLWFKG	
Bpa ⁴⁸⁹ -13-1 ⁴⁵⁹⁻⁴⁹²	RAKANWLRAF NKVRMQLQEARGE GEMSKSLfFKG	
Bpa ^{464,489} -13-1 ⁴⁵⁹⁻⁴⁹²	RAKANfLRAF NKVRMQLQEARGE GEMSKSLfFKG	
ub13-2	CQARAHWFRAVTKVRLQLQEIS	ubMunc13-2 (382-402)
Bp ^N -ub13-2	Bp-CQARAHWFRAVTKVRLQLQEIS	
Bpa ³⁸⁷ -ub13-2	CQARAHfFRAVTKVRLQLQEIS	
R ³⁸⁷ -ub13-2	CQARAHRFRAVTKVRLQLQEIS	
ub13-2 ³⁸²⁻⁴¹⁵	QARAHWFRAVTKVRLQLQEISDDGDP SLPQWLPE	ubMunc13-2 (382-415)
Bpa ³⁸⁷ -ub13-2 ³⁸²⁻⁴¹⁵	QARAHfFRAVTKVRLQLQEISDDGDP SLPQWLPE	
Bpa ⁴¹² -ub13-2 ³⁸²⁻⁴¹⁵	QARAHWFRAVTKVRLQLQEISDDGDP SLPQfLPE	
Bpa ^{387, 412} -ub13-2 ³⁸²⁻⁴¹⁵	QARAHfFRAVTKVRLQLQEISDDGDP SLPQfLPE	
b13-2a	CKLSRAIHHFRLALQGVFQKLENN	bMunc13-2 (572-594)
Bpa ⁵⁸⁰ -b13-2a	CKLSRAIHHfRLALQGVFQKLENN	
R580-b13-2a	CKLSRAIHHRLALQGVFQKLENN	
b13-2b	CINNFKNV LREKRLRQKKLLQELV	bMunc13-2 (719-742)
Bpa ⁷²³ -b13-2b	CINNfKNV LREKRLRQKKLLQELV	
R723-b13-2b	CINN RKNV LREKRLRQKKLLQELV	
13-3a	CKFGSTLQRAKSALEV VWNK	Munc13-3 (786-804)
Bpa ⁷⁸⁷ -13-3a	CKfGSTLQRAKSALEV VWNK	
R787-13-3a	CKRGSTLQRAKSALEV VWNK	
13-3b	CSFKEAALRAYKKQMAELEEK	Munc13-3 (961-980)
Bpa ⁹⁶² -13-3b	CSfKEAALRAYKKQMAELEEK	
R962-13-3b	CSRKEAALRAYKKQMAELEEK	

2.1.3. Photoaffinity labeling (PAL)

For the initial PAL experiments, 5 μ M salt-free bovine brain CaM (product number P2277, Sigma) and 5 μ M peptidic photoprobe were incubated for 2 h at room temperature under light exclusion in 250 mM ammonium acetate (pH 8) in the presence of 2 mM EGTA or 3 mM CaCl_2 . DTT (5 mM) was included to prevent intermolecular disulfide bond formation of the N-terminal Cys residues present in all peptides used. The exact concentrations of CaM stock solutions were determined by amino acid analysis. Activation of the photophore with UV light was performed on ice using an Ultratech 400 W halogen metal vapor lamp (Osram) and a B270 glass screen (Schott) to filter protein-damaging wavelengths below 300 nm (Jahn et al., 2002). Unless stated otherwise, UV irradiation was carried out for 20 min. Following UV irradiation, photoadducts were separated from non-labeled CaM by denaturing SDS-PAGE on pre-cast NuPAGE 12 % Bis-Tris gels (Invitrogen) using a MOPS buffer system according to the manufacturer's instructions. Gels were fixed for one hour in ethanol/acetic acid and proteins were visualized using a colloidal Coomassie staining with Coomassie Brilliant Blue G-250 according to Neuhoff (Neuhoff et al., 1988).

The competition and cross competition reactions were carried out as above in the presence of increasing concentrations (0-50 μ M) of the wild-type or CaM-binding-deficient control peptides as competitors.

Buffer stocks:

250 mM ammonium acetate, pH 8.0

50 mM EGTA, pH 8.0

50 mM CaCl_2

MOPS running buffer (20X): 1 M MOPS, 1 M Tris base, 20.5 mM EDTA, 2% SDS

Fixing solution: 40% (v/v) ethanol, 10% (v/v) acetic acid

Colloidal Coomassie dye stock solution: 0.1% (w/v) Coomassie Brilliant Blue G250, 2% (w/v) *o*-phosphoric acid, 10% (w/v) ammonium sulfate; activated with ¼ parts of 100% methanol

2.1.4. Detection of photoadducts by mass spectrometry

For detection of photoadducts by matrix-assisted laser desorption/ionization (MALDI) time-of-flight (TOF) mass spectrometry, aliquots of the irradiated PAL reaction mixture were desalted on the basis of reversed-phase chromatography by using C18 ZipTips (Millipore) according to the manufacturer's instructions. Sinapinic acid was used to prepare a matrix sandwich for the application of the samples on a ground steel sample support: a saturated sinapinic acid solution in ethanol was deposited

onto the sample position, which resulted in a microcrystalline matrix layer after evaporation of the solvent. Onto these precoated positions, 1 μ l of a premix consisting of equal volumes of the ZipTip eluate and of a saturated sinapinic acid solution (acetonitrile/0.1 % TFA, 1:2) was deposited and allowed to dry. After drying, the crystalline sample was washed once with 2 μ l 0.1 % TFA. A mixture of three standard proteins ranging from 12,360-23,981 Da (Protein Calibration Mix 2, LaserBio Labs) was prepared accordingly and used for external calibration. Positively charged ions in the mass-to-charge (m/z) range 5,000-30,000 were analyzed with a Bruker Ultraflex I MALDI-TOF mass spectrometer operated in the linear mode under the control of the FlexControl 2.4 operation software (Bruker Daltonics). Post-processing and calibration of the mass spectra was performed with the post-processing software FlexAnalysis 2.4 (Bruker Daltonics).

2.1.5. PAL-based Ca^{2+} titration assay

To investigate the Ca^{2+} sensitivity of the Munc13-CaM interaction, a PAL-based Ca^{2+} titration assay was established. For that purpose, bovine brain CaM and peptidic photoprobe were incubated as described above for PAL, with the exception that a titration PAL buffer more closely resembling the presynaptic conditions was used. Defined concentrations of free Ca^{2+} were achieved by different Ca^{2+} /chelator buffer systems. Maxchelator (<http://www.stanford.edu/~cpatton/maxc.html>), a program for determining the free metal concentration in the presence of chelators (Patton et al., 2004) was used to calculate the Ca^{2+} /chelator ratios needed to obtain the desired concentrations of free Ca^{2+} . For free Ca^{2+} concentrations in the range of 1-1000 nM, 10 mM EGTA was included into the titration buffer and 0.06-8.5 mM CaCl_2 were added (Table 2). Only reagents of highest purity were used for the Ca^{2+} titration experiments.

Table 2. Ca^{2+} /EGTA buffer composition for free Ca^{2+} concentrations in the nanomolar range

Free [Ca^{2+}]	EGTA	[Ca^{2+}] added
0	10 mM	-
1 nM	10 mM	0.057 mM
3 nM	10 mM	1.68 mM
10 nM	10 mM	0.54 mM
20 nM	10 mM	1.03 mM
30 nM	10 mM	1.46 mM
50 nM	10 mM	2.22 mM
100 nM	10 mM	3.63 mM
300 nM	10 mM	6.31 mM
1 μ M	10 mM	8.51 mM

Separation of the photoadducts from non-labeled CaM by SDS-PAGE and visualization of the proteins by colloidal Coomassie staining were performed as described above.

Buffer stocks:

PAL buffer: 10 mM HEPES 150 mM KCl, pH 7.2

50 mM EGTA, pH 7.2

50 mM CaCl₂

2.1.6. Documentation and quantification of SDS-PAGE gels

All gels were documented with a near-infrared fluorescence imager (Odyssey system; LI-COR). Quantification of proteins was carried out on the basis of the Coomassie fluorescence that can be recorded in the 700 nm channel as this fluorescence is linearly correlated to the amount of Coomassie-stained protein in the concentration range used in this study (Luo et al., 2006).

2.1.7. Determination of trace calcium

Trace calcium in virtually calcium-free samples was determined by inductively coupled plasma mass spectrometry (ICP-MS) using a quadrupole instrument equipped with a dynamic reaction cell (ELAN DRC II, Perkin Elmer). Ammonia at a flow rate of 1 ml/min was used as reaction gas ($R_{pq} = 0.5$) to eliminate plasma-based interferences such as $^{40}\text{Ar}^+$. Calcium was detected on the basis of its isotopes $^{42}\text{Ca}^+$, $^{43}\text{Ca}^+$, and $^{44}\text{Ca}^+$ to enable the quantification of trace calcium in the presence of a high excess of potassium ($^{39}\text{K}^+$). The detection limit for calcium was approximately 20 ppb. Measurements were performed by Klaus Simon at the Department of Geochemistry, University of Göttingen.

2.2. Structural analysis of photoadducts by LC-MALDI-MS

2.2.1. Calmodulin

Recombinant CaM and ^{15}N -CaM were generated by Fernando Rodriguez-Castañeda as described (Haberz et al., 2006). Transformed *E. coli* were grown in minimal medium containing NH_4Cl or $^{15}\text{NH}_4\text{Cl}$ as nitrogen source. CaM was first enriched by a bulk purification step on the basis of TCA precipitation and further purified through hydrophobic interaction chromatography on a phenylsepharose column. Collected fractions were analyzed by SDS-PAGE. Recombinant CaM was compared with bovine brain CaM in the different PAL experiments described above

in order to examine its photoadduct yield, complex stoichiometry, and Ca^{2+} sensitivity, and thus applicability for the structural analysis of the Munc13/CaM interaction.

2.2.2. PAL

The PAL experiments for the structural analysis were carried out in the presence of 30 nM free Ca^{2+} under the quasi physiological conditions as described in Section 2.1.5. As before, 5 μM recombinant CaM and 5 μM photoprobe were used. Equimolar solutions of ^{15}N -CaM were prepared in the same buffer but in the absence of photoprobe, and handled in parallel. UV light irradiation was performed as described and equal volumes of the PAL sample and the ^{15}N -CaM control sample were mixed. Photoadduct formation was monitored by denaturing SDS-PAGE and colloidal Coomassie staining as outlined above. MALDI-TOF-MS was used to co-detect CaM, ^{15}N -CaM, and the respective photoadducts at the level of intact proteins.

2.2.3. HPLC/MALDI-TOF-MS for analysis of photoreaction mixtures

The photoreaction mixtures were alkalized to pH 8.0 and directly subjected to in-solution digest with recombinant porcine trypsin (Roche) for 16 hours (100 ng trypsin, 2 M urea, 10 % acetonitrile). The resulting mixtures of tryptic peptides were acidified with 1 μl TFA and separated on a Dionex Hypersil C18 BDS column (0.3 x 150 mm; particle size 3 μm , pore size 100 Å). The column was operated at a flow rate of 4 $\mu\text{l}/\text{min}$ using an ABI 140B syringe pump (Applied Biosystems) connected to an Accurate splitter (Dionex). Linear gradients formed by 0.1 % TFA and 0.1 % TFA containing 80 % acetonitrile were applied for elution. The separation was monitored by UV detection at 214 and 280 nm. Using a Probot microfraction collector (Dionex), 30 s -fractions of the eluate were automatically spotted onto a Bruker 600/384 AnchorChip target. Targets were pre-coated with α -cyano-4-hydroxycinnamic acid (HCCA) matrix as described (Jahn et al., 2006). To ensure uniform preparations independently of the eluent composition, the samples were re-crystallized with tetrahydrofurane:acetone:0.1%TFA = 7:2:1 (0.5 $\mu\text{l}/\text{spot}$). All peptide survey and fragment ion mass spectra were recorded on a Bruker Ultraflex I MALDI-TOF/TOF mass spectrometer. Positively charged ions in the m/z range 500 to 5500 were analyzed automatically in the reflector mode under the control of the FlexControl 2.4 operation software (Bruker Daltonics). Mass spectra were automatically post-

processed with the FlexAnalysis 2.4 software (Bruker Daltonics) and then manually searched for candidate cross-linked peptides. Peptides of interest were selected as precursors for the manual acquisition of fragment ion spectra, which were annotated with the help of the BioTools 3.0 software (Bruker Daltonics). Relevant sample spots were subjected to on-target cyanogen bromide (CNBr) cleavage.

For comparison with observed mass spectrometric data, theoretical isotope distributions of signals corresponding to ^{14}N - and ^{15}N -containing peptides were simulated with the MS-Isotope tool of the ProteinProspector program suite (<http://prospector.ucsf.edu>). This tool allows simulations with variable resolution and isotope content.

2.2.4. Secondary proteolytic cleavage of exceptionally large cross-linked peptides with endoproteinase Asp-N

In the cases when cross-linking with the Munc13-derived photoprobes took place within the largest tryptic CaM fragment CaM(38-74), the photoadducts were isolated by rpHPLC under the conditions described above, dried in a vacuum centrifuge, and subjected to in-solution digest with endoproteinase Asp-N (*Pseudomonas fragi*, Roche) for 16 hours (100 ng Asp-N, 25 mM Tris pH 8.0, 2 M urea, 10% acetonitrile).

2.2.5. On-target CNBr cleavage of PAL-cross-linked peptides

Spot positions containing candidate cross-linked peptides were treated on-target with CNBr to directly test whether a Met side chain was involved as site of photoincorporation into CaM (Kage et al., 1996). For that purpose, 2 μl of a saturated CNBr solution in 70% (v/v) formic acid were applied onto the spot positions of interest. Spots were covered with small glass vials containing a filter paper soaked with the CNBr solution and the reaction was allowed to proceed over night at room temperature. After the reaction was terminated by evaporation of the CNBr solution, the target was directly introduced into the mass spectrometer. The corresponding peptide survey spectra were compared with those recorded before the CNBr cleavage and thereby screened for newly appearing signals corresponding to methylthiocyanate derivatives of the benzophenone-containing tryptic peptides derived from the photoprobes (monoisotopic mass shift +73.00 mass units, Fig. 10). The identity of such derivatives was confirmed by MS/MS sequencing.

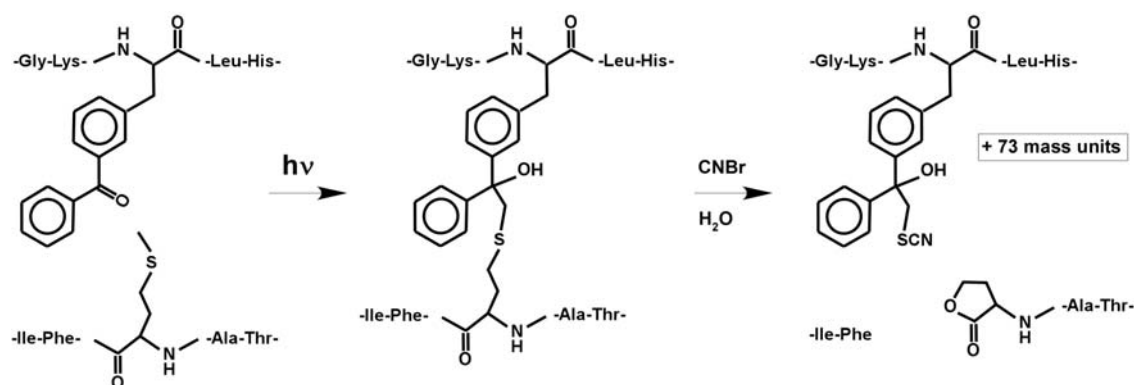


Figure 10. Mechanism of CNBr-induced ligand release of p-benzoyl-L-phenylalanine-labeled photoadducts cross-linked at a Met residue. CNBr digest of Met-cross-linked photoadducts leads to release of the photoprobe with a mass increment of 73 mass units. Adapted from (Kage et al., 1996).

2.3. Molecular Biology

2.3.1. Materials

2.3.1.1. Bacterial strains

E. coli, XL-1 Blue competent cells (Stratagene)
E. coli, ElectroTen-Blue competent cells (Stratagene)
E. coli, BL21DE3 competent cells (Stratagene)

2.3.1.2. Vectors

pGEX-4T-1 (GE Healthcare Life Sciences)
 pCR2.1-TOPO (Invitrogen)
 pBlueScript II KS (-) (Fermentas)

2.3.1.3. Plasmids

pEGFP-N1-bMunc13-2 (provided by Prof. Nils Brose)
 pEGFP-N1-Munc13-3 (provided by Prof. Nils Brose)
 pVENUS-VGLUT (provided by Dr. Etienne Herzog)
 pGEX-Munc13-1(309-567) (provided by Dr. Andrea Betz)
 pGEX-bMunc13-2(366-780) (as generated in this study)
 pGEX-bMunc13-2(366-780)F580R (as generated in this study)
 pGEX-bMunc13-2(366-780)F723R (as generated in this study)
 pGEX-bMunc13-2(366-780)F580R/F723R (as generated in this study)
 pGEX-bMunc13-2(366-780)F723R/K724E/K728E/R731E (as generated in this study)
 pGEX-Munc13-3(711-1063) (as generated in this study)
 pGEX-Munc13-3(711-1063)F787R (as generated in this study)
 pGEX-Munc13-3(711-1063)F962R (as generated in this study)

pGEX-Munc13-3(711-1063)F787R/F962R (as generated in this study)

pVENUS-N1-bMunc13-2 (as generated in this study)

pVENUS-N1-bMunc13-2 F723R/K724E/K728E/R731E (as generated in this study)

pVENUS-N1-Munc13-3 (as generated in this study)

pVENUS-N1-Munc13-3 F962R (as generated in this study)

2.3.1.4. Oligonucleotides

Table 3. Synthetic oligonucleotides used in this study (synthesis done in the MPI-EM DNA Core Facility on an ABI 5000 DNA/RNA Synthesizer)

Primer#	Sequence	Rest. sites
12135	5' -GCGC <u>G</u> AATTCATCAAGGGCTTAGTTTCCTACCAAAG -3'	EcoRI
12136	5' -CGCGATC <u>T</u> CGAGCTACCCTTCTGGGAGCCACTGAGG -3'	XhoI
12141	5' -CGC <u>G</u> AATTCCTCCATGCCCTGGATTGGATAATG -3'	EcoRI
12142	5' -CGCGTACTC <u>G</u> AGCTAGTTCAGGGATGTCCTGATAACCATAGC -3'	XhoI
12412	5' -CGATCCACCACCGCCGTTTGGCTCTTCAG -3'	-
12413	5' -CTGAAGAGCCAAACGGCGGTGGTGGATCG -3'	-
12414	5' -CCTTAACAAATGCATCAACAATCGTAAAAACGTCCTAAGAG -3'	-
12415	5' -CTCTTAGGACGTTTTTACGATTGTTGATGCATTTGTTAAGG -3'	-
12416	5' -CCTTTAAGTTCCCCAAACGT <u>G</u> GATCCACTCTTCAGAGG -3'	BamHI
12417	5' -CCTCTGAAGAGT <u>G</u> GATCCACGTTTGGGGAACCTTAAAGG -3'	BamHI
12418	5' -GAGAATCCGACCTTCCCGCAAAGAAGCAGCTTTAAGG -3'	-
12419	5' -CCTTAAAGCTGCTTCTTTGCGGGAAGGTCGGATTCTC -3'	-
13357	5' -GCATCAACAATCGTGAAAACGTCCTAGAAGAGAAAGAGCTGAGGCAGAAAAAC-3'	-
13358	5' -GTTTTTCTGCCTCAGCTCTTTCTTCTAGGACGTTTTCACGATTGTTGATGC-3'	-
13731	5' -GCTAGAAAACAGG <u>A</u> CTAGTGTGACTGAAGTAG -3'	SpeI
13732	5' -GCTTCTTTTCGCGAAGGTCGGATTCTCTTTGG -3'	-
13733	5' -CCAAAGAGAATCCGACCTTCGCGAAAAGAAGC -3'	-
13911	5' -CAGGGACAC <u>C</u> CGGGCACATGTACTTAGAAGAC -3'	SmaI
13940	5' -GCAGATATGCGTGAAGGATTACTGC -3'	-
13941	5' -GAGAACCGCCCAGGAGCCTATGAAC -3'	-

2.3.2. Methods

2.3.2.1. Electroporation of plasmid DNA into competent bacteria

An aliquot (40 µl) of electrocompetent *E. coli* of the appropriate strain was let thaw on ice and 20 ng of plasmid DNA or 1 µl of a ligation reaction were added, mixed gently and incubated for one minute on ice in a pre-cooled electroporation cuvette (0.1 cm, BioRad). The cuvette was administered an electric pulse of 1.80 kV (E.coli pulser, BioRad). Immediately following the electroporation the bacterial cells were retrieved from the cuvette with 0.8 ml pre-warmed Luria-Bertani (LB) Medium and allowed to recover and express their antibiotic resistance for 1 hour at 37°C under moderate shaking. For plasmid DNA electroporation 5-10 µl of bacteria were plated on the appropriate selection plates; in case of ligation reactions, the bacteria were carefully centrifuged and the entire pellet was resuspended in 100 µl LB Medium and plated on the appropriate selection plates.

Buffer stocks and materials:

LB Medium, per liter Millipore water: 10 g NaCl, 10 g Bacto-Tryptone, 5 g Bacto-yeast extract, 100 µl NaOH (10N stock); autoclaved

LB plates: 15 g Bacto-agar per 1 l LB medium; autoclaved. Required selection antibiotic added before plates are poured.

2.3.2.2. Small scale plasmid-DNA preparation

Small amounts of plasmid DNA were isolated from 1,5 ml overnight bacterial culture using the PureLink™ Quick Plasmid Miniprep Kit (Invitrogen) following the protocol supplied by the manufacturer or by the lysozyme-boiling method (Holmes and Quigley, 1981) as a rapid screening tool for ligation and/or transformation efficiency. According to this method the bacterial culture was pelleted for 30 s at 16,000 xg and resuspended in 300 µl STET buffer. After addition of 250 µg of lysozyme the suspension was boiled for 1 min at 100°C (water bath) and centrifuged for 10 min at 16,000 xg. The cell debris/protein pellet was removed with a toothpick and 100 µl of ammonium acetate (7.5 M) and 400 µl of isopropanol (100 %) were added to the supernatant. The sample was mixed and centrifuged immediately for 30 min at 16,000 xg. The pellet was let to air-dry and resuspended in 50 µl TE buffer for 30 min at 37°C upon mild shaking.

Buffer stocks:

STET: 8% sucrose, 0.5% Triton X-100, 10 mM Tris-HCl pH 8.0, 50 mM EDTA

Lysozyme: 10 mg/ml in Millipore water

7.5 M ammonium acetate

TE buffer: 10mM Tris-HCl pH 7.4, 1mM EDTA

2.3.2.3. Medium scale plasmid DNA preparation

For midi preparations of Plasmid DNA, a 100 ml bacterial culture was grown overnight. The DNA preparation was carried out using the PureLink™ Quick Plasmid Midiprep Kit (Invitrogen) following the protocol supplied by the manufacturer. The DNA pellet was redissolved in 100 µl TE buffer at 37°C.

2.3.2.4. Determination of DNA concentration

For the determination of the DNA concentration of aqueous solutions, a Genesys 6 Spectrophotometer (Thermo Spectronic) was used for absorption measurement at 260 nm wavelength (for double-stranded DNA 1 OD₂₆₀ = 50 mg/ml).

2.3.2.5. Sequencing of DNA

All DNA sequence analysis was done in the MPI-EM DNA Core Facility on an Applied Biosystems 373 DNA Sequencer.

2.3.2.6. DNA digest with restriction endonucleases

Analytical and preparative DNA digests were carried out for screening/sequence confirmation purposes and for the use of the DNA fragments in further subcloning steps. Instructions in the New England Biolabs manual were followed for the appropriate restriction endonuclease/buffer combination and overall reaction conditions. Generally digests were performed for 1.5 – 3 hrs at the enzyme specific temperature. When a consecutive digest with a second restriction enzyme was required, reactions were precleaned using the Invisorb® MSB spin PCRapace kit (Invitex).

2.3.2.7. Dephosphorylation of 5' DNA-ends

Dephosphorylation of the 5'-ends of DNA plasmids cut with a single restriction endonuclease was carried out in order to prevent recircularization of vectors in further DNA ligation reactions. The plasmid DNA was treated with alkaline phosphatase (calf intestine, Roche) in the supplied buffer according to manufacturer's instructions. Before further use, the DNA was purified by extraction with phenol:chloroform (see below).

2.3.2.8. Refilling of cohesive 5' DNA fragment ends

For the fill-in of the 5' overhangs of DNA fragments to be ligated into blunt-end vectors *Pfu* DNA polymerase (Stratagene) or the Klenow fragment of DNA polymerase I (New England Biolabs) were used. For refilling with *Pfu* the precleaned DNA fragment was supplemented with dNTPs, *Pfu* buffer and the *Pfu* DNA polymerase in a total of 100 µl and incubated for 1 hour at 72°C. For refilling with Klenow the precleaned DNA fragment was supplemented with dNTPs, the supplied buffer and the Klenow fragment and incubated for 20 min at room temperature. In both cases the DNA was extracted with phenolchloroform before further use (see below).

2.3.2.9. DNA Ligation

For ligation, digested plasmid and insert with compatible ends were mixed in a molar ratio of 1:4 and supplemented with T4 DNA ligase (Invitrogen) and the ligase-specific buffer in a total of 20 µl reaction volume. The ligation reaction was allowed to proceed for 16-20 hours at 16°C. Before electroporation into competent bacteria, the DNA was precipitated with ethanol (see below).

2.3.2.10. Ethanol precipitation of DNA

In order to increase the DNA concentration available for the electroporation of ligation products the ligation reaction (20 µl) was supplemented with 2 µl of kalium acetate (3 M) and 60 µl ethanol (100 %) and placed at -80°C for 2 hours. The precipitate was pelleted for 30 min at 16,000 xg in a pre-cooled bench-top centrifuge, the pellet was washed with 70 % ethanol and resuspended in 5 µl distilled water.

Buffer stocks:

3 M kalium acetate (10X)

2.3.2.11. Phenolchloroform extraction

Phenolchloroform extraction was performed on DNA samples following dephosphorylation or fill-in reactions in order to remove any enzymes and impurities that could compromise DNA ligation efficiency. For that purpose the DNA sample was dissolved in a total of 300 µl Millipore water, 300 µl of phenol were added and the mixture was vortexed thoroughly until turbid. The mixture was centrifuged for 3 min at 16,000 xg to achieve phase separation. The upper aqueous phase was

transferred to a clean vial, 300 µl of phenolchloroform (1:1) were added and the mixture was vortexed thoroughly. Following a centrifugation step the upper aqueous phase was transferred to a clean vial and washed twice with 300 µl chloroform as described above to remove all phenol. The DNA in the aqueous phase was precipitated with ethanol and kalium acetate (see above).

2.3.2.12. Agarose gel electrophoresis

For the analysis or purification of DNA restriction fragments the reactions were subjected to agarose-gel electrophoresis on 0.7 - 2 % agarose gels in TBE buffer including ethidium bromide (Roth). The negatively charged DNA fragments were separated at constant voltage (80-120 V) in TBE buffer and visualized by ethidium bromide under UV-light (254 or 314 nm). DNA fragment sizes were estimated by a GeneRuler DNA Ladder Mix sample (Fermentas) run on the gel in parallel.

Buffer stocks:

TBE running buffer (10X): 0.5 M Tris-Base, 0.5 M boric acid, 20 mM EDTA, pH 8.0

Ethidium bromide (2000X): 10 mg/ml

2.3.2.13. Agarose gel extraction of DNA fragments

DNA fragments of interest were excised and isolated from agarose gel with the PureLink™ Quick gel extraction kit (Invitrogen) according to the protocol supplied by the manufacturer.

2.3.2.14. Polymerase Chain Reaction (PCR)

Amplification of DNA *in vitro* was carried out by PCR. The reaction included double-stranded DNA template, oligonucleotide primers, dNTPs, the high-fidelity *Pfu* DNA polymerase (Stratagene) and the supplied buffer. All PCR reactions were run on Gene Amp 9700 PCR cycler (Applied Biosystems) with the basic cycle parameters as follows:

- | | |
|---------|---|
| Step 1: | 94°C for 3 min |
| Step 2: | 94°C for 20 s |
| Step 3: | <i>Annealing temperature</i> for 30 s |
| Step 4: | 72°C for <i>extension time</i> (30-40 cycles from step 2) |
| Step 5: | 72°C for 10 min |

Annealing temperatures were chosen at 5°C lower than the mean calculated melting temperature of the primers used in the reaction; extension time was adjusted according to the length of the PCR product. PCR products to be used in subcloning reactions were purified with the Invisorb® MSB spin PCRapace kit (Invitex).

2.3.2.15. Subcloning in TOPO pCR ® 2.1 vectors

The TOPO® TA cloning Kit (Invitrogen) was used for the rapid subcloning of PCR products. Protocols supplied by manufacturer were closely followed.

2.3.2.16. Cloning strategies for constructs generated and used in this study*pGEX-bMunc13-2(366-780)*

Primers 12135/12136 were used on a pEGFP-N1-bMunc13-2 template for PCR amplification of a 1264 bp long fragment corresponding to amino acids 366-780 in bMunc13-2 from *Rattus Norvegicus* (GenBank accession number U24071). The fragment was directly subcloned in pCR2.1TOPO, further excised with EcoRI/XhoI (restriction sites introduced via the primers) and ligated into the corresponding sites of pGEX-4T1.

pGEX-Munc13-3(711-1063)

Primers 121341/12142 were used on a pEGFP-N1-Munc13-3 template for PCR amplification of a 1080 bp long nucleotide fragment corresponding to amino acids 711-1063 in Munc13-3 from *Rattus Norvegicus* (GenBank accession number U75361). The fragment was directly subcloned in pCR2.1TOPO, further excised with EcoRI/XhoI (restriction sites introduced via the primers) and ligated into the corresponding sites of pGEX-4T1.

pVENUS-N1-bMunc13-2

The VENUS cassette was excised from pVENUS-VGLUT with AgeI/NotI and ligated in the same restriction sites on pEGFP-N1-bMunc13-2, replacing EGFP. Primer 13940 was designed for the sequencing confirmation of the in-frame position of the VENUS cassette N-terminally of bMunc13-2.

pVENUS-N1-bMunc13-2 F723R/K724E/K728E/R731E

PstI and NotI were used to excise a 1.2 kb fragment from pGEX-bMunc13-2(366-780)F723R/K724E/K728E/R731E containing the CaM-insensitive mutated sequence and the fragment was subcloned into the corresponding restriction sites of pBluescript II KS (-), giving rise to pBluescript II KS –bMunc13-2-T1. A 2 kb fragment containing the 5'- end of bMunc13-2 was excised with EcoRI and PstI from pVENUS-N1-bMunc13-2 and subcloned into the corresponding restriction sites of the pBluescript II KS –bMunc13-2-T1, giving rise to pBluescript II KS –bMunc13-2-

T2. *SpeI* and *BstEII* were used to excise a 2.1 kb fragment from pBluescript II KS – bMunc13-2-T2 covering the CaM-insensitive mutation sequence and inserted it into the same restriction sites of pVENUS-N1-bMunc13-2, giving rise to pVENUS-N1-bMunc13-2 F723R/K724E/K728E/R731E.

pVENUS-N1-Munc13-3

The VENUS cassette was excised from pVENUS-VGLUT with *AgeI*/*NotI* and ligated in the same restriction sites on pEGFP-N1-Munc13-3, replacing EGFP. Primer 13941 was designed for the sequencing confirmation of the in-frame position of the VENUS cassette N-terminally of Munc13-3.

pVENUS-N1-Munc13-3 F962R

Primers 13731/12732 were used for directed mutagenesis and PCR amplification of a 250 bp fragment from pVENUS-N1-Munc13-3 that contains a 5'- *Spe I* restriction site and the F962R CaM binding mutation. Primers 13733/13911 were used for the site-directed mutagenesis and PCR amplification of a 1.4 kb fragment from pVENUS-N1-Munc13-3 that contains the F962R CaM binding mutation and a 3'- *Sma I* restriction site. The two fragments were used in a fill-in PCR reaction, giving rise to a 1.6 kb fragment which was subcloned into pCRII-TOPO. This construct was digested with *SpeI* and *SmaI* and the resulting 1.6 kb fragment was ligated into the same restriction sites of pVENUS-N1-Munc13-3, giving rise to pVENUS-N1-Munc13-3 F962R.

2.3.2.17. Site-directed mutagenesis

The following plasmids containing Munc13 constructs with mutations as specified were generated using a QuikChange® Site-Directed Mutagenesis Kit (Invitrogen) under conditions suggested in the manufacturer's manual. Numbering of the primers used for the site-directed mutagenesis refers to Table 3.

- *pGEX-bMunc13-2(366-780)F580R*, primers 12412/12413
- *pGEX-bMunc13-2(366-780)F723R*, primers 12414/12415
- *pGEX-bMunc13-2(366-780)F580R/F723R*, primers 12414/12415 on template *pGEX-bMunc13-2(366-780)F580R*
- *pGEX-bMunc13-2(366-780)F723R/K724E/K728E/R731E*, primers 13357/13358 on template *pGEX-bMunc13-2(366-780)F723R*

- *pGEX-Munc13-3(711-1063)F787R*, primers 12416/12417
- *pGEX-Munc13-3(711-1063)F962R*, primers 12418/12419
- *pGEX-Munc13-3(711-1063)F787R/F962R*, primers 12418/12419 on template *pGEX-Munc13-3(711-1063)*

2.4. Co-sedimentation assays

2.4.1 Expression of GST-fusion proteins

The GST Gene Fusion System (GE Healthcare Life Sciences) was used for the bacterial expression of GST-fused bMunc13-2 and Munc13-3 fragments. pGex-4T-1 plasmids carrying different constructs were transformed by electroporation into *E. coli* of the BL21DE3 strain. Single colonies were transferred into 5 ml of LB medium supplied with ampicillin (100 µl/ml) and incubated with vigorous shaking overnight at 37°C. This preculture was diluted in 50 ml of LB medium supplied with ampicillin and incubated further at 37°C until the optical density of the culture at 600 nm reached ~0.85. The bacterial culture was let to cool down to room temperature, 0.1 mM isopropyl β-D-1-thiogalactopyranoside (IPTG) was added for the induction of protein expression and the culture was shaken for 2 hours at room temperature. The bacteria were sedimented for 20 min by centrifugation (4500 xg, 4°C) and the pellet was washed with 5 ml PBS and resuspended in buffer A supplied with the protease inhibitors 0.1 mM PMSF, 0.1 mM aprotinin, 0.1 mM leupeptin and 0.1 mM DTT. The cells were lysed by sonification using the Macro-tip from the *Labsonic U Sonifiers* (Braun) (5 pulses x 10 seconds). Triton X-100 (0.1%) was added to the suspension to solubilize the protein and it was shaken for 20 minutes on ice. The cell debris were pelleted by ultracentrifugation (100,000 xg, 30 minutes, 4°C) and the clear supernatant containing the soluble GST-fusion proteins was filtrated through a sterile 0.22 µm Millipore filter.

2.4.2. CaM co-sedimentation assay

Glutathione sepharose 4B beads were prepared as outlined in the GST Gene Fusion System handbook (GE Healthcare Life Sciences) and were incubated overnight at 4°C with the filtrated bacterial supernatant to allow adsorption of the GST-fusion proteins. The beads were washed 4 times with buffer A containing protease inhibitors and DTT, then equilibrated with either buffer E or buffer C and incubated with 30 ng/µl of CaM (bovine brain, Roche) in the respective buffers for 4

hours at 4°C. The beads were washed 3 times with either buffer E or buffer C, boiled for 3 min in SDS sample buffer and analyzed by denaturing SDS PAGE on pre-cast NuPAGE 12 % Bis-Tris gels (Invitrogen) using a MOPS buffer system according to the manufacturer's instructions.

The Coomassie fluorescence signals from the bands corresponding to the GST-fusion proteins (apparent molecular weight ~65 kDa) and the CaM co-sedimented under each condition (apparent molecular weight ~17 kDa) were quantified based on 2 independent experiments, and the signal-intensity/kDa values were used for the estimation of the stoichiometry of the interactions.

Buffer stocks:

0.5 M IPTG (500X)

10% Triton X-100

PBS (10X)

Buffer A (2X): 40 mM Tris/HCl, pH 7.5; 300 mM NaCl, 2 mM EDTA

Buffer E (2X): 100 mM Tris/HCl, pH 7.5; 300 mM NaCl; 2 mM EDTA;

Buffer C (2X): 100 mM Tris/HCl, pH 7.5; 300 mM NaCl; 2 mM EDTA; 8 mM CaCl₂

CaM, bovine brain: 1 mg/ml in 10 mM HEPES, pH 7.5

SDS sample buffer (3X): (163 mM Tris/HCl pH 6.8, 26% glycerol, 6% SDS, 0.03% bromophenol blue, 13% β-mercaptoethanol)

1.5 M DTT

100 mM PMSF (1000X)

100 mM aprotinin (1000X)

100mM leupeptin (1000X)

3. RESULTS

3.1. Characterization of the CaM interactions of bMunc13-2 and Munc13-3

3.1.1. Screening for CaM binding sites in bMunc13-2 and Munc13-3

The Munc13 isoforms bMunc13-2 and Munc13-1 do not contain a conserved CaM binding site with sequence homology to those found in Munc13-1 and ubMunc13-2. The first indication of the presence of a non-conserved CaM recognition motif in bMunc13-2 was provided by co-sedimentation experiments using GST-fusion proteins of bMunc13-2 fragments; these experiments identified bMunc13-2(627-755) as a minimal CaM-binding sequence (A. Betz and N. Brose, unpublished data). This amino acid sequence was therefore used as input for the web-based bioinformatic CaM-recognition-motif prediction tool available at the CaM target database (<http://calcium.uhnres.utoronto.ca/ctdb>). Based on this prediction amino acids 719-742 of bMunc13-2 were identified as a potential CaM binding site (black dotted bar, Fig. 11). Although unrelated in amino acid sequence, this site corresponded to the established CaM binding sites Munc13-1(459-479) and ubMunc13-2 (382-402), with respect to its distance from the C1 domain (Fig. 11). Surprisingly, when the input for the prediction algorithm was extended to encompass the 500 amino acids N-terminally of the C1 domain in bMunc13-2, a second sequence with high propensity for CaM binding was identified (amino acids 573-592, white dotted bar, Fig. 11).

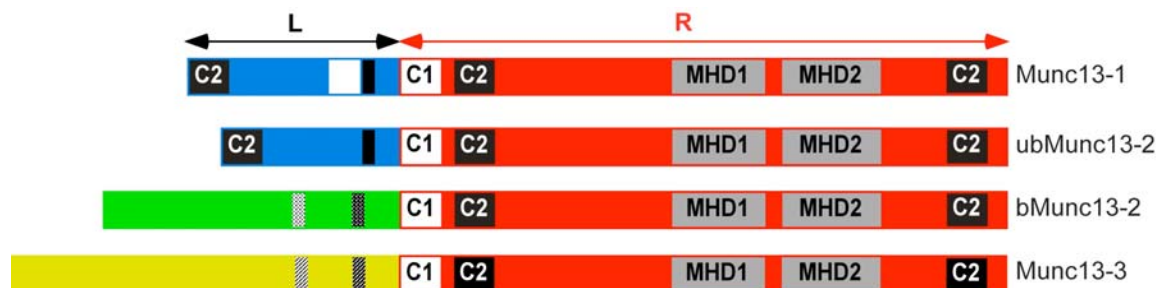


Figure 11. Established and potential CaM binding sites in the Munc13 proteins. Established conserved CaM binding sites in Munc13-1 and ubMunc13-2 are represented by black bars. Bioinformatically predicted non-conserved CaM binding sites in bMunc13-2 and Munc13-3 are represented by dotted and hatched bars, respectively. See Fig. 2 for details on the domain structure of Munc13.

Analysis of the corresponding part of Munc13-3 (500 amino acids N-terminal of the C1 domain) with the prediction algorithm also revealed two potential CaM binding sites in this isoform. The positions of the two sites, comprising amino acids 786-804 and 961-980, resembled those of potential CaM binding sites in bMunc13-2 (Fig.

11). When the corresponding sequences of Munc13-1 and ubMunc13-2 were used as input for the prediction algorithm, no additional CaM binding sites were identified.

3.1.2. Peptide design

On the basis of the bioinformatic screening, four novel model peptides were synthesized covering the potential CaM binding sites of bMunc13-2 and Munc13-3. The potential CaM binding peptides, bMunc13-2(572-594) (b13-2a), Munc13-3(786-804) (13-3a), bMunc13-2(719-742) (b13-2b), and Munc13-3(961-980) (13-3b) were synthesized and used in parallel with the previously characterized CaM binding peptides Munc13-1(459-479) (13-1) and ubMunc13-2(382-402) (ub13-2). All six CaM recognition motifs are at least related to the Ca^{2+} -dependent 1-5-10 or 1-8-14 motifs, and are therefore characterized by a hydrophobic anchor residue in position 1 of the motifs (Chin and Means, 2000) (Trp in 13-1 and ub13-2, and Phe in b13-2a/b and 13-3a/b).

For the application of these Munc13-derived model peptides in PAL, the anchor residues were replaced with the photoreactive amino acid derivative p-Benzoyl-Phe to generate the benzophenone (Bpa) photoprobes Bpa⁴⁶⁴-13-1, Bpa³⁸⁷-ub13-2, Bpa⁵⁸⁰-b13-2a, Bpa⁷²³-b13-2b, Bpa⁷⁸⁷-13-3a, and Bpa⁹⁶²-13-3b (Fig. 12). By applying this strategy, the photophore was directly introduced into the CaM binding site without changing the hydrophobic, bulky, and aromatic characteristics of the corresponding anchor position, thus minimizing interference with CaM binding. In addition to the wild-type peptides and their corresponding photoprobes, binding-deficient homologs were synthesized based on the finding that Trp/Arg mutations within the CaM binding site abolish CaM binding of Munc13-1 and ubMunc13-2 (Junge et al., 2004). To test whether this mutation effect is also seen at the peptide level and, if so, to verify it for bMunc13-2 and Munc13-3, we replaced the hydrophobic anchor residues with charged and hydrophilic Arg (R⁴⁶⁴-13-1, R³⁸⁷-ub13-2, R⁵⁸⁰-b13-2a, R⁷²³-b13-2b, R⁷⁸⁷-13-3a, and R⁹⁶²-13-3b; Fig. 12).

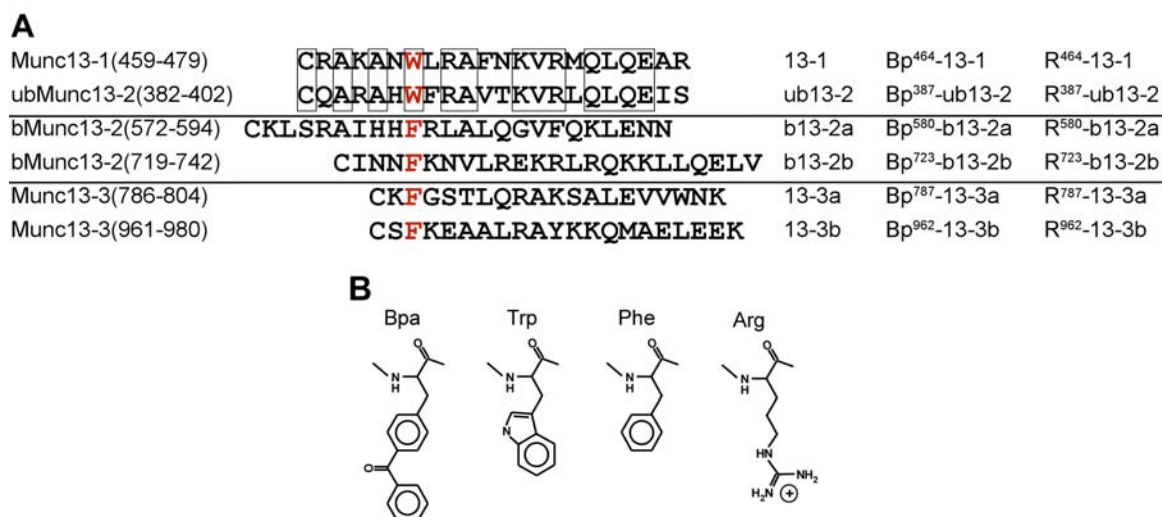


Figure 12. (A) Amino acid sequences of the model peptides covering the CaM binding sites of the different Munc13 isoforms. The sequences of the wild-type peptides are shown with the proposed hydrophobic anchor residue in red. The full names including the amino acid numbering and the abbreviations used throughout the text are given to the left and right of the sequences, respectively. The corresponding photoprobes and binding-deficient controls were generated by replacement of the anchor residue by p-Benzoyl-Phe (Bpa) and Arg (R), respectively. The Munc13-1- and ubMunc13-2-derived peptides display a high homology (59 % identity, identical residues are boxed), whereas the other sequences are unrelated. **(B) Structures of Bpa (photoreactive residue), Trp/Phe (hydrophobic anchor residue), and Arg (substitution in binding deficient controls).** Based on structural similarity the Bpa exchange was considered conservative.

3.1.3. Detection of the photoadducts

Bpa⁴⁶⁴-13-1, Bpa³⁸⁷-ub13-2, Bpa⁵⁸⁰-b13-2a, Bpa⁷²³-b13-2b, Bpa⁷⁸⁷-13-3a, and Bpa⁹⁶²-13-3b were used in PAL experiments followed by gel-electrophoretic analysis of the photoreaction products to demonstrate the Ca²⁺-dependent CaM binding of the novel Munc13-derived photoprobes. First, photoadduct formation of the established N-terminally modified versions of the Munc13-1/ubMunc13-2-derived photoprobes, Bp^N-13-1 and Bp^N-ub13-2 (Junge et al., 2004), was compared with that of the corresponding analogs generated by replacement of the anchor residues, Bpa⁴⁶⁴-13-1 and Bpa³⁸⁷-ub13-2. SDS-PAGE and colloidal Coomassie staining showed that the intensity of the Ca²⁺-dependent 20 kDa species corresponding to the photoadducts was similar for Bp^N-13-1 and Bpa⁴⁶⁴-13-1, as well as for Bp^N-ub13-2 and Bpa³⁸⁷-ub13-2 (Fig.13A). Thus, the photoadduct yields were independent of the position of the photophore in the peptide, indicating that the photoprobes retained their affinity for CaM even after substitution of the anchor residue by p-Benzoyl-Phe. The photoadduct pattern of Bpa⁴⁶⁴-13-1 and Bpa³⁸⁷-ub13-2 appeared

to be more homogenous compared to those of Bp^N-13-1 and Bp^N-ub13-2 (Fig. 13A). This can be explained by a greater flexibility of the benzophenone group at the N-terminus of the peptides and its potential to cross-link CaM in different positions, generating photoadducts of altered electrophoretic mobility.

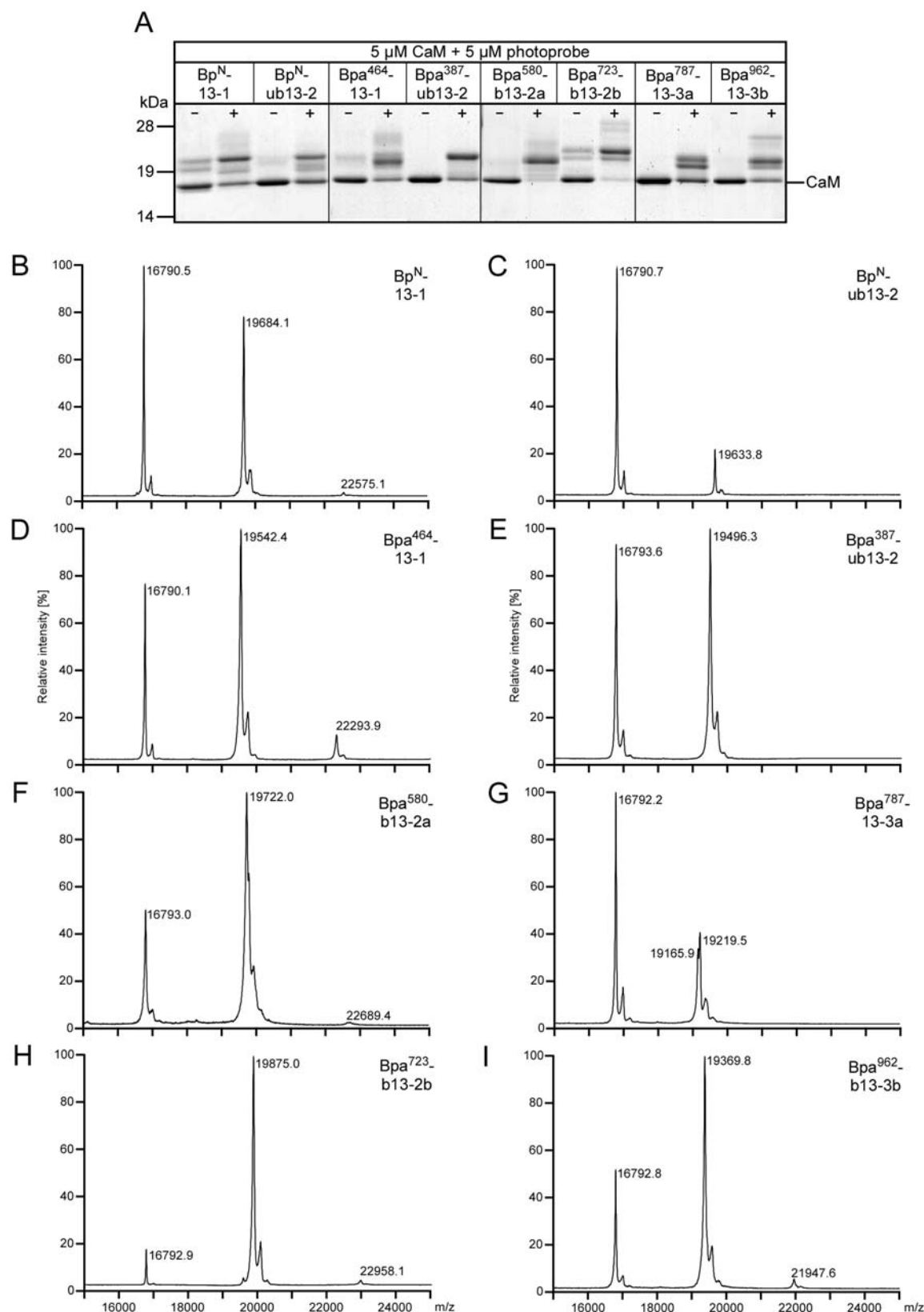


Figure 13. Detection of CaM and its photoadducts by SDS PAGE and mass spectrometry.

(A) Coomassie-stained SDS gels showing the photoadduct formation of the novel photoprobes Bpa⁴⁶⁴-13-1, Bpa³⁸⁷-ub13-2, Bpa⁵⁸⁰-b13-2a, Bpa⁷²³-b13-2b, Bpa⁷⁸⁷-13-3a and Bpa⁹⁶²-13-3b in the absence (-) and presence (+) of Ca²⁺. The N-terminally modified photoprobes Bp^N-13-1 and Bp^N-ub13-2, which were used previously to study CaM binding of Munc13-1 and ubMunc13-2 (Junge et al., 2004), were included for comparison. (B-I) Mass spectra showing, that all photoadducts were in principle represented by single signals corresponding to 1:1 species, even if a heterogeneous pattern was observed in the SDS gel. Only the mass spectra obtained from the PAL reactions in the presence of Ca²⁺ are displayed. Mass spectra were acquired by MALDI-TOF mass spectrometry using sinapinic acid as matrix. The mass increment of $m/z = 206$ detected for all signals was due to the known photochemically generated adducts of sinapinic acid. The calculated masses (M_{calc}) of CaM and its respective photoadducts were as follows: $M_{\text{calc}}(\text{CaM}) = 16790.4$ (B-I), $M_{\text{calc}}(\text{CaM+Bp}^{\text{N}}\text{-13-1}) = 19687.8$ (B), $M_{\text{calc}}(\text{CaM+Bp}^{\text{N}}\text{-ub13-2}) = 19638.7$ (C), $M_{\text{calc}}(\text{CaM+Bpa}^{464}\text{-13-1}) = 19544.7$ (D), $M_{\text{calc}}(\text{CaM+Bpa}^{387}\text{-ub13-2}) = 19495.6$ (E), $M_{\text{calc}}(\text{CaM+Bpa}^{580}\text{-b13-2a}) = 19716.8$ (F), $M_{\text{calc}}(\text{CaM+Bpa}^{787}\text{-13-3a}) = 19159.2$ (G), $M_{\text{calc}}(\text{CaM+Bpa}^{723}\text{-b13-2b}) = 19877.1$ (H), $M_{\text{calc}}(\text{CaM+Bpa}^{962}\text{-13-3b}) = 19367.4$ (I). The maximal mass deviation was only 300 ppm.

In order to investigate whether the predicted CaM binding sites in bMunc13-2 and Munc13-3 are functional, PAL experiments were performed with Bpa⁵⁸⁰-b13-2a, Bpa⁷⁸⁷-13-3a, Bpa⁷²³-b13-2b, and Bpa⁹⁶²-13-3b, and the photoreaction products analyzed as before. Similar to Munc13-1 and ubMunc13-2, Ca²⁺-dependent 20 kDa photoadducts species were detected for all four photoprobes employed (Fig. 13A), confirming the presence of two CaM binding sites in bMunc13-2 and Munc13-3, respectively. Interestingly, the photoadducts of Bpa⁷²³-b13-2b and Bpa⁷⁸⁷-13-3a were not as homogenous as those of the other photoprobes, but rather appeared as distinct double-bands (Fig. 13A). This finding indicated a more flexible mode of CaM binding of Bpa⁷²³-b13-2b and Bpa⁷⁸⁷-13-3a, which in turn would result in the formation of two defined photoadducts with different electrophoretic mobilities. Mass spectrometric analysis was used to determine whether these double-bands correspond to isomeric 1:1 photoadducts or to photoadducts of higher stoichiometric order. Only unmodified CaM and 1:1 photoadducts were detected for Bp^N-ub13-2, Bpa³⁸⁷-ub13-2, and Bpa⁷⁸⁷-13-3a (Fig. 13C, E, G). In the mass spectra obtained for Bp^N-13-1, Bpa⁴⁶⁴-13-1, Bpa⁵⁸⁰-b13-2a, Bpa⁷²³-b13-2b, and Bpa⁹⁶²-13-3b additional signals corresponding to a 1:2 stoichiometry were observed, but only with intensities close to the detection limit (Fig. 13B, D, F, H, I). The presence of these minor signals was in agreement with the Ca²⁺-dependent 25 kDa species observed as faint smeary bands after gel-electrophoretic analysis of the respective photoreaction products (Fig. 13A). These barely detectable 1:2 species were considered as

artifacts probably due to the very high Ca^{2+} -concentrations and/or the relatively long irradiation times. The photoprobes Bp^N-13-1, Bpa⁴⁶⁴-13-1, Bpa⁷²³-b13-2b also exhibited some Ca^{2+} -independent CaM binding capacity (Fig. 13A), which was not seen with full-length Munc13 proteins and was therefore considered as artifact due to protein truncation (Junge et al., 2004). Taken together, these initial PAL experiments demonstrated that all four Munc13-isoforms bind CaM in a Ca^{2+} -dependent manner and with a 1:1 stoichiometry.

3.1.4. Specificity of photoadduct formation

Competition experiments were employed in order to investigate the specificity of the synthetic photoprobes in their interactions with CaM. For that purpose increasing concentrations of the corresponding wild-type parent peptides were included into the PAL reaction, and the photoadduct formation was analyzed by gel electrophoresis as before. When 13-1 and ub13-2 were used as competitors for CaM binding of Bpa⁴⁶⁴-13-1 and Bpa³⁸⁷-ub13-2, respectively, photoadduct formation was suppressed already at equimolar levels (Fig. 14A, B), indicating that photoreactive and unmodified forms of the peptides bind with similar affinity to the same binding site. Up to ten-fold higher concentrations of b13-2a and 13-3a, respectively, were required to significantly suppress photoadduct formation of Bpa⁵⁸⁰-b13-2a, Bpa⁷²³-b13-2b, Bpa⁷⁸⁷-13-3a and Bpa⁹⁶²-13-3b (Fig. 14C, D, E, F) indicating that these photoprobes exhibit increased binding affinities rather than that the photoreactive and unmodified forms use different binding sites. It has been previously reported that amphipatic model peptides exhibit an increased affinity for CaM upon incorporation of a Trp residue into the N-terminal part of the motif (O'Neil et al., 1989), indicating a correlation between the affinity of these peptides to CaM and the bulkiness and hydrophobicity of their anchor residues. Accordingly, the replacement of Trp by p-Benzoyl-Phe as performed in Bpa⁴⁶⁴-13-1 and Bpa³⁸⁷-ub13-2, (Fig. 13A) did not significantly alter the biophysical characteristics of the anchor positions, and therefore resulted in similar affinities of the photoreactive and unmodified forms. In contrast, replacement of Phe by p-Benzoyl-Phe as performed in Bpa⁵⁸⁰-b13-2a, Bpa⁷²³-b13-2b, Bpa⁷⁸⁷-13-3a and Bpa⁹⁶²-13-3b rendered the anchor position more hydrophobic, bulky, and aromatic, which equipped the photoprobes with higher affinities to CaM than those of the wild-type parent peptides.

On the basis of the data from the competition experiments, it was concluded that each of the four Munc13-derived photoprobes and their respective wild-type counterparts target the same binding site on CaM. In comparison to the wild type peptides, the affinity of the photoprobes was not decreased upon incorporation of the photophore, indicating an identical binding mode and suitability for later PAL-based structural studies.

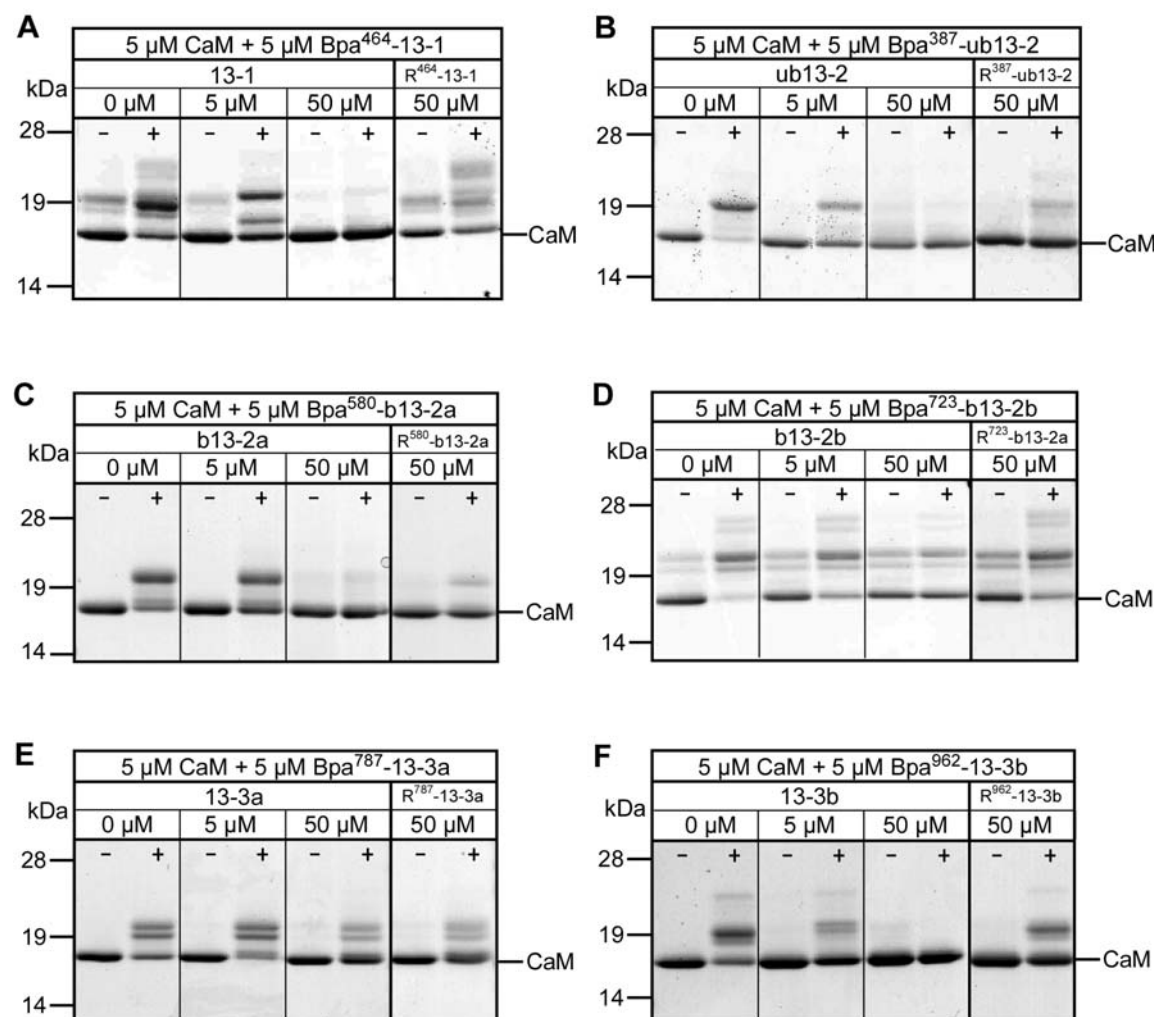


Figure 14. Competition experiments. Coomassie-stained SDS gels showing photoadduct formation of Bpa⁴⁶⁴-13-1 (A), Bpa³⁸⁷-ub13-2 (B), Bpa⁵⁸⁰-b13-2a (C), Bpa⁷²³-b13-2b (D), Bpa⁷⁸⁷-13-3a (E) and Bpa⁹⁶²-13-3b (F) in the absence (0 μ M), equimolar presence (5 μ M) and excess presence (50 μ M) of their respective unlabeled peptide homologs. Absence (-) and presence (+) of Ca²⁺ is indicated. Competition experiments in the presence of 50 μ M of the respective binding deficient homologs (Arg variants) are shown in the right-most lane of each panel.

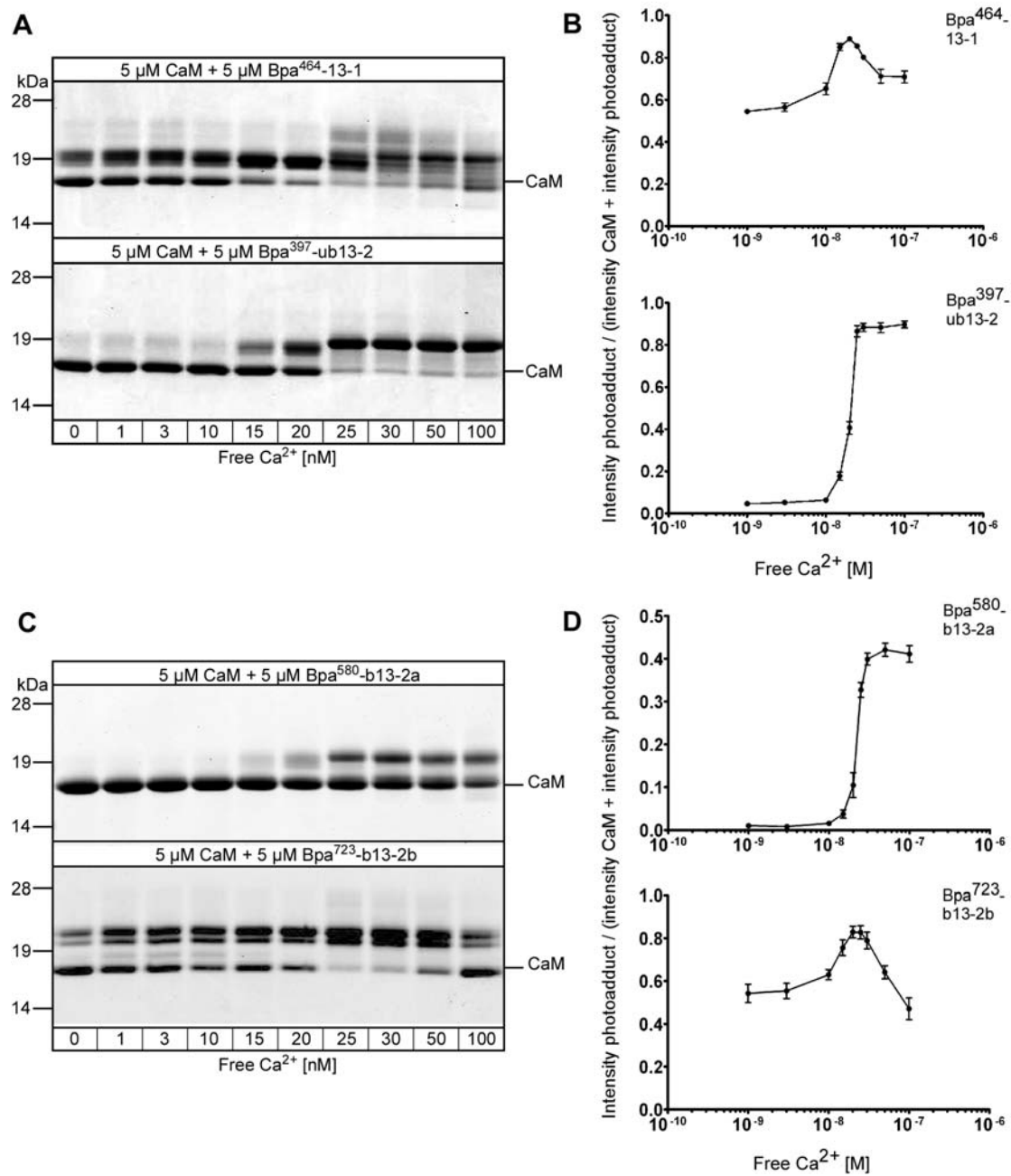
The competition approach was also used to test whether model peptides containing an Arg instead of the hydrophobic anchor residue were devoid of CaM binding, as seen with full-length Munc13-1 and ubMunc13-2 (Junge et al., 2004). For that purpose, R⁴⁶⁴-13-1, R³⁸⁷-ub13-2, R⁵⁸⁰-b13-2a, R⁷²³-b13-2b, R⁷⁸⁷-13-3a, and R⁹⁶²-13-3b were synthesized as binding-deficient homologs and used as competitors in PAL experiments. As anticipated, the ability of R⁴⁶⁴-13-1 and R³⁸⁷-ub13-2 to suppress photoadduct formation of Bpa⁴⁶⁴-13-1 and Bpa³⁸⁷-ub13-2 was considerably lower than that of the wild-type peptides (Fig. 14A, B). This effect of decreased affinity to CaM upon incorporation of Arg in position of the anchor residue held true - at least as a trend - for all binding-deficient homologs (Fig. 14). Taken together, the data from the competition experiments confirmed the essential role of the anchor residue for CaM binding of b13-2a/b and 13-3a/b, as well. This information, together with the knowledge that two CaM binding sites are present in bMunc13-2 and Munc13-3, respectively, was later used for the generation of CaM-insensitive variants of these Munc13 isoforms for future functional studies.

3.1.5. Ca²⁺ sensitivity of photoadduct formation

Due to the established role of the CaM/Munc13 interaction in STP processes in response to elevations in residual Ca²⁺ at the presynapse, it was of interest to establish the Ca²⁺ concentrations required to trigger the CaM/Munc13 association. This question was addressed using the Munc13 peptide model system, and a new PAL-based Ca²⁺ titration assay was established in order to analyze the Ca²⁺ sensitivity of photoadduct formation. The PAL experiments with the Munc13-derived photoprobes were performed in the presence of defined concentrations of free Ca²⁺, achieved by Ca²⁺/chelator buffer systems, followed by gel-electrophoretic analysis of the photoreaction products. After Coomassie-staining, the bands corresponding to CaM and the respective photoadducts were quantified with a near-infrared fluorescence imager on the basis of the Coomassie fluorescence. The quantification data from several independent experiments were pooled and plotted as a titration curve, from which the effective Ca²⁺ concentration range could be deduced.

As pilot experiments employing free Ca²⁺ in the concentration range of 0-10 μ M indicated that photoadduct formation is induced already in the presence of nanomolar concentrations of free Ca²⁺, the PAL-based titration assays were carried out in a concentration range of 0-100 nM free Ca²⁺. Ca²⁺-dependent photoadduct

formation of all Munc13-derived photoprobes was initiated already at free Ca^{2+} concentrations as low as 20 – 30 nM (Fig. 15).



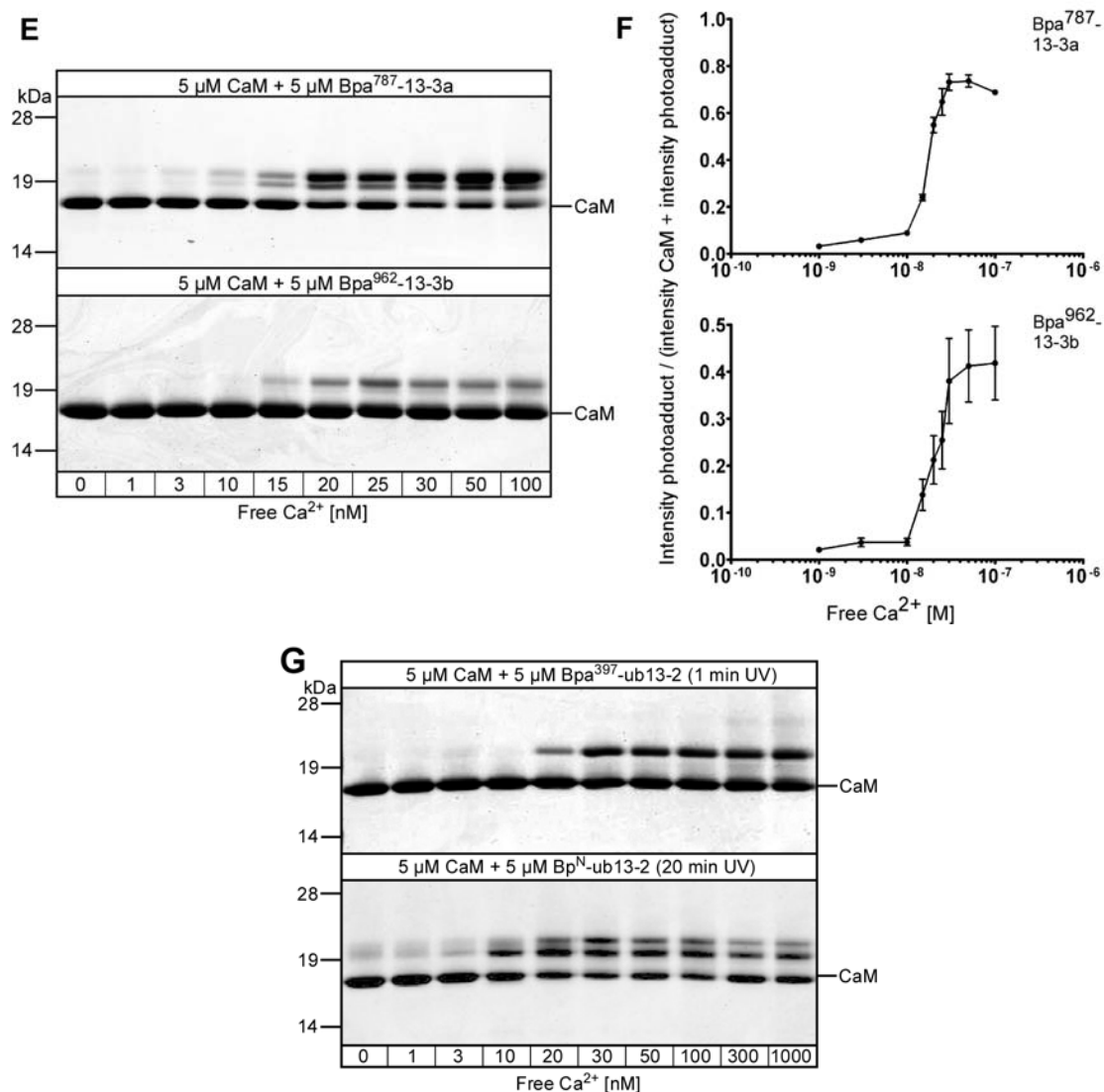


Figure 15. PAL-based Ca²⁺ titration assay. (A, C, E) Representative Coomassie-stained SDS gels showing the photoadduct formation of Bpa⁴⁶⁴-13-1, Bpa³⁸⁷-ub13-2, Bpa⁵⁸⁰-b13-2a, Bpa⁷²³-b13-2b, Bpa⁷⁸⁷-13-3a, and Bpa⁹⁶²-13-3b after 20 min of irradiation in the presence of increasing free Ca²⁺ concentrations indicated below the gel images. For each photoprobe, quantification data from three independent PAL experiments with gels run in duplicate were pooled ($n = 6$) and plotted against the Ca²⁺ concentration to generate the titration curves shown in (B, D, F). To compensate for variations in the total protein load, relative photoadduct yields were calculated by dividing the intensity of the photoadduct band(s) by the summed up intensities of the CaM and photoadduct bands, and depicted in the graphs. Error bars indicate the standard deviation. (G) Coomassie-stained SDS gels showing the Ca²⁺-dependent photoadduct formation of Bpa³⁸⁷-ub13-2 after 1 min of irradiation (upper panel), and of Bp^N-ub13-2 after 20 min of irradiation (lower panel). Free Ca²⁺ concentrations are indicated below the gel images as before.

These results prompted the question whether the observed high Ca^{2+} sensitivities of photoadduct formation were a consequence of the non-equilibrium reaction conditions reached after extensive irradiation. Under these PAL conditions, the interaction partners are irreversibly transferred into a covalent complex and thereby removed from the equilibrium. This effect particularly applied to Bpa⁶⁴⁶-13-1, Bpa³⁸⁷-ub13-2 and Bpa⁷²³-b13-2b, as these photoprobes showed an almost quantitative photoadduct yield at their optimum Ca^{2+} concentrations (Fig. 15A, 15C lower panel). To address this question the duration of irradiation was varied in time course studies in order to identify exposition times which left the majority of CaM unlabeled and could be therefore considered at least as semi-equilibrium conditions. As shown here for Bpa³⁸⁷-ub13-2, the Ca^{2+} concentration sufficient to initiate photoadduct formation remained in the same range even when only 25 % of CaM took part in photoadduct formation after one minute of exposure to UV light (Fig. 15G, upper panel).

Based on these observations it could be ruled out that the duration of irradiation, and thus the photoadduct yield, had a significant influence on the outcome of the titration experiments. Considering the significant influence of the anchor residue on peptide affinity to CaM as outlined above, there was a concern that the high Ca^{2+} sensitivities of photoadduct formation might be an artifact due to incorporation of the photophores in position of the anchor residues. To address this issue, titration experiments were carried out under the same conditions using the N-terminally modified photoprobe Bp^N-ub13-2 (Fig. 15G, lower panel). In agreement with the results obtained for Bpa³⁸⁷-ub13-2, the onset of photoadduct formation of Bp^N-ub13-2 was at the same nanomolar concentrations of free Ca^{2+} , excluding the possibility that the position of the photophore within the peptide had a significant influence on the Ca^{2+} sensitivity of the interaction.

When the densitometric data were plotted as titration curves, it became apparent that Bpa⁴⁶⁴-13-1 and Bpa⁷²³-b13-2b exhibited an atypical Ca^{2+} dependence of photoadduct formation, as photoadduct yields peaked at approximately 30 nM free Ca^{2+} , but dropped with higher Ca^{2+} concentrations (Fig. 15A upper panel, 15C lower panel). This observation was in clear contrast to the Ca^{2+} dependence of photoadduct formation of Bpa³⁸⁷-ub13-2, Bpa⁵⁸⁰-b13-2a, Bpa⁷⁸⁷-13-3a, and Bpa⁹⁶²-13-3b, which was represented by sigmoidal titration curves (Fig. 15B lower panel, 15D upper panel, 15F). Interestingly, Bpa⁴⁶⁴-13-1 and Bpa⁷²³-b13-2b, the photoprobes showing the atypical titration profile, did also show artificial Ca^{2+} -

independent CaM binding and tended to form secondary complexes of 1:2 stoichiometry in the preceding PAL experiments (Fig. 13). However, it remains to be established whether these effects are all artifacts due to the use of model peptides or, at least in part, represent inherent properties of the corresponding full-length proteins Munc13-1 and bMunc13-2.

Taken together, these findings indicated that Ca^{2+} concentrations as low as 20-30 nM are sufficient to trigger binding of the Munc13-derived model peptides to CaM. However, these values should not be considered as absolutely exact as it is experimentally difficult to control nanomolar Ca^{2+} concentrations with chelator buffer systems, mainly due to contaminating Ca^{2+} (Patton et al., 2004). In order to avoid that small changes in total Ca^{2+} due to contamination lead to drastic changes in free Ca^{2+} (Patton et al., 2004) higher chelator concentrations (10 mM EGTA) were used. To estimate the apparent Ca^{2+} contamination, aliquots of the virtually Ca^{2+} -free samples (see lanes "0 nM free Ca^{2+} " in Fig. 3 A) from all titration experiments were pooled and submitted for ICP-MS analysis of total Ca^{2+} concentration (measurement performed by Klaus Simon, University of Göttingen). The level of contaminating Ca^{2+} was found to be in the 200 ppb range, which is equivalent to approximately 5 μM Ca^{2+} . Within the critical buffer range around 30 nM free Ca^{2+} , this low level of contaminating Ca^{2+} would lead to only small increases in free Ca^{2+} (less than 10 %) in the presence of 10 mM EGTA (Patton et al., 2004).

All PAL experiments described above employing bovine brain CaM have been reproduced with recombinant CaM showing no difference in photoadduct yield, complex stoichiometry and Ca^{2+} sensitivity (not shown). Therefore, recombinant CaM was used in PAL for the further structural analysis of the Munc13/CaM interaction.

3.1.6. Stoichiometry of the interaction of CaM with bMunc13-2 and Munc13-3

The presence of two predicted CaM binding sites in bMunc13-2 and Munc13-3 posed the question of what their function and mechanism of interaction with CaM might be. It was possible that the isoform-specific Munc13 peptides are recognized by different interaction sites on CaM and bind simultaneously, that they employ different CaM sites with only one being occupied at a time due to allosteric effects, or that they compete for the same binding pocket in CaM. To address this issue of binding site preference and occupancy in CaM by each pair of Munc13 peptides using PAL, CaM was incubated with an equimolar mixture of each Munc13-derived photoprobe pair. Based on the SDS-PAGE analysis of the resulting photoadducts possibility for simultaneous binding of the two peptides to CaM was excluded as no trimeric photoadduct was observed (Fig. 16).

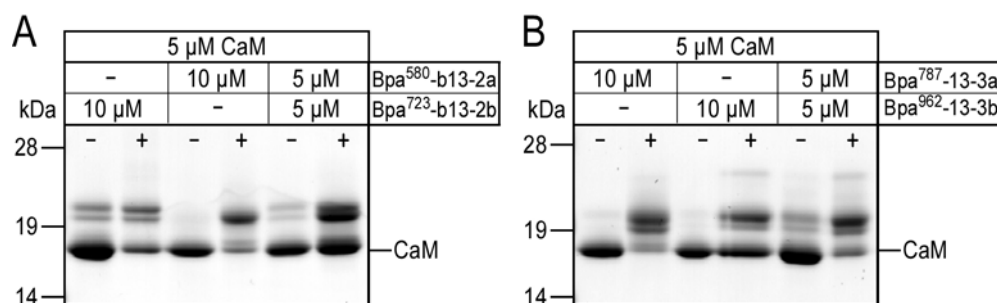


Figure 16. PAL-based heterotrimer formation assay. Comparison of the binding pattern of an equimolar mixture of Bpa⁵⁸⁰-b13-2a and Bpa⁷²³-b13-2b (**A**), or Bpa⁷⁸⁷-13-3a, and Bpa⁹⁶²-13-3b (**B**) with that of an equal total peptide concentration of each photoprobe independently, in the absence (-) and presence (+) of 25 nM free Ca²⁺ concentration.

Rather, the photoadducts in the cross-linking reactions containing both photoprobes appeared like a combination between the two electrophoretic profiles observed in the PAL reactions employing each individual peptide. This outcome could not exclude any of the two remaining possible modes of interaction. Further experiments were designed to address the functional relevance and structural details of each CaM binding site in bMunc13-2 and Munc13-3.

3.1.7. Co-sedimentation assays with GST-fusion proteins of bMunc13-2(366-780) and Munc13-3(711-1063)

The PAL experiments detailed above were very useful for the identification and initial characterization of the novel CaM binding sites in the bMunc13-2 and Munc13-3 isoforms but, as all peptide model systems, offered only limited insight into the behavior of individual domains in a full-length protein context. Thus, they did not resolve questions of significance, function and mechanism of the two CaM binding sites identified in each isoform. To address these questions GST-fusion protein fragments were designed that covered both predicted CaM binding sequences in the two proteins: bMunc13-2(366-780) and Munc13-3(711-1063). These constructs were used in co-sedimentation assays in order to verify their Ca^{2+} -dependent binding to CaM and to examine the stoichiometry of these interactions. For that purpose GST-bMunc13-2(366-780) and GST-Munc13-3(711-1063) were immobilized on glutathione sepharose 4B beads and incubated with bovine brain CaM in the presence or absence of Ca^{2+} . Following several washing steps the beads were boiled in sample buffer and the protein extracts were separated by SDS-PAGE and visualized by colloidal Coomassie staining. Both GST-bMunc13-2(366-780) and GST-Munc13-3(711-1063) interacted with CaM in a strictly Ca^{2+} -dependent manner (Fig. 17), in contrast with the GST-Munc13-1(445-567) control construct which, as anticipated, exhibited also Ca^{2+} -independent CaM binding (Junge et al., 2004).

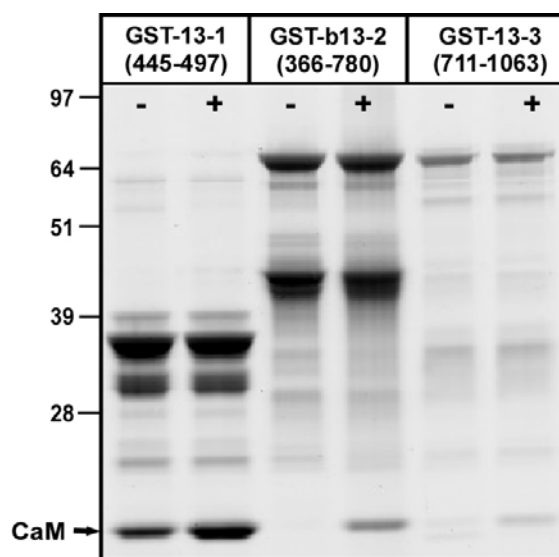


Figure 17. Co-sedimentation assays with GST-fusion proteins of bMunc13-2(366-780) and Munc13-3(711-1063)

Representative Coomassie-stained SDS gel showing CaM binding of the GST-fusion proteins of bMunc13-2(366-780) and Munc13-3(711-1063) in the absence (-) and presence (+) of Ca^{2+} . A GST-fusion construct of the CaM-binding site in Munc13-1 (445-497) was used as positive control. Mass spectrometric analysis of the 40 kDa protein species observed in the co-sedimentation assay of GST-bMunc13-2(366-780) showed that it corresponds to a truncated GST-bMunc13-2 fragment not containing any of the 2 predicted CaM binding sites and was thus not considered for quantification.

Quantification of the Coomassie fluorescence signal from the bands corresponding to the GST-fusion proteins and the CaM co-sedimented under each condition (see section 2.4.2. in Methods) showed a 1:1 stoichiometry for these interactions suggesting that only one of the two predicted CaM binding sites in each isoform have functional relevance at the level of full length proteins.

To determine which of the two CaM binding sequences is responsible for the interaction at the protein level different mutated GST-bMunc13-2(366-780) and GST-Munc13-3(711-1063) constructs were generated (Table 4) and tested for their Ca^{2+} -dependent affinity for CaM. The constructs carried Arg mutations in place of the anchor Phe residues as these mutations were established as non-binding controls at the peptide level in the PAL experiments (see section 3.1.4.).

Table 4. Mutant GST-fusion constructs of bMunc13-2(366-780) and Munc13-3(711-1063) used in the co-sedimentation assays. Respective mutations shown in superscript.

GST- bMunc13-2(366-780)	GST- Munc13-3(711-1063)
GST-bMunc13-2 ^{F580R}	GST-Munc13-3 ^{F787R}
GST-bMunc13-2 ^{F723R}	GST-Munc13-3 ^{F962R}
GST-bMunc13-2 ^{F580R/F723R}	GST-Munc13-3 ^{F787R/F962R}
GST-bMunc13-2 ^{F723R/K724E/K728E/R731E}	

In the case of bMunc13-2, mutation of Phe580 to Arg did not impair CaM co-sedimentation while there was substantial (~70%) reduction of CaM binding by GST-bMunc13-2^{F723R} and GST-bMunc13-2^{F580R/F723R} (Fig. 18A), indicating that only bMunc13-2(719-742) interacts with CaM at the level of the full length protein.

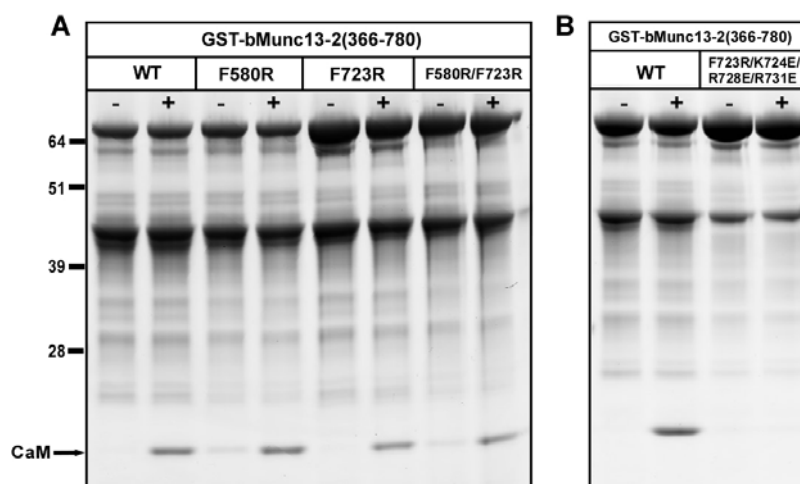


Figure 18. Co-sedimentation assays with GST-bMunc13-2(366-780) and its mutant variants. Coomassie-stained SDS-gels showing the CaM binding of GST-bMunc13-2(366-780) fusion proteins GST-bMunc13-2^{F580R}, GST-bMunc13-2^{F723R} and GST-bMunc13-2^{F580R/F723R} (**A**) and GST-bMunc13-2^{F723R/K724E/K728E/R731E} (**B**) in the absence (-) and presence (+) of Ca²⁺.

The Phe723Arg mutation in bMunc13-2 significantly reduces CaM binding but does not abolish it entirely. However, for the functional establishment and initial electrophysiological characterization of the bMunc13-2/CaM interaction in rescue experiments, a variant with complete loss of binding is required. Therefore, another GST-bMunc13-2(366-780) construct was designed where, together with the Phe723Arg, several amino acids making up the basic side of the amphiphilic helix that defines the CaM binding site were mutated to Glu (GST-bMunc13-2^{F723R/K724E/K728E/R731E}). These mutations led to complete disruption of binding to CaM (Fig. 18B) and were further considered in the design of viral vectors for neuronal infection and electrophysiological rescue experiments.

When the mutations in the GST-Munc13-3(711-1063) were examined for their sensitivity to CaM it became clear that mutation of Phe787 to Arg has no effect on CaM binding, while Phe962 seems to be essential for the interaction, as its mutation to Arg led to complete loss of binding, also seen in the case where both anchoring residues were exchanged with Arg (Fig. 19).

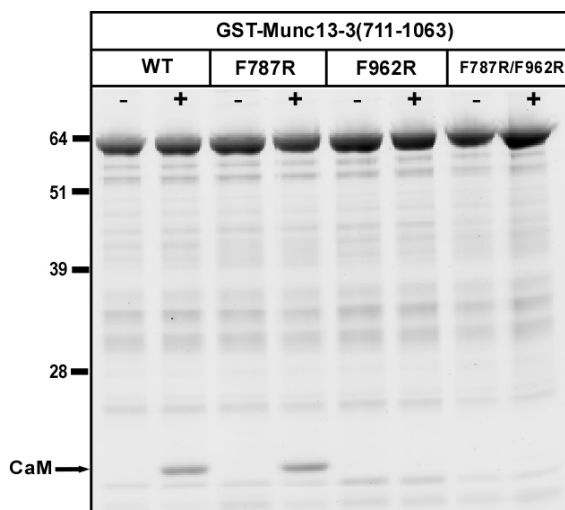


Figure 19. Co-sedimentation assays with GST-Munc13-3(711-1063) and its mutant variants.

Coomassie-stained SDS-gels showing the CaM binding of GST-Munc13-3(711-1063) fusion proteins GST-Munc13-3^{F787R}, GST-Munc13-3^{F962R} and GST-Munc13-3^{F787R/F962R} in the absence (-) and presence (+) of Ca²⁺.

Thus, based on the co-sedimentation experiments it became clear that of the two predicted CaM binding sites in bMunc13-2 and Munc13-3 only the ones adjacent to the C1 domain of the proteins have functional relevance in the context of larger GST-fusion protein fragments. Despite lacking sequence homology with the characterized CaM binding sites in Munc13-1 and ubMunc13-2, these novel CaM interaction sites share the same position in the Munc13 sequence relative to the C1 domain.

3.2. Structural characterization of the Munc13/CaM interaction by PAL

Elucidation of the molecular mechanisms underlying the regulation of Munc13 proteins by CaM is greatly dependent on knowledge of the structure of the Munc13/CaM complexes. Such structural data have been missing so far, partly due to technical difficulties involving the production of recombinant full-length Munc13 proteins. To circumvent this problem, a PAL-based analytical strategy using Munc13-derived photoprobes (see section 3.1.2.) was developed. For the initial establishment of this workflow (see below) the conserved CaM binding sites of the already functionally characterized Munc13 isoforms, Munc13-1 and ubMunc13-2 (Junge et al., 2004) were employed.

3.2.1. Analytical strategy

The covalent complexes of the Munc13 photoprobes and CaM generated by PAL represent a suitable structural model of this interaction and, due to the design of the photoprobes, can convey important information about contact sites between Munc13 and CaM. Bpa⁴⁶⁴-13-1, Bpa³⁸⁷-ub13-2, Bpa⁵⁸⁰-b13-2a, Bpa⁷⁸⁷-13-3a, Bpa⁷²³-b13-2b, and Bpa⁹⁶²-13-3b all carry the photoactivatable Bpa moiety in place of their potential anchor residues (Trp or Phe) and, since this amino acid exchange preserves the hydrophobic, bulky, and aromatic characteristics of the anchor position, PAL should lead to a regioselective photoincorporation within the immediate binding cavity of CaM. Mass spectrometric analysis of the CaM/Munc13 complexes can provide direct identification of the amino acids of CaM involved in cross-link formation and thus in coordinating the anchor residue of the peptides.

To implement this concept experimentally an innovative analytical strategy was established for the mapping of the sites of photoincorporation into CaM (Fig. 20). The workflow is characterized by the introduction of an MS-based dimension of separation by using two variants of recombinant CaM - "light" CaM produced under standard conditions (L-CaM) and "heavy" CaM metabolically labeled with ¹⁵N (H-CaM). Only L-CaM was employed in the PAL reactions with Bpa⁴⁶⁴-13-1, Bpa³⁸⁷-ub13-2, Bpa⁵⁸⁰-b13-2a, Bpa⁷⁸⁷-13-3a, Bpa⁷²³-b13-2b, and Bpa⁹⁶²-13-3b while H-CaM was handled in parallel without being subjected to the reaction with the photoprobes. Following irradiation, labeled L-CaM and H-CaM were combined in an equimolar ratio and the resulting mixture was analyzed by gel electrophoresis and MS, and finally subjected to in-solution digest with trypsin. Because of the experimental design and the inclusion of H-CaM as reference protein, there were three different

theoretical peak patterns expected in the peptide survey spectra obtained by the HPLC/MALDI-MS analysis of the tryptic digests. Most of the signals should appear as characteristic doublet peaks with a fixed intensity ratio (ideally of 1:1) and a mass difference corresponding to the number of nitrogen atoms present in the respective CaM fragment. These would represent CaM sequences unaffected by the PAL reaction. The second signal pattern should be identical to the doublet peaks described above, with the exception that the "light" peak has an appreciably reduced intensity compared to its "heavy" counterpart. These would represent CaM sequences directly involved in photoadduct formation. The third species should be unpaired peaks with a natural isotope distribution. These masses are not compatible with tryptic CaM peptides and therefore represent fragments of the free photoprobe (which can be sorted out easily) or cross-linked peptides, consisting of the "down-regulated" CaM fragment and the Bpa-containing fragment of the photoprobe. As off-line LC/MALDI-MS circumvents the time limitations of on-line LC/MS couplings, these cross-linked peptides could be subjected to extensive mass spectrometric sequencing or even to on-target manipulations such as CNBr cleavage.

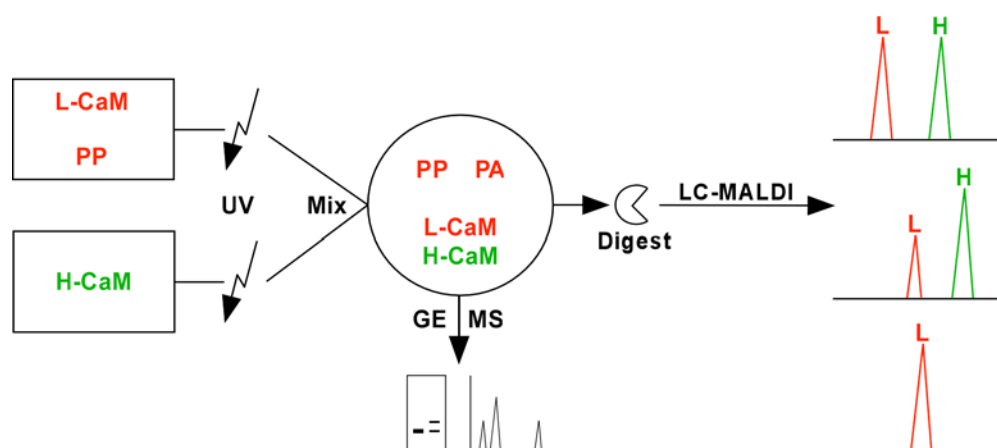


Figure 20. Analytical strategy for mapping the sites of photoincorporation into CaM. The experimental design is based on the use of normal "light" CaM (L-CaM) as binding partner for the photoprobe (PP) and ^{15}N -labeled "heavy" CaM (H-CaM) as reference protein, both of which are combined after irradiation. The resulting mixture (containing L-CaM, H-CaM, the photoadduct (PA), and unreacted PP) was analyzed by gel electrophoresis (GE) and MS, and finally subjected to in-solution digest followed by HPLC/MALDI-MS analysis. Three defined peak patterns were expected in the peptide survey spectra: (i) CaM fragments not involved in photoadduct formation appear as "light" (L) and "heavy" (H) doublets of similar abundance, (ii) L-CaM fragments involved in photoadduct formation are less abundant compared to their H-CaM counterparts, and (iii) unpaired "light" signals represent candidate cross-linked peptides (see text for details).

3.2.2. Detection of intact CaM complexes

Due to the complexity of the analytical strategy described above, only the photoadducts of Munc13-1 and ubmunc13-2 were initially selected for structural analysis. As a first step in this analytical workflow CaM was incubated at physiological concentrations (5 μ M) with equimolar amounts of Bpa⁴⁶⁴-13-1 or Bpa³⁸⁷-ub13-2 in the presence of 30 nM free Ca²⁺, a concentration deduced as optimal from the Ca²⁺ titration experiments (Fig. 20), and the reaction was subjected to UV light for PAL. Using SDS-PAGE, a Ca²⁺-dependent complex of CaM with the photoprobe was detected as a band of an apparent molecular weight of 20 kDa (Fig. 21 insets). The high photoadduct yields of at least 50 % were in agreement with the Ca²⁺ titration experiments using bovine brain CaM described earlier (See Fig. 15). MS was used to show that the homogenous gel bands corresponding to fractions of unreacted CaM indeed contained a mixture of L-CaM and H-CaM, differing by 177 mass units. While the signals for L-CaM and H-CaM were of similar abundance when PAL was performed in the absence of Ca²⁺, the intensity of the signal for L-CaM is considerably reduced upon PAL in the presence of Ca²⁺ (Fig. 21). The corresponding photoadducts of L-CaM were detected at their expected *m/z* values, though not with the expected abundance, which probably reflects selective losses of the more hydrophobic complexes during ZipTip desalting prior to MS.

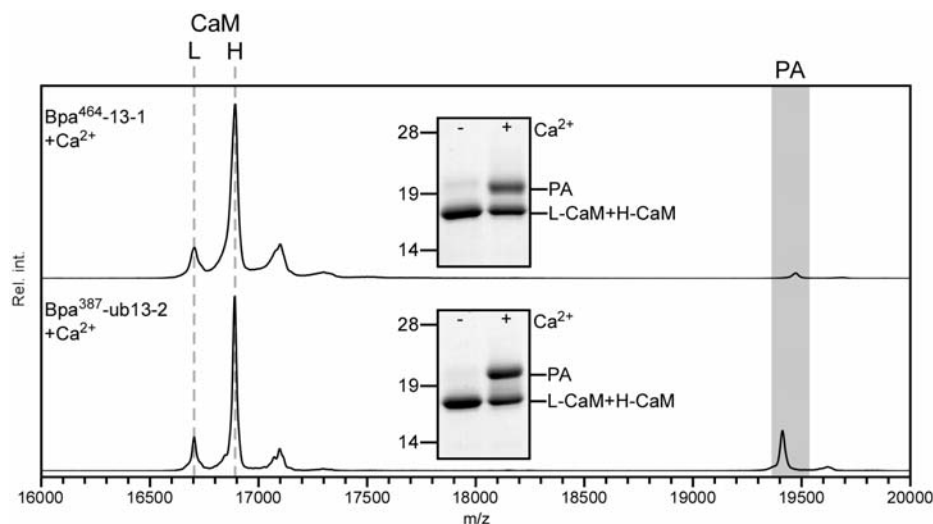


Figure 21. Detection of intact photoadducts by SDS-PAGE and MS. In the Coomassie-stained SDS gels (insets), the CaM photoadducts (PA) of Bpa⁴⁶⁴-13-1 (upper panel) and Bpa³⁸⁷-ub13-2 (lower panel) appeared Ca²⁺-dependently at an apparent molecular mass of 20 kDa. Due to experimental design (see Fig. 20), the CaM band contained L-CaM and H-CaM, which could not be distinguished by SDS-PAGE (mass difference 177 Da). This was possible by MS as shown in the mass spectra of the same fractions. Upon PAL in the presence of Ca²⁺, the signals for L-CaM dropped from equiabundant levels (not shown) to drastically reduced intensities compared to those of H-CaM. This was due to the involvement of L-CaM in the formation of photoadducts, which were detected at their expected *m/z* range (underlined in grey). Due to the use of sinapinic acid as matrix, all mass signals showed an adduct peak with a mass increment of 206 mass units.

3.2.3. Identification of cross-linked peptides

As follows, the detailed detection and characterization of the cross-linked peptides is exemplified with the data acquired for the Munc13-1/CaM complex for the sake of conciseness. According to the analytical strategy (Fig. 20), the photoreaction mixture containing L-CaM, H-CaM, the photoadduct, and unreacted photoprobe was next subjected to a tryptic digest followed by HPLC/MALDI-MS analysis. In the peptide survey spectra obtained, most tryptic CaM fragments were detected as equiabundant doublet signals, corresponding to a CaM sequence coverage of at least 93 % (Fig. 22).

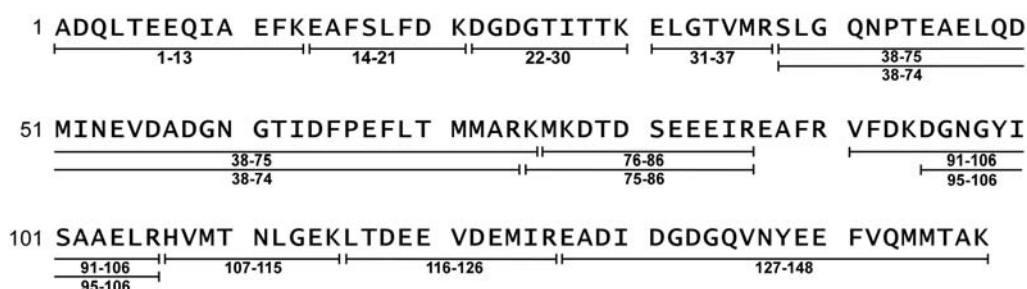


Figure 22. Peptide mapping of recombinant CaM by mass spectrometry. Detected tryptic peptides of CaM are underlined. The corresponding ranges of amino acids are given below the sequence.

These doublet signals consisted of a "light" peak derived from L-CaM involved in PAL and an equiabundant "heavy" peak derived from H-CaM included as reference protein, as shown as an example for CaM(78-86) (Fig. 23A). Consistent with the peptide sequence DTDSEEEIR containing 12 nitrogen atoms, the observed mass increment between both monoisotopic peaks was 11.98 mass units (Fig. 23A).

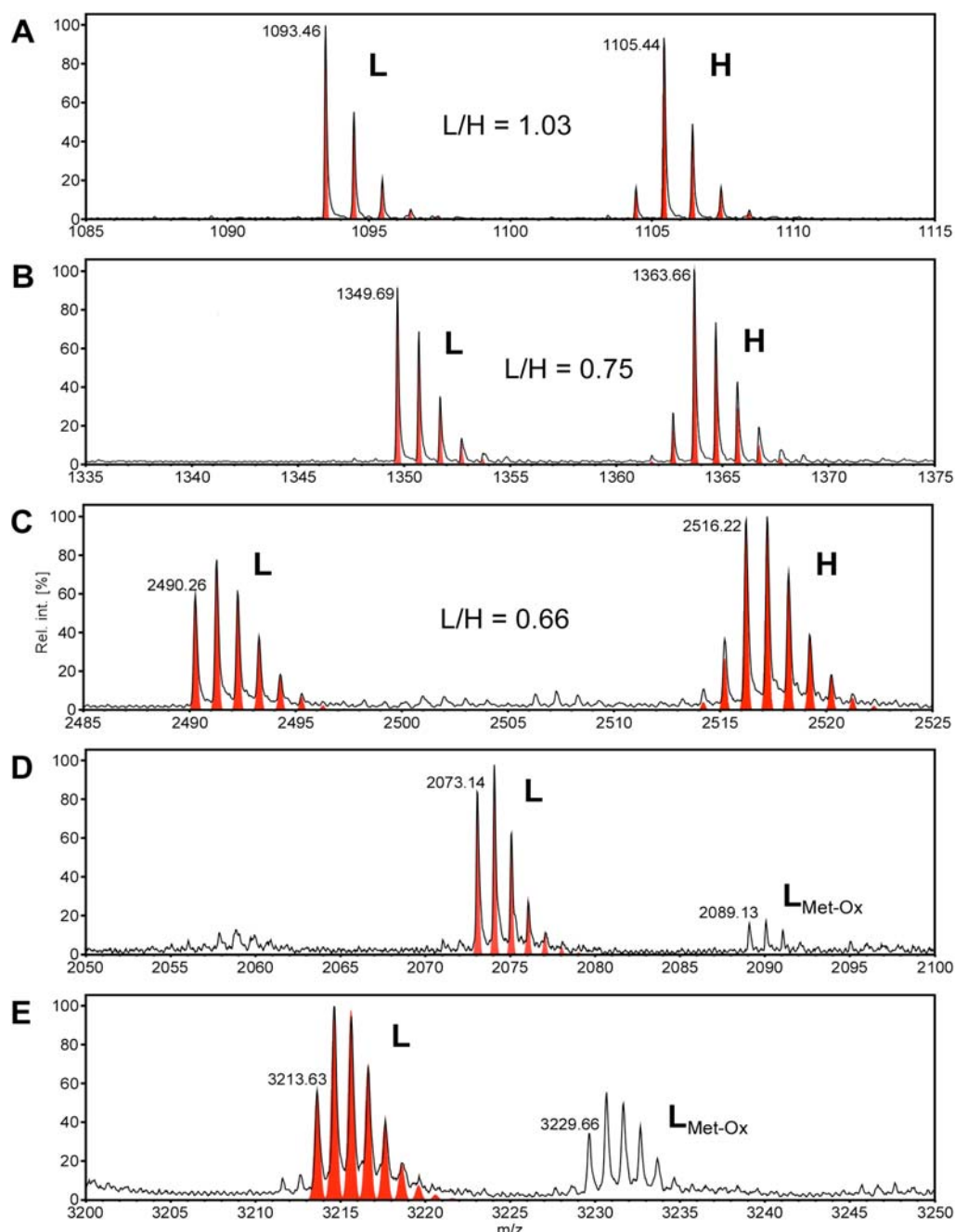


Figure 23. Identification of cross-linked peptides by HPLC/MALDI-MS. Selected peptide survey spectra showing characteristic peak patterns for a CaM fragment not involved in photoadduct formation (CaM(78-86), $[M+H]^+_{\text{calc,mono}} = 1093.46/1105.40$) (A), CaM fragments involved in photoadduct formation (CaM(116-126), $[M+H]^+_{\text{calc,mono}} = 1349.63/1363.62$) (B) and (CaM(127-148), $[M+H]^+_{\text{calc,mono}} = 2490.08/2516.00$) (C), and the cross-linked peptides (Bpa⁴⁶⁴-13-1(5-9)-CaM(116-126), $[M+H]^+_{\text{calc,mono}} = 2073.00$) and (Bpa⁴⁶⁴-13-1(5-9)-CaM(127-148), $[M+H]^+_{\text{calc,mono}} = 3213.45$) (E). For the CaM fragments, the light-to-heavy ratios (L/H) were calculated on the basis of the peak areas of the entire isotope clusters. Isotope distributions of the simulated peaks (shown as filled red signals) were calculated with the MS-Isotope tool using the resolution of the corresponding observed peaks. For simulating the isotope distributions of H-CaM-related peaks, incorporation of ¹⁵N was set to 98.7 %. In panels D and E, the signals at m/z 2089.13 and 3229.66 did not display the typical isotope distribution of an H-CaM fragment and were assigned as the Met sulfoxide variant of the respective cross-linked peptide (monoisotopic mass shift +16.00 mass units).

The atypical isotope distribution observed in peaks corresponding to H-CaM tryptic peptides (see "heavy" peaks in the mass spectra of Fig. 23) is due to the incomplete incorporation of ^{15}N into CaM (98.7 %, as determined on the basis of simulated isotope distributions). This incomplete isotope incorporation turned out to be an advantage, as a signal could be readily assigned as "light" or "heavy" just on the basis of its characteristic isotope distribution without the need to know the mass distance to its respective counterpart. When the mass spectra were screened for doublet signals with reduced intensity of the "light" peak compared to its "heavy" counterpart, such a peak pattern was observed for CaM(116-126) (ratio light/heavy = 0.75; Fig. 23 B) and CaM(127-148) (ratio light/heavy = 0.66; Fig. 23 C), indicating that Bpa⁴⁶⁴-13-1 labeled CaM in its C-terminal domain. The corresponding cross-linked peptides consisting of one of the "down-regulated" CaM fragments CaM(116-126) or CaM(127-148) and the Bpa-containing photoprobe fragment Bpa⁴⁶⁴-13-1 (5-9) were detected as unpaired peaks with a natural isotope distribution at m/z 2073.14 ($[\text{M}+\text{H}]^+_{\text{calc,mono}} = 2073.00$; Fig. 23 D) and m/z 3213.63 ($[\text{M}+\text{H}]^+_{\text{calc,mono}} = 3213.45$; Fig. 23 E), respectively. Similarly, characteristic peak patterns with reduced intensity of the "light" peak for CaM(116-126) (ratio light/heavy = 0.88) and CaM(127-148) (ratio light/heavy = 0.61) were found when Bpa³⁸⁷-ub13-2 was used for PAL. The corresponding cross-linked peptides modified by Bpa³⁸⁷-ub13-2(5-9) were detected at m/z 2130.18 ($[\text{M}+\text{H}]^+_{\text{calc,mono}} = 2130.00$) and m/z 3270.68 ($[\text{M}+\text{H}]^+_{\text{calc,mono}} = 3270.45$). Based on the observation that the "light" peak of CaM(127-148) was always more markedly reduced in intensity than that of CaM(116-126), the outermost C-terminus of CaM was considered as the major, and the adjacent sequence stretch as the minor contact site of Bpa⁴⁶⁴-13-1, Bpa³⁸⁷-ub13-2. Thus, the workflow allows for a semi-quantitative estimation of binding-site usage.

Although not elaborated further here, corresponding analysis of the CaM photoadducts with the bMunc13-2- and Munc13-3-derived photoprobes showed down-regulation of the tryptic CaM peptides, CaM(116-126) and CaM(127-148), as well (data not shown). This finding was considered as sufficient evidence that all Munc13 isoforms share the same binding site in the C-terminal domain of CaM. Therefore, the focus on Munc13-1 and ubMunc13-2 was maintained for the further characterization of the cross-linked peptides. As above, the strategy is exemplified on the basis of data on the Munc13-1/CaM complex.

3.2.4. Identification of contact sites between Munc13 and CaM by PAL

Following the detection of cross-linked peptides these were further analyzed by MS/MS sequencing in order to identify the amino acids in CaM labeled by the Munc13-derived photoprobes. In the case of Bpa⁴⁶⁴-13-1 the smaller cross-linked peptide Bpa⁴⁶⁴-13-1(5-9)-CaM(116-126) yielded a conclusive fragment ion series, which was best compatible with a linkage of Bpa⁴⁶⁴-13-1(5-9) to the side chain of Met124 (Fig. 24A).

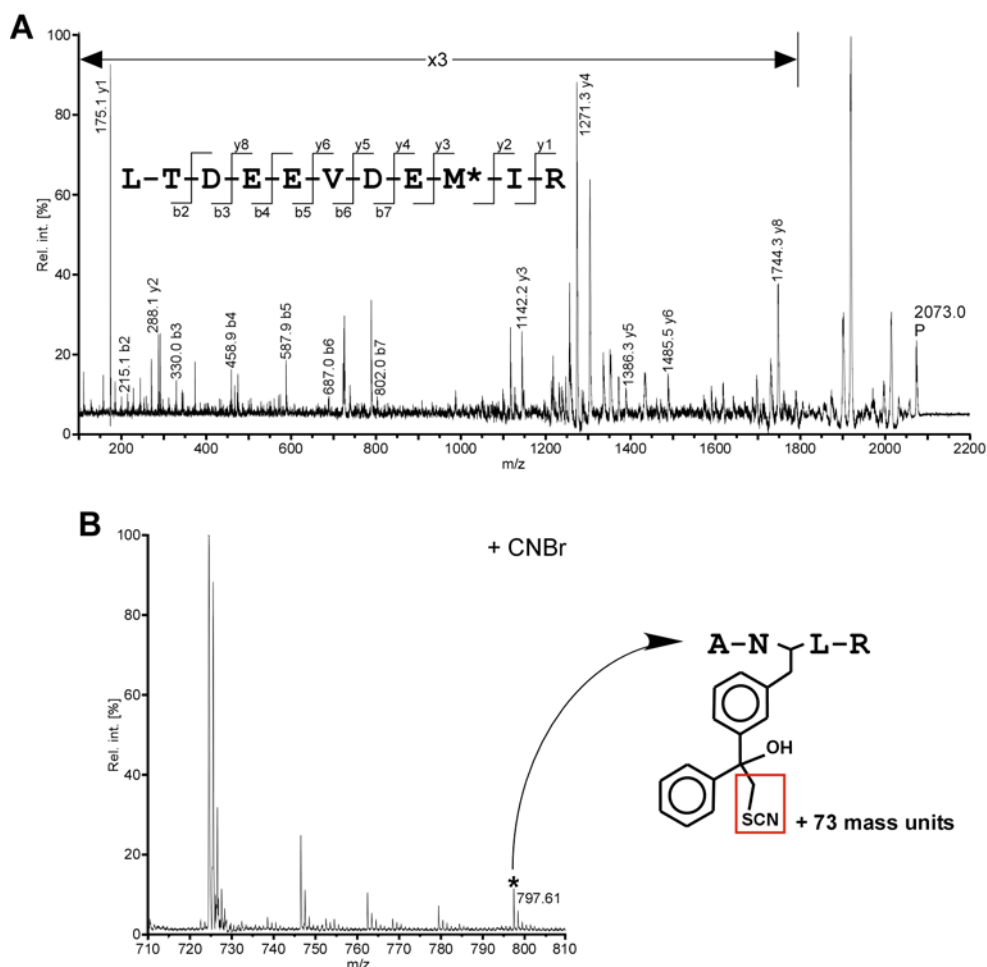


Figure 24. Characterization of the photoadducts at the amino acid level. (A) Fragment ion mass spectrum of the cross-linked peptide Bpa⁴⁶⁴-13-1(5-9)-CaM(116-126). P denotes the precursor ion ($[M+H]^+_{\text{calc, mono}} = 2073.00$) and only b- and y-ions are labeled for the sake of clarity. While the N-terminal b-ion series excluded the amino acid stretch LTDEEVD as the site of modification, the y-ion series provided positive evidence that the photoprobe fragment Bpa⁴⁶⁴-13-1(5-9) is linked through the side chain of Met-124 of CaM (marked by an asterisk). Note that the high abundance of the y8 and particularly of the y4 ion is in agreement with facile amide bond cleavages C-terminal of Asp. (B) Verification of Met124 cross-linking by on-target CNBr cleavage. CNBr treatment of the cross-linked peptide species Bpa⁴⁶⁴-13-1(5-9)-CaM(116-126) gave rise to a newly occurring signal representing the methylthiocyanate derivative of Bpa⁷-13-1(5-9) (m/z 797.56, marked by an asterisk). The structure indicates the mass increment of 73 mass units. See Fig. 10 for details on the CNBr cleavage procedure.

In contrast, the fragment ion mass spectrum of the rather large cross-linked peptide Bpa⁷-13-1(5-9)-CaM(127-148) ($[M+H]^+_{\text{calc,mono}} = 3213.45$) did not contain instructive sequence information, but the few assignable signals indicated labeling of Met present in position 144 and 145. To test this further, the cross-link-containing sample spots were subjected to on-target CNBr cleavage. According to Kage et al. (Fig10; Kage et al., 1996), the bond between the γ -carbon and sulfur in the Met side chain is cleaved upon treatment with CNBr, which leads to the formation of a methylthiocyanate derivative and thereby release of the benzophenone-containing photoprobe fragment. This release happens only when photoincorporation has taken place into the terminal methyl group of a Met side chain and is indicated by the appearance of a specific signal at an m/z value 73 mass units higher than that of the unmodified photoprobe fragment (Kage et al., 1996). As a proof of principle, this method was first applied to the cross-linked peptide Bpa⁴⁶⁴-13-1(5-9)-CaM(116-126) and indeed detected the methylthiocyanate derivative of Bpa⁴⁶⁴(5-9) (Fig. 24B). This result clearly demonstrated labeling of the side chain of Met-124 and was in full agreement with the MS/MS data (Fig. 24A).

Next, the larger cross-linked peptide Bpa⁴⁶⁴-13-1(5-9)-CaM(127-148) was subjected to on-target CNBr cleavage, leading to the complete disappearance of the signals at m/z 3213.63 and m/z 3229.66 corresponding to Bpa⁴⁶⁴-13-1(5-9)-CaM(127-148) and its sulfoxide variant, respectively, whereas the signal at m/z 724.34 was not affected (Fig. 25).

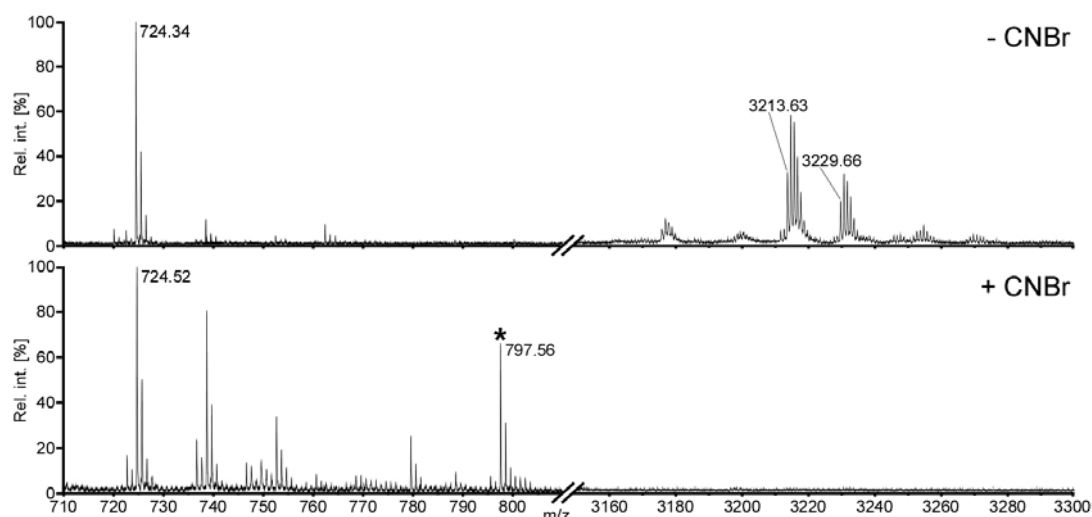


Figure 25. On-target CNBr cleavage of the cross-linked peptide Bpa⁴⁶⁴-13-1(5-9)-CaM(127-148). The mass spectra were recorded from the same cross-link-containing sample spot prior to (- CNBr, upper panel) and after (+ CNBr, lower panel) on-target CNBr cleavage. The m/z range 810 to 3150 was excluded from the x-axes to enable an appropriate display of the relevant parts of the mass spectra. Prior to cleavage, Bpa⁴⁶⁴-13-1(5-9)-CaM(127-148) (m/z 3213.63) and its Met sulfoxide variant (m/z 3229.66) were present together with the co-eluting free photoprobe fragment Bpa⁴⁶⁴-13-1(5-9) (m/z 724.34). After cleavage, the cross-linked peptide species disappeared completely, giving rise to the methylthiocyanate derivative of Bpa⁴⁶⁴-13-1(5-9) (m/z 797.56, marked by an asterisk).

Interestingly, MS/MS sequencing revealed that this signal corresponded to Bpa⁴⁶⁴-13-1 (5-9) (Fig. 26), indicating that the free photoprobe fragment Bpa⁴⁶⁴-13-1 (5-9) co-eluted with the cross-linked peptide Bpa⁴⁶⁴-13-1 (5-9)- CaM(127-148).

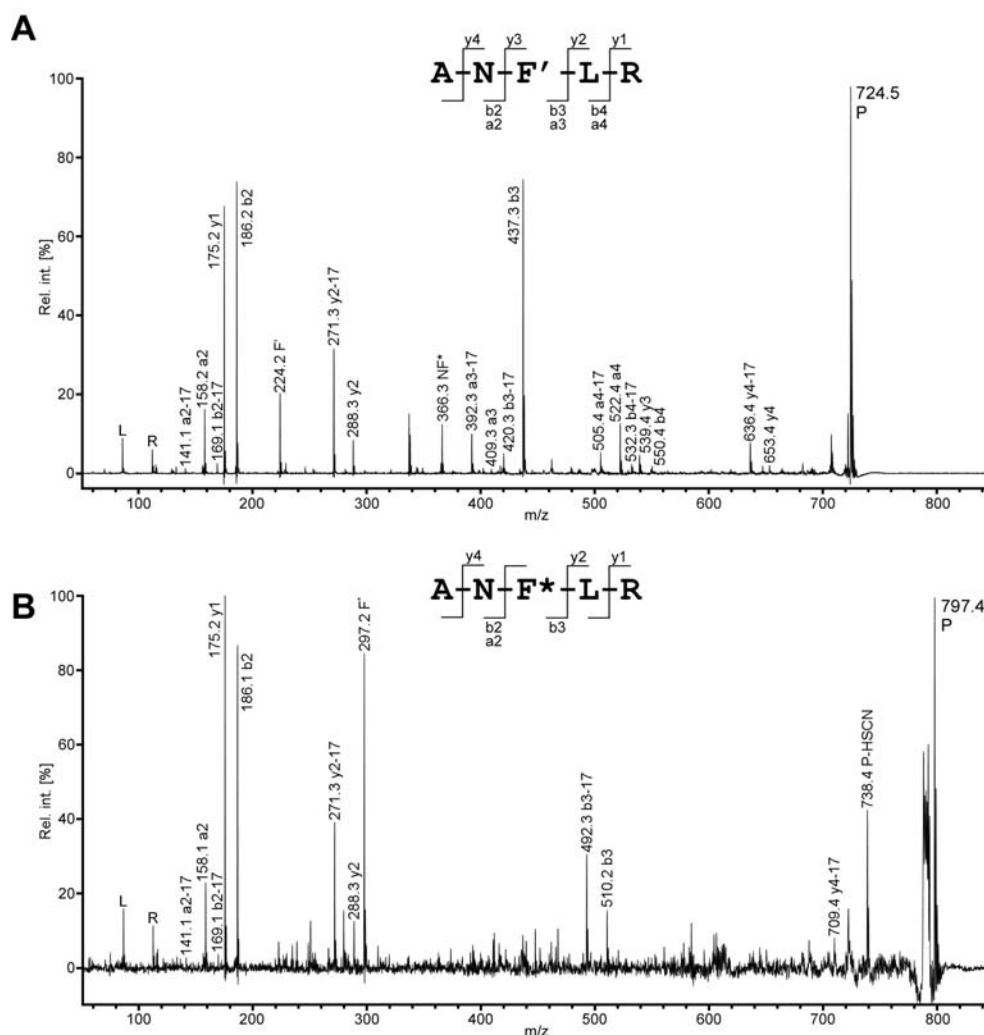


Figure 26. Fragment ion mass spectra of the photoprobe fragment Bpa⁴⁶⁴-13-1(5-9) (A) and its methylthiocyanate derivative (B). P denotes the precursor ions. The identities of both peptides were confirmed on the basis of the conclusive fragment ion series obtained. In the amino acid sequences, F' indicates p-Benzoyl-Phe (Bpa) and F* its methylthiocyanate derivative. Note the presence of the corresponding immonium ions at m/z 224.19 (indicating F' in A) and m/z 297.19 (indicating F* in B). In mass spectrum B, the signal at m/z 738.39 most likely corresponds to the loss of thiocyanic acid from the precursor.

As the presence of the free photoprobe fragment was not a general feature of cross-link-containing fractions, its release from the cross-linked peptide during mass spectrometric analysis was considered rather unlikely, an assumption further supported by the fact that benzophenones almost exclusively form stable C-C bonds (Dorman and Prestwich, 1994). More importantly, a newly appearing signal at m/z 797.56 was detected (Fig. 25) and confirmed by MS/MS sequencing to correspond to the methylthiocyanate derivative of Bpa⁴⁶⁴-13-1(5-9) (Fig. 26). Thereby, labeling of CaM at Met-144/145 was demonstrated. Labeling of CaM at Met-124 and Met-144/145 was also confirmed for Bpa³⁸⁷-ub13-2.

Thus, in complement with MS/MS sequencing, the on-target CNBr cleavage emerged as a useful method to test for photoincorporation at Met residues, when the cross-linked peptides were too large for a conclusive MS-based sequence analysis. An alternative approach to confront the large size of the photoadducts - the use of endoproteinase AspN in combination with trypsin for shortening the cross-linked peptides – was not practical in this study for several reasons. CaM appeared to be hardly accessible for AspN. Together with the unusual abundance of potential AspN cleavage sites (17 Asp and 21 Glu residues), this led to a variety of incomplete digestion products. As a consequence, the cross-link was distributed into several peptides, which often complicated or even prevented the identification of cross-linked peptides. Moreover, incomplete cleavages often hampered the recognition of the characteristic peak patterns, which in our experimental design indicated the involvement of a particular CaM fragment in cross-link formation (see above).

In summary, the structural characterization of the Munc13/CaM interaction by PAL revealed that Munc13 binding takes place in the C-terminal domain of CaM where the coordination of the hydrophobic anchor residue in Munc13 is achieved by key Met residues. The PAL methodology, however, was limited in providing structural information concerning the global orientation of the peptides in the complex and the overall CaM fold. These issues were further investigated in the framework of two collaborative studies. The question of peptide orientation was addressed by chemical cross-linking experiments involving the short Munc13-1 and ubMunc13-2 peptides and CaM (as described in the discussion). For the elucidation of the overall structure of the Munc13/CaM complex, a combination of PAL and NMR experiments using C-terminally elongated Munc13-derived peptides was employed (see below).

3.3. PAL and structural characterization of the CaM interaction of C-terminally elongated Munc13-1- and ubMunc13-2-derived peptides

In the timeline of this study, a collaboration was initiated with Fernando Rodríguez-Castañeda and colleagues from the Department for NMR-Based Structural Biology at the Max Planck Institute for Biophysical Chemistry (MPI-BC) (Göttingen) who are investigating structural aspects of the Munc13/CaM interaction by NMR methods. They used a 34 amino acid Munc13-1-derived peptide (further C-terminally elongated compared to the established CaM binding site; Junge et al., 2004) in NMR titration experiments with CaM to address the structural dynamics of binding between Munc13-1 and CaM. These experiments provided evidence that the Munc13-1 peptide may bind to CaM through two independent domains – a “classical” interaction involving the anchor Trp464 residue and the hydrophobic binding pocket in the C-terminal lobe of CaM (as seen in the PAL-based structural analysis described in section 3.2.), as well as a “novel” contact of Leu488 and Trp489 (positions 25/26 relative to the anchor Trp residue in position 464) with the side chains of Met36, Val55 and Ile 52 in the N-terminus of CaM ((Rodríguez-Castaneda, 2007); Rodríguez-Castañeda, et al., in preparation).

RAKAN W LRAFNKVRMQLQEAR	13-1 ⁴⁵⁹⁻⁴⁷⁹
RAKAN W LRAFNKVRMQLQEARGE GEMSKSL W FKG	13-1 ⁴⁵⁹⁻⁴⁹²
QARAH W FRAVTKVRLQLQEIS	ub13-2 ³⁸²⁻⁴⁰²
QARAH W FRAVTKVRLQLQEISDDGDPSLPQ W LPE	ub13-2 ³⁸²⁻⁴¹⁵

Figure 27. Amino acid sequences of the model peptides covering the extended CaM binding sites in Munc13-1 and ubMunc13-2. Trp residues shown in red were substituted with p-Benzoyl-Phe (Bpa) individually or simultaneously to generate photoreactive peptides for PAL experiments. The sequences of the peptides used in the initial structural characterization of the Munc13/CaM complexes (see section 3.2.) are shown in parallel.

To support this observation biochemically using the PAL methodology, Trp464, Trp489, or both were substituted with Bpa in Munc13-1(459-492)-derived peptide employed in the NMR study (Fig .27) to generate mono-functional (Bpa⁴⁶⁴-13-1⁴⁵⁹⁻⁴⁹², Bpa⁴⁸⁹-13-1⁴⁵⁹⁻⁴⁹²) and bi-functional (Bpa^{464,489}-13-1⁴⁵⁹⁻⁴⁹²) photoprobes. As seen with the short photoprobes carrying Bpa in place of Trp464 (Bpa⁴⁶⁴-13-1, Fig. 13), Bpa⁴⁶⁴-13-1⁴⁵⁹⁻⁴⁹² interacted with CaM specifically, with a 1:1 stoichiometry, and in a largely Ca²⁺-dependent manner, with some observable Ca²⁺-independent photoadduct formation (Fig. 28). Interestingly, a specific and Ca²⁺-dependent

interaction with CaM was also observed for Bpa⁴⁸⁹-13-1⁴⁵⁹⁻⁴⁹² (Fig. 28), validating the presence of the novel CaM binding element in Munc13-1 indicated by the NMR results. The somewhat lower photoadduct yield observed compared to Bpa⁴⁶⁴-13-1⁴⁵⁹⁻⁴⁹² implied that the binding of the C-terminal of Munc13-1⁴⁵⁹⁻⁴⁹² is less tight than that of its N-terminus.

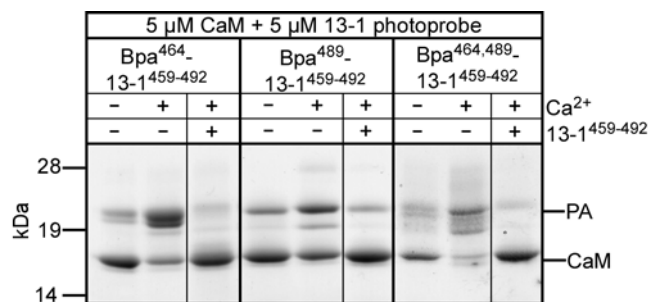


Figure 28. Photoaffinity labeling of CaM with Munc13-1(458-492)-derived photoprobes. Coomassie-stained SDS gels showing the photoadduct (PA) formation of Bpa⁴⁶⁴-13-1⁴⁵⁹⁻⁴⁹², Bpa⁴⁸⁹-13-1⁴⁵⁹⁻⁴⁹² and Bpa^{464,489}-13-1⁴⁵⁹⁻⁴⁹² in the absence and presence of excess Ca²⁺ (1 mM). Photoprobe binding was considered specific as PA formation is suppressed in presence of ten-fold molar excess of wild type competitor. Like in Fig. 13 mass spectrometry (not shown here) revealed that only unlabeled CaM and 1:1 photoadduct species were present even in the samples showing photoadduct double bands, which were most likely due to conformational effects on electrophoretic mobility. The 1:2 photoadduct species detected to some extent at an apparent molecular mass of 28 kDa were probably related to the artificially high Ca²⁺ concentration of 1 mM, as these artifacts were not observed under physiological Ca²⁺ concentrations (see Fig 29).

PAL-based Ca²⁺ titration assays revealed that CaM becomes sensitive to both Bpa⁴⁶⁴-13-1⁴⁵⁹⁻⁴⁹² and Bpa⁴⁸⁹-13-1⁴⁵⁹⁻⁴⁹² at free Ca²⁺ concentrations in the lower nanomolar range (Fig. 29), reproducing the effective Ca²⁺ concentrations observed for the CaM interactions of the shorter Munc13 derived CaM binding peptides (Fig. 14). Further structural characterization of the photoadducts of the extended Munc13-derived photoprobes was therefore performed on PAL reactions that had been carried out in the presence of 50 nM free Ca²⁺.

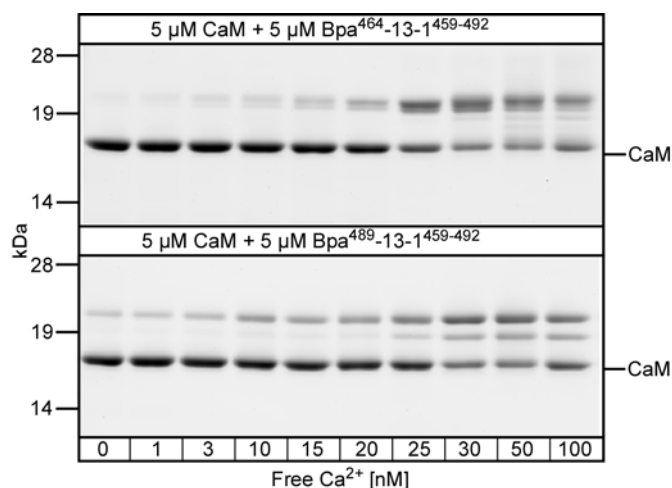


Figure 29. PAL-based Ca²⁺ titration assay. Representative Coomassie-stained SDS gels showing photoadduct formation of Bpa⁴⁶⁴-13-1⁴⁵⁹⁻⁴⁹² and Bpa⁴⁸⁹-13-1⁴⁵⁹⁻⁴⁹² after 20 min of irradiation in the presence of increasing free Ca²⁺ concentrations as indicated below the gel images.

The covalent complexes formed by CaM and Bpa⁴⁶⁴-13-1⁴⁵⁹⁻⁴⁹² and Bpa^{464,489}-13-1⁴⁵⁹⁻⁴⁹² were subjected to the newly established workflow for the structural characterization of CaM photoadducts described in section 3.2. in order to confirm that Trp464 of Munc13-1 behaves consistently in the shorter (13-1⁴⁵⁹⁻⁴⁷⁹) and longer (13-1⁴⁵⁹⁻⁴⁹²) Munc13-1-derived peptides. Indeed, mass spectrometric analysis showed that Trp464 reproducibly contacts Met124 and Met144 of CaM during binding, irrespective of the length of peptide (cross-link identification, MS/MS sequencing and CNBr digest results identical to Bpa⁴⁶⁴-13-1, therefore omitted here).

To identify the contact sites of Trp489 of Munc13-1⁴⁵⁹⁻⁴⁹² in CaM, the photoadducts of CaM with the bi-functional photoprobe Bpa^{464,489}-13-1⁴⁵⁹⁻⁴⁹² were characterized structurally as above. Trypsin digestion followed by HPLC/MALDI-TOF-MS revealed that the site of photoincorporation of Bpa489 into CaM is located within the tryptic peptide CaM³⁸⁻⁷⁴. As the corresponding cross-linked peptide consisting of the tryptic fragments CaM³⁸⁻⁷⁴ and Bpa^{464,489}-13-1⁴⁸⁷⁻⁴⁹² has a mass of 4.9 kDa and is therefore not available for mass spectrometric sequencing, it was isolated by HPLC and truncated further by proteolysis with the endoproteinase AspN. By this approach, the site of photoincorporation was narrowed down to CaM⁵⁰⁻⁵⁷, and MS/MS sequencing of the cross-linked peptide revealed a linkage between Bpa489 of the photoprobe and Met51 of CaM (Fig. 30). This finding was also confirmed for the mono-functional photoprobe Bpa⁴⁸⁹-13-1⁴⁵⁹⁻⁴⁹² (data not shown). Thus, in the bound

state, Trp489 of Munc13-1⁴⁵⁹⁻⁴⁹² contacts Met51 of CaM, a residue that is also part of the hydrophobic cleft of the N-terminal CaM domain as are the residues that showed chemical shift perturbation in the NMR experiments - Met 36, Val 55 and Ile52.

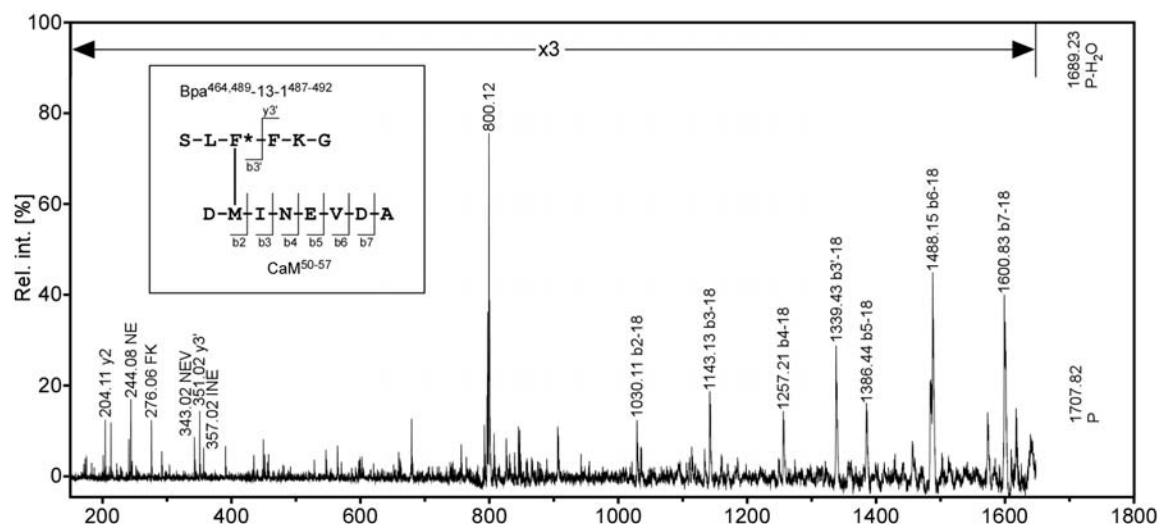


Figure 30. Characterization of the photoadduct of Bpa^{464,489}-13-1⁴⁸⁷⁻⁴⁹² and CaM at the amino acid level. Fragment ion mass spectrum of the cross-linked peptide consisting of CaM⁵⁰⁻⁵⁷ and Bpa^{464,489}-13-1⁴⁸⁷⁻⁴⁹². P denotes the precursor ion ($[M+H]^+_{\text{calc}} = 1707.79$) and primed ion designators indicate fragmentation in the photoprobe chain. After an immediate loss of water (P-H₂O), a conclusive N-terminal b-ion series is formed, demonstrating that the sequence CaM⁵²⁻⁵⁷ (INEVDA) was not modified. As modification of Asp50 can be ruled out on the basis of the AspN cleavage specificity, only Met51 remains as site of photoincorporation (see inset, F* encodes Bpa). The dominant signal at $m/z = 800.12$ is most likely related to Bpa^{464,489}-13-1⁴⁸⁷⁻⁴⁹² and may be explained by concurrent release and radicalic rearrangement of the benzophenone moiety under post-source decay conditions (Leite et al., 2003).

Comparison of the sequences of Munc13-1 and ubMunc13-2 in the region of their CaM recognition motifs showed that, apart from the high homology and the conserved distribution of hydrophobic residues in their established CaM binding sites, they also share the Trp in position 26 relative to the anchor Trp residue (Fig 27). The sequence surrounding Trp412 in ubMunc13-2, however, is less homologous to Munc13-1, and is characterized by the presence of three non-conserved Pro residues, amino acids known to have profound influence on the secondary structure of proteins. This raised the question whether the proposed novel CaM recognition motif is common to both Munc13 isoforms, despite the differences present in primary structure. To address this, photoprobes derived from the sequence of ubMunc13-2(382-415) where Trp387, Trp412, or both were replaced with p-Benzoyl-Phe (Bpa³⁸⁷-ub13-2³⁸²⁻⁴¹⁵, Bpa⁴¹²-ub13-2⁴⁵⁹⁻⁴⁹², and Bpa^{387,412}-ub13-2⁴⁵⁹⁻⁴⁹²) were employed in PAL experiments with CaM (Fig. 31).

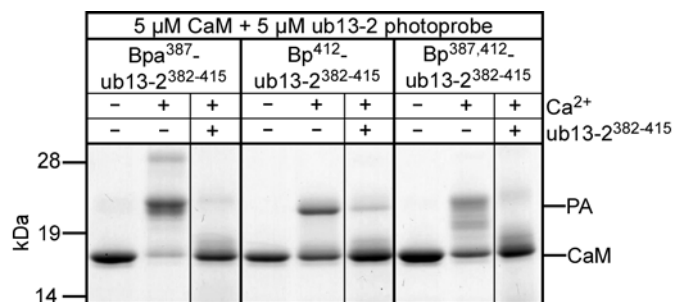


Figure 31. Photoaffinity labeling of CaM with ubMunc13-2(382-415)-derived photoprobes.

Coomassie-stained SDS gels showing the photoadduct (PA) formation of Bpa³⁸⁷-ub13-2³⁸²⁻⁴¹⁵, Bpa⁴¹²-ub13-2³⁸²⁻⁴¹⁵ and Bpa^{387,412}-ub13-2³⁸²⁻⁴¹⁵ in the absence and presence of excess Ca²⁺ (1 mM). Photoprobe binding was considered specific as PA formation is suppressed in presence of ten-fold molar excess of wild type competitor. Like in Fig. 13 mass spectrometry (not shown here) revealed that only unlabeled CaM and 1:1 photoadduct species were present even in the samples showing photoadduct double bands, which were most likely due to conformational effects on electrophoretic mobility. The 1:2 photoadduct species detected to some extent at an apparent molecular mass of 28 kDa were probably related to the artificially high Ca²⁺ concentration of 1 mM.

As observed for Munc13-1(459-492), CaM photoadducts of the longer ubMunc13-2(382-415)-derived photoprobe carrying Bpa in place of Trp387 showed an electrophoretic profile (Fig. 31) identical to the one of the short, Bpa³⁸⁷-ub13-2³⁸²⁻⁴⁰², photoprobe (Fig. 13). This identity could be reproduced in the MS-based structural analysis of the covalent photoadducts as it confirmed that Trp387 of ubMunc13-2 contacts Met124 and Met 144 in CaM and thus shares the same binding site in the C-terminal domain of CaM with Trp⁴⁶⁴ of Munc13-1 (see section 3.2.3).

More importantly, PAL experiments of CaM and Bpa⁴¹²-ub13-2³⁸²⁻⁴¹⁵ showed that the interaction through the Trp residue in position 26 relative to the anchor Trp387 is conserved between Munc13-1 and ubMunc13-2, and takes place with comparable efficiency (based on the similar photoadduct yields observed for the two isoforms (Fig. 28 and Fig. 31). Employing the bi-functional photoprobe Bpa^{387,412}-ub13-2³⁸²⁻⁴¹⁵ and the analytical strategy described above led to the identification of a cross-linked peptide consisting of the proteolytic fragments CaM⁶⁴⁻⁷⁴ and Bpa^{387,412}-ub13-2⁴⁰³⁻⁴¹⁵ indicating that the C-terminus also of ubMunc13-2³⁸²⁻⁴¹⁵ bind to the N-terminal CaM domain. MS/MS sequencing of the cross-linked peptide revealed a linkage between Bpa412 of the photoprobe and Met71 of CaM (Fig. 32), a finding that was also confirmed for the mono-functional photoprobe Bpa⁴¹²-ub13-2³⁸²⁻⁴¹⁵ (data not shown). Thus, in the bound state, Trp412 of ubMunc13-2³⁸²⁻⁴¹⁵ contacts Met71 of CaM, a

residue that is at least in close spatial proximity to the hydrophobic cleft of the CaM N-terminal domain.

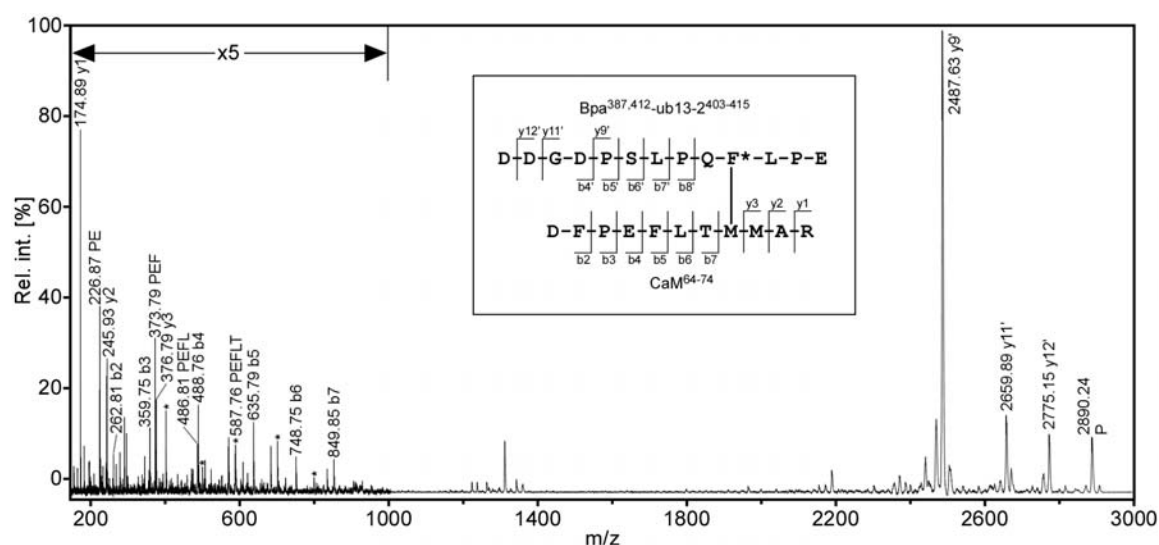


Figure 32. Characterization of the photoadduct of Bpa^{387,412}-ub13-1³⁸²⁻⁴¹⁵ and CaM at the amino acid level. Fragment ion mass spectrum of the cross-linked peptide consisting of CaM⁶⁴⁻⁷⁴ and Bpa^{387,412}-ub13-2⁴⁰³⁻⁴¹⁵. P denotes the precursor ion ($[M+H]^+_{\text{calc}} = 2890.30$) and primed ion designators indicate fragmentation in the photoprobe chain. The detection of a C-terminal y- (y1-y3) and an N-terminal b-ion series (b2-b7) revealed Met71 as the site of photoincorporation (see inset, F* encodes Bpa). Within the enlarged region $m/z < 1000$, fragment ions derived from cleavages in the photoprobe chain are only marked by an asterisk for the sake of clarity. The high abundance of the y9' ion at $m/z = 2487.63$ is in agreement with facile amide bond cleavages N-terminal of Pro and C-terminal of Asp.

In summary, the PAL-based analytical workflow for the structural characterization of CaM photoadducts established here was successfully employed for the biochemical verification of the novel mode of interaction, which was indicated for the CaM/Munc13-1 complex on the basis of dynamic NMR experiments. Furthermore, the PAL strategy was fast and efficient in providing evidence that this novel mode of interaction with CaM holds true for the ubMunc13-2 isoform, as well, a finding that was later also supported by NMR titration experiments.

4. DISCUSSION

4.1. Munc13 proteins interact with CaM via structurally distinct non-conserved binding sites

Genetic, morphological, cell-biological, biochemical and electrophysiological evidence accumulated over the past decade has led to the notion of an essential role of the Munc13 proteins in synaptic transmission, at the step of maturation of docked synaptic vesicles to a fusion-competent state (Aravamudan et al., 1999; Augustin et al., 1999b; Betz et al., 1998; Brose et al., 2000; Maruyama and Brenner, 1991; Richmond et al., 1999; Varoqueaux et al., 2002). Functional analyses have been focused mainly on Munc13-1, the isoform present throughout the brain, and the ubiquitously expressed isoform ubMunc13-2, while less information is available on the two other known Munc13 variants – the brain-specific bMunc13-2, and Munc13-3. The major interest in Munc13-1 is easily justified by its indispensable role in priming of synaptic vesicles at glutamatergic synapses – loss of Munc13-1 leads to a 90% reduction in the pool of readily releasable vesicles and a corresponding decrease in neurotransmission (Augustin et al., 1999b). In contrast, lack of Munc13-2 or Munc13-3 alone does not cause strong phenotypic changes, implying that their function may be largely redundant with that of Munc13-1 (Augustin et al., 2001; Varoqueaux et al., 2002).

Genomic, cDNA and protein sequence comparison of the members of the Munc13 family showed that their general structure comprises two distinct modules: a C-terminal unit, highly conserved across isoforms, and a largely variable N-terminal unit, bearing homology only in Munc13-1 and ubMunc13-2 (Betz et al., 2001; Brose et al., 1995b; Brose et al., 2000; Varoqueaux et al., 2002). The high conservation of the C-terminal module is an indication that its sequence has been subject to string selection pressure because it contributes to the essential functions of the Munc13 proteins. This notion has been supported by more recent studies showing that the isolated C-terminal module of Munc13 is sufficient for the priming of synaptic vesicles (Basu et al., 2005; Stevens et al., 2005). However, the priming efficiency of such isolated C-terminal constructs is significantly lower than observed for the full-length protein, indicating that further structures within the N-terminal part of Munc13s have important facilitating and modulating roles in Munc13 function. Thus, while bMunc13-2 and Munc13-3 are not, by themselves, essential for synaptic transmission in the presence of Munc13-1, they may, through their differing N-terminal sequences, and their expression pattern of complex redundancy, provide a

platform for further specific regulation of priming and modulation of synaptic strength.

Munc13-1 and ubMunc13-2 have emerged as key regulators of adaptive mechanisms defining short-term plasticity characteristics of neurons (Rosenmund et al., 2002). They contain a conserved calmodulin (CaM) binding site in their N-termini and the Ca^{2+} -dependent interaction of these Munc13 isoforms with CaM constitutes a molecular mechanism that transduces residual Ca^{2+} signaling to the synaptic exocytotic machinery (Junge et al., 2004). To address the question whether such Ca^{2+} /CaM regulatory mechanisms are present in the bMunc13-2 and Munc13-3 isoforms, bioinformatics tools were used for the identification of potential non-conserved CaM recognition motifs in their non-homologous N-terminal sequences. The *in silico* analysis led to the prediction of two potential CaM-binding sequences in each isoform and these were used as templates for the synthesis of Munc13-derived model peptides to be used in photoaffinity labeling (PAL) experiments with CaM. These peptides were designed such that their proposed anchor residues (Trp or Phe) for CaM binding were replaced with the photoreactive amino acid derivative p-Benzoyl-Phe (Fig. 12). By applying this strategy, the photophore was directly introduced into the CaM binding site without changing the hydrophobic, bulky, and aromatic characteristics of the corresponding anchor position, thus minimizing interference with the biopotency of the peptides. The photoprobes covering established (for Munc13-1 and ubMunc13-2) and newly proposed (for bMunc13-2 and Munc13-3) CaM binding sites were used in PAL experiments and mass spectrometric analysis to demonstrate their stoichiometric and Ca^{2+} -dependent interaction with CaM (Fig. 13).

The bioinformatics prediction of two CaM binding sites in the N-termini of bMunc13-2 and Munc13-3 and their confirmation at the peptide level in the PAL assays raised questions concerning the functional relevance of multiple CaM binding domains within the full-length Munc13 proteins. Based on co-sedimentation assays with recombinant protein constructs of ~40 kDa, containing both predicted CaM binding sites in bMunc13-2 and Munc13-3, it became evident that, for both isoforms, only the CaM binding site closest in position to the conserved central C1 domain has functional relevance within larger protein fragments, and, consequently, the full-length proteins (Fig. 18 and 19). Thus, these experiments constitute the first biochemical proof that bMunc13-2 and Munc13-3 interact with CaM in a stoichiometric and Ca^{2+} -dependent manner. The results of the co-sedimentation

assays illustrated both the strengths and limitations of bioinformatics tools for the prediction of protein/protein interactions and emphasized the need for biochemical cross-validation of predicted interactions in the context of at least larger protein fragments. While isolated shorter peptides may convey the optimal requirements for recognition by a target protein, structural factors brought about by other parts of the protein may have decisive influence on whether this interaction is physiologically feasible.

In summary, the combination of bioinformatics sequence analysis, peptide-based PAL experiments and co-sedimentation assays with larger Munc13-derived protein fragments established the presence of non-conserved CaM binding sites in bMunc13-2 and Munc13-3, and demonstrated that these Munc13 isoforms bind CaM in a stoichiometric and Ca^{2+} -dependent manner. Despite lacking homology with the characterized CaM binding sites in Munc13-1 and ubMunc13-2, these novel CaM interaction sites share the same position in the Munc13 sequence relative to the C1 domain, indicating that they are a product of convergent evolution and convey to bMunc13-2 and Munc13-3 similar roles in processes of presynaptic STP.

4.2. Munc13/CaM complex formation is triggered at Ca^{2+} concentrations in the lower nanomolar range

Sensing of and response to transient increases in the residual presynaptic Ca^{2+} levels are important adaptive mechanisms that define the short-term plasticity characteristics of neurons (Zucker and Regehr, 2002). The CaM/Munc13 interaction was put forward as a Ca^{2+} sensor/effector complex transducing residual Ca^{2+} signaling to the exocytotic machinery at the presynapse, prompting questions regarding the Ca^{2+} sensitivity of formation of this complex. The PAL-based Ca^{2+} titration assay established in this study revealed that CaM binding of all four Munc13 isoforms is sensitive to Ca^{2+} concentrations in the range of 20-30 nM (Fig. 15). Although these unexpectedly low Ca^{2+} concentrations may still be afflicted with some uncertainty due to technical limitations in controlling free Ca^{2+} in the nanomolar range, they can be considered as physiological on the basis of a recent study reporting basal presynaptic Ca^{2+} levels of as low as 25 nM (Korogod et al., 2005). Indeed, Ca^{2+} affinities in the lower nanomolar range have been reported previously for other CaM/target peptide complexes (Murase and Iio, 2002; Olwin and Storm, 1985; Peersen et al., 1997). However, several comparative studies have

shown that full-length CaM binding proteins require effective Ca^{2+} concentrations up to one order of magnitude higher than the corresponding peptides to induce CaM-dependent effects (Crouch et al., 1981; Fitzsimons et al., 1992; Yagi et al., 1989). In agreement with these observations, a half-maximal effective Ca^{2+} concentration of approximately 100 nM has been recently determined for the binding of fluorescent full-length GFP-ubMunc13-2 to CaM-coated beads (Zikich et al., 2008). Considered in the context of synaptic function and plasticity at low Ca^{2+} concentrations, the Ca^{2+} sensitivity of CaM interaction for all Munc13 isoforms reported here indicates that bMunc13-2 and Munc13-3 may have STP characteristics similar to those previously established for Munc13-1 and ubMunc13-2 (Junge et al., 2004). Thus, all Munc13 proteins and CaM form Ca^{2+} sensor/effector complexes, which are functional already at slightly elevated Ca^{2+} levels and capable of sensing small increases in presynaptic Ca^{2+} concentration, that are thought to be necessary for the induction of STP phenomena (Korogod et al., 2005).

So far, neither bMunc13-2 nor Munc13-3 have been studied in detail at the functional level. However, preliminary data indicate that both isoforms convey Ca^{2+} -dependent STP characteristics to synapses, much like ubMunc13-2 (J.-S. Rhee, unpublished observations). Future experiments will have to determine whether the STP characteristics conveyed by bMunc13-2 and Munc13-3 are caused by the Ca^{2+} /CaM binding sites characterized in the present study.

4.3. Structural characterization of the Munc13/CaM interaction

4.3.1. A novel PAL- based strategy for interaction site mapping

The new PAL-based workflow for the structural characterization of peptide/protein interactions established in this study comprises the use of benzophenone photoprobes, an isotopically labeled target protein (here CaM), and mass spectrometry for an in-depth analysis of the photoadducts (Fig. 20). Within the experimental strategy, typical shortcomings of more common PAL workflows have been addressed, which are often related to (i) photoprobe design, (ii) identification of the cross-linked peptides (i.e. localization of the region of photoincorporation), and (iii) sequence analysis of the cross-linked peptides (i.e. identification of the exact site of photoincorporation). First, photoprobe design is facilitated by the use of Bpa as this photoreactive amino acid can replace the hydrophobic, bulky, and aromatic anchor residues Trp and Phe that are frequently present in CaM-binding motifs,

without changing the overall biophysical properties of the peptide. Bpa substitution of the anchor residues promotes regioselective photoincorporation within the immediate binding cavity of CaM and thereby facilitates the direct identification of the amino acids of CaM involved in coordinating the anchor residue of the peptides.

Moreover, benzophenones have a unique photochemistry, allowing for reversible activation even in the presence of water (Dorman and Prestwich, 1994), and are therefore the photophores of choice when high photoadduct yields are required to obtain enough material for subsequent analysis. Second, identification of the cross-linked peptides is facilitated by the inclusion of isotopically labeled CaM (H-CaM) as reference protein. Due to this experimental design, CaM sequences involved in photoadduct formation are represented by doublet peaks, the "light" peak of which has a reduced intensity compared to its "heavy" counterpart. Accordingly, candidate masses of corresponding cross-linked peptides can be easily derived and the mass spectra can be screened for such masses appearing as unpaired peaks with natural isotope distributions. When different CaM fragments are involved in photoadduct formation, the regulation factor of the L-CaM/H-CaM doublet peaks contain semi-quantitative information of binding-site usage, which cannot be derived from the mass spectrometric detection of the cross-linked peptide alone. Third, sequence analysis of the cross-linked peptides is facilitated by the use of off-line rather than on-line LC/MS techniques. Whereas the chromatographic peak width defines the analysis time in on-line couplings, LC/MALDI-MS is not limited in this respect and even enables on-target manipulations such as CNBr cleavage.

In conclusion, this PAL-based workflow can find further use in the future research on novel CaM binding partners as it allows for a rapid structural screening of peptide-CaM interactions when data on the atomic structure of the complexes are lacking. Applications can also be extended to other peptide-protein interactions, especially in combination with NMR methods where isotopically labeled proteins are often available.

4.3.2. CaM interacts with Munc13 through key Met residues

Mass spectrometric analysis of the Munc13/CaM photoadducts showed that photoincorporation of the Bpa groups from the Munc13-derived photoprobes takes place exclusively at Met-124 and Met-144 of CaM (Fig. 24 and 25). This apparent

'Met preference' can be explained the observation that C-H bonds adjacent to heteroatoms are particularly reactive sites for photoincorporation of benzophenones (Dorman and Prestwich, 1994). In the case of Met, the thioether may be involved in the formation of an intermediate radical anion/cation pair to account for the high reactivity of the Met side chain (O'Neil et al., 1989). Consistently, labeling of Met side chains was found in numerous PAL studies using benzophenone-derivatized peptides (see (Behar et al., 2000; Kage et al., 1996; O'Neil et al., 1989; O'Neil and DeGrado, 1989; Sachon et al., 2003) and references therein). More importantly, however, CaM is an extraordinarily Met-rich protein (Met frequency of 6.1 %), and the Met residues constitute virtually half of its hydrophobic binding interfaces that are exposed to the solvent upon Ca^{2+} binding (Peersen et al., 1997; Yamniuk and Vogel, 2004). Consequently, essentially all Met side chains are involved in van der Waals interactions with the MLCK- and CaMKII-derived peptides as seen in the high-resolution structures of these CaM complexes (Ikura et al., 1992; Meador et al., 1992; Meador et al., 1993). The CaM residues shown here to be involved in cross-linking with the Munc13 peptides - Met-124 and Met-144 – have been previously reported in initial PAL studies on CaM using artificial model peptides with Bpa in the N-terminus of a basic amphiphilic α -helix (O'Neil et al., 1989; O'Neil and DeGrado, 1989). In these studies, modeling approaches were used to demonstrate that, depending on the orientation of the Bpa residue, labeling occurred either at Met-124 or Met-144, both of which line opposite sides of a hydrophobic cavity in the C-terminal domain of CaM. Based on these arguments it was concluded that the photoincorporation of Bpa⁴⁶⁴(Munc13-1) and Bpa³⁸⁷(ubMunc13-2) into the side chains of Met-144 and Met-124 in CaM is an accurate correlate of the contact sites between CaM and the anchor Trp of Munc13-1 and ubMunc13-2.

Taking together all lines of evidence obtained in the PAL experiments, it was postulated that, in the bound state, the anchor residues Trp-464 of Munc13-1 and Trp-387 of ubMunc13-2 contact Met-124 and Met-144 of CaM, the latter representing the major contact site.

4.3.3. Integration of PAL and chemical cross-linking constraints for molecular modeling of the CaM/Munc13 complex

The contacts revealed by PAL constituted exceptionally valuable constraints for molecular modeling as they were deduced from virtually "zero-length" cross-links. However, PAL approaches have the inherent limitation that they usually provide only a low number of constraints and have been insufficient to address questions regarding the orientation of the Munc13 peptides in the complex with CaM. For this reason, complementary chemical cross-linking experiments on the CaM/Munc13-1 complexes were performed using the homobifunctional amine-reactive cross-linkers BS³ and BS²G, with spacer lengths of 11.4 Å and 7.7 Å, respectively. The different molecular distance constraints for Lys residues in CaM and the Munc13-1-derived peptides obtained in these chemical cross-linking experiments were combined with the constraints from PAL acquired in this study and used for the structural modeling of the CaM/Munc13-1 complexes. All chemical cross-linking (Inez Pottratz, Christian Ihling) and molecular modeling (Stefan Kalkhof) experiments were performed in the group of Prof. Andrea Sinz at the University of Halle.

The Munc13-1 peptide (predicted to adopt an α -helical structure, based on bioinformatics analysis and modeling) was docked to a variety of different CaM structures with simultaneous consideration of the constraints from PAL (Trp-C ^{η 2}-Met-S ^{γ} distances of 0-8 Å) and chemical cross-linking (Lys-C ^{α} -Lys-C ^{α} -distances of 5-19 Å). The best fit with the experimental data sets was obtained for the structure of CaM in complex with a peptide derived from neuronal NO synthase (nNOS, pdb entry 2O60) (Fig. 33). As a result of the combination of two complementary sets of constraints derived from different cross-linking techniques the modeled structures of CaM/Munc13 peptide complexes exhibited only subtle structural differences with an overall rmsd value of less than 5 Å. When only the constraints from PAL were applied for docking, numerous different orientations particularly of the peptide C-terminus were obtained (Fig. 33B). In contrast, the overall orientation of the peptide was already quite well described on the basis of the relatively loose constraints from chemical cross-linking alone, but exact localization of the peptide N-terminus was not possible due to the lack of rather tight constraints from PAL (Fig. 33C). Further model refinement confirmed the structure of CaM from the CaM/nNOS peptide complex as best-fitting structure (Fig. 33D).

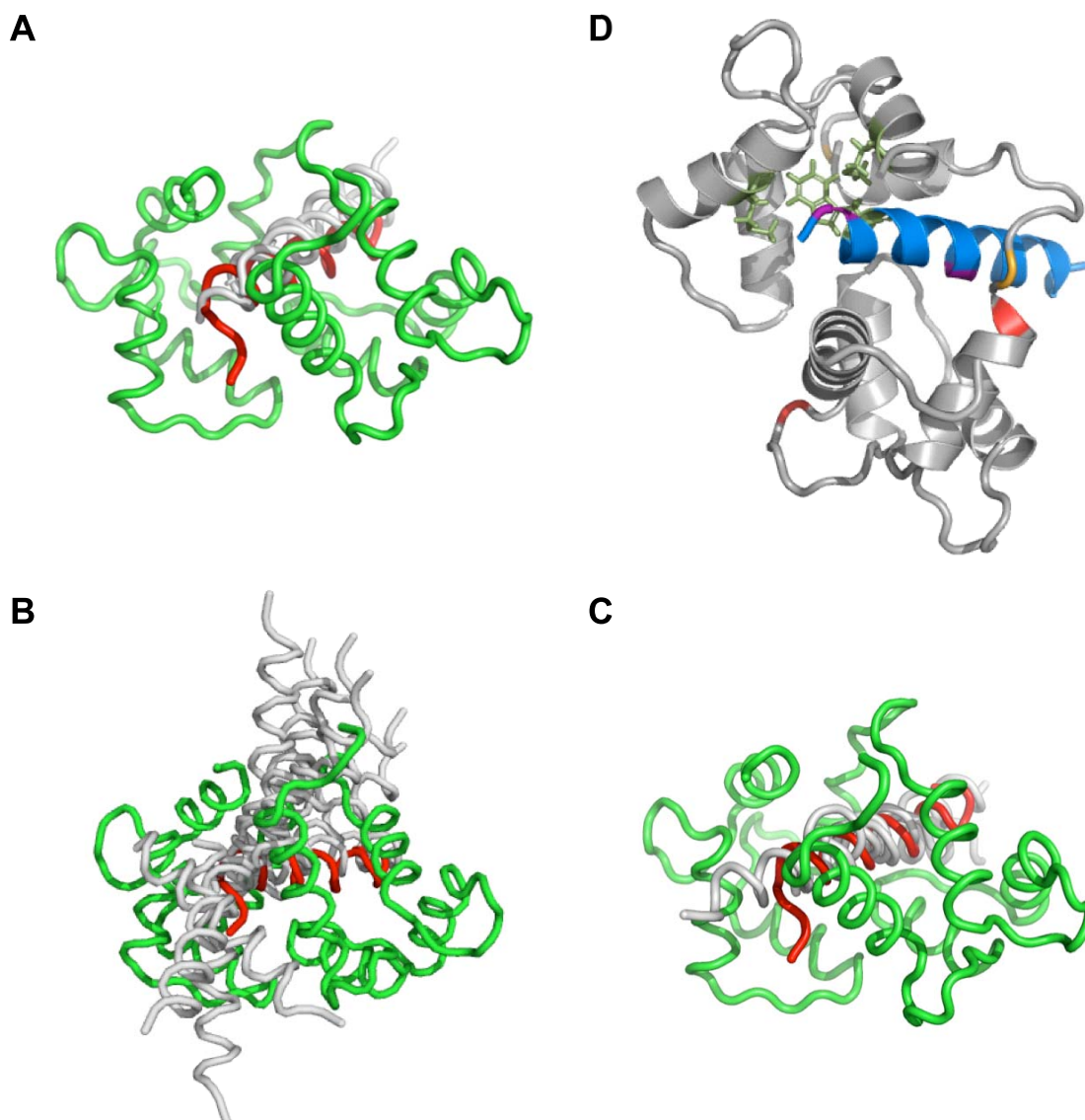


Figure 33. Molecular modeling of the Munc13-1/CaM complex. (A-C) Structures of the Munc13-1/CaM complex created by PatchDock on the basis of the constraints from PAL and chemical cross-linking (A), PAL alone (B), and chemical cross-linking alone (C). The structure of CaM from the CaM/nNOS peptide complex (pdb entry 2O60) as best-fitting structure is shown in green. Docking solutions for 13-1 are shown in gray and were limited to ten representative structures in (B). As shown in (A), only two peptide structures were possible (clustering rmsd < 5 Å) when the constraints from PAL and chemical cross-linking are combined. For comparison, the structure of the nNOS peptide (pdb entry 2O60) is shown in red. (D) Model of the complex formed by Munc13-1 (blue) and CaM (gray) after structural refinement using the RosettaDock server. The color code of the Lys residues is as follows: CaM Lys-77/94, yellow; CaM Lys-21/75, red; 13-1 Lys-4/13, purple. The amino acid side chains involved in PAL (Trp-7 of 13-1 and Met-124/144 of CaM) are presented in green. Visualization was performed by PyMol. Figure courtesy of Stefan Kalkhof and Andrea Sinz.

Corresponding chemical cross-linking experiments and subsequent molecular modeling of the ubMunc13-2/CaM interaction revealed an antiparallel orientation and similar overall conformation of this complex to the one observed for Munc13-1.

Thus, due to the complementary nature of PAL and chemical cross-linking, insights were gained into both binding sites (mainly by PAL) and overall conformations (mainly by chemical cross-linking) of CaM in complex with Munc13-1. Based on the integration of all molecular distance constraints, a molecular model of this interaction was proposed, which, despite its low resolution, provides important structural information: CaM and the Munc13 proteins interact in an antiparallel orientation through a 1-5-8 motif. In the energetically most likely structure CaM adopts a fold similar to the one reported for its complex with neuronal NOS (pdb entry 2O60). NOS (like MLCK) contains a so-called 1-5-8-14 CaM binding motif, indicating the presence of hydrophobic anchor amino acids in positions 1, 5, 8, and 14 of the motif (Rhoads and Friedberg, 1997). Munc13-1 and ubMunc13-2 exhibit a similar CaM binding motif, with hydrophobic amino acids in positions 1, 5, 8, 10 and 12 (Fig. 6). However, the hydrophobic residue in position 14 of the CaM binding motif is missing, as is the N-terminal cluster of basic amino acids, which usually determines the orientation of the target protein in the CaM complex (Vetter and Leclerc, 2003). This led to the conclusion that Munc13 has an unusual motif with a CaM binding mode similar, but not identical to that of nNOS. Support for this conclusion comes from the molecular models, in which the C-terminus of 13-1 differs in its conformation from that of the NOS peptide as the charged Glu residue in position 14 of the motif cannot be accommodated in the hydrophobic cleft of the N-terminal CaM domain (Fig. 33A, 33D). Due to the lack of tight PAL constraints for the C-terminal parts of the Munc13 peptides, it cannot be ruled out that the N-terminal CaM domain may adopt a rather extended conformation while the peptides bind through the 1-5-8 motif to the C-terminal CaM domain. Such a structure has been described for the complex formed by CaM and C20W, a peptide derived from plasma membrane Ca^{2+} pump (Elshorst et al., 1999). On the basis of the complementary cross-linking data the CaM binding motif of Munc13 could be unambiguously classified as a member of the antiparallel 1-5-8 motif family, but high-resolution structural studies were needed to elucidate the exact binding mode underlying the CaM-Munc13 interaction.

4.3.4. The high-resolution structure of the CaM/Munc13 complex reveals a novel 1-26 CaM recognition motif

The low-resolution structural model of CaM in complex with Munc13-derived peptides described above found its validation in the high-resolution NMR structure of the Munc13-1⁴⁵⁸⁻⁴⁹²/4Ca²⁺-CaM complex in solution obtained recently by Fernando Rodriguez-Castañeda and colleagues at the Department for NMR-Based Structural Biology of the MPI-BPC (Göttingen). Using C-terminally elongated peptides compared to the ones employed in the cross-linking approaches (Fig. 27), they showed that Munc13-1 interacts with the C-terminal domain of CaM in an antiparallel orientation through its hydrophobic anchor residues in positions 1-5-8. More interestingly, they observed a second module of Munc13/CaM interaction where the Trp residue in position 26 relative to the first hydrophobic anchor residue is attached to the N-terminal lobe of CaM, representing a novel CaM/peptide binding mode.

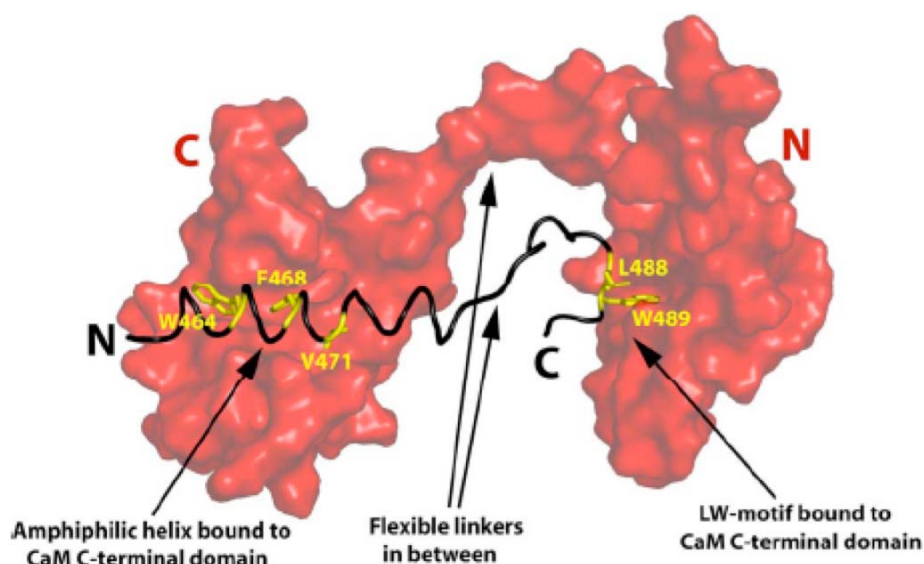


Figure 34. High-resolution structure of the Munc13-1⁴⁵⁸⁻⁴⁹²/4Ca²⁺-CaM complex. Ca²⁺-saturated CaM (red) interacts with Munc13-1⁴⁵⁸⁻⁴⁹² (black) in an open conformation. The complex features two modules: an amphiphilic α -helical 1-5-8 motif bound to the CaM C-terminal domain and the 25-26 LW motif attached to the CaM N-terminal domain. The side-chains of the anchoring residues are highlighted as yellow sticks. Figure courtesy of Fernando Rodriguez-Castañeda.

Biochemical support for these structural features came from the PAL data on the Munc13-1⁴⁵⁹⁻⁴⁹²/CaM complex described herein, showing that Trp489 in position 1 of the 1-5-8-26 motif contacts Met124 and Met144 in the hydrophobic cleft of the C-terminal CaM domain, while Trp464 in position 26 contacts Met51 in the

hydrophobic cleft of the N-terminal CaM domain (Fig. 30). This bipartite mode of interaction involving hydrophobic anchor residues at positions 1-5-8-26 seems to be conserved in ubMunc13-2 as well, as PAL revealed that the Trp residue in position 26 of the ubMunc13-2 motif interacts specifically and in a Ca^{2+} dependent manner with Met71 in the N-terminal domain of CaM (Fig. 32). Met51 and Met71 are positioned at opposite sites of the hydrophobic cavity in the N-terminal lobe of CaM, indicating that Munc13-1 and ubMunc13-2 have a very similar, if not identical, mode of interaction with CaM in an extended conformation. The subtle difference in the CaM coordination of the C-terminal parts of the two Munc13-derived peptides most likely originates from the presence of three non-conserved Pro residues in ubMunc13-2 and their potential influence on secondary structure.

In summary, the combination of different cross-linking techniques, mass spectrometry, and molecular modeling is a powerful tool to complement NMR and X-ray crystallography. In the present example, this approach rapidly yielded structural information with a reasonable technical effort, and, most importantly, enabled the characterization of a peptide-protein interaction under physiological solvent and concentration conditions.

5. CONCLUSIONS AND OUTLOOK

This study provides evidence for the presence of non-conserved CaM binding sites in the bMunc13-2 and Munc13-3 proteins. PAL and co-sedimentation experiments demonstrated that all four Munc13 isoforms bind CaM in a stoichiometric and Ca^{2+} -dependent manner and that only slightly elevated intracellular Ca^{2+} concentrations are sufficient to trigger these interactions. These findings support the conclusion that convergent evolution has generated structurally distinct but functionally similar Ca^{2+} /CaM binding sites in Munc13-1/ubMunc13-2, bMunc13-2, and Munc13-3, all of which can contribute to presynaptic short term plasticity. On-going expression cloning and electrophysiological work is aimed at elucidating the role of the CaM regulation of bMunc13-2 and Munc13-3 in the context of short term plasticity.

A PAL-based analytical strategy was established that allows for the rapid structural characterization of peptide/protein interactions. It is especially valuable in providing details about the binding sites accommodating such interactions and was applied here in the identification of critical Met side chains in the C-terminal domain of CaM that coordinate the anchor Trp residues of Munc13 proteins. Further integration of PAL and chemical cross-linking approaches allowed the generation of a molecular model of the Munc13/CaM complex demonstrating its antiparallel orientation. Moreover, the PAL methodology emerged as an important complement to high-resolution NMR studies on the Munc13/CaM interaction, providing biochemical evidence for a novel 1-26 CaM binding motif in Munc13-1 and ubMunc13-2.

The structural data on the CaM-Munc13 complex offer new options for future studies towards a deeper understanding of the role of the Munc13 proteins in synaptic vesicle priming and short-term plasticity. Structural information facilitates the design of Munc13 mutants with altered affinities for CaM, which, alongside the previously established CaM-insensitive variants (W464R in Munc13-1 and W387R in ubMunc13-2; Junge et al., 2004), will be extremely useful tools in the further electrophysiological characterization of these proteins.

6. REFERENCES

- Aebersold, R., and Mann, M. (2003). Mass spectrometry-based proteomics. *Nature* 422, 198-207.
- Aravamudan, B., Fergestad, T., Davis, W. S., Rodesch, C. K., and Broadie, K. (1999). *Drosophila* UNC-13 is essential for synaptic transmission. *Nat Neurosci* 2, 965-971.
- Ashery, U., Varoqueaux, F., Voets, T., Betz, A., Thakur, P., Koch, H., Neher, E., Brose, N., and Rettig, J. (2000). Munc13-1 acts as a priming factor for large dense-core vesicles in bovine chromaffin cells. *Embo J* 19, 3586-3596.
- Augustin, I., Betz, A., Herrmann, C., Jo, T., and Brose, N. (1999a). Differential expression of two novel Munc13 proteins in rat brain. *Biochem J* 337, 363-371.
- Augustin, I., Korte, S., Rickmann, M., Kretschmar, H. A., Sudhof, T. C., Herms, J. W., and Brose, N. (2001). The cerebellum-specific Munc13 isoform Munc13-3 regulates cerebellar synaptic transmission and motor learning in mice. *J Neurosci* 21, 10-17.
- Augustin, I., Rosenmund, C., Sudhof, T. C., and Brose, N. (1999b). Munc13-1 is essential for fusion competence of glutamatergic synaptic vesicles. *Nature* 400, 457-461.
- Basu, J., Shen, N., Dulubova, I., Lu, J., Guan, R., Guryev, O., Grishin, N. V., Rosenmund, C., and Rizo, J. (2005). A minimal domain responsible for Munc13 activity. *Nat Struct Mol Biol* 12, 1017-1018.
- Behar, V., Bisello, A., Bitan, G., Rosenblatt, M., and Chorev, M. (2000). Photoaffinity cross-linking identifies differences in the interactions of an agonist and an antagonist with the parathyroid hormone/parathyroid hormone-related protein receptor. *Journal of Biological Chemistry* 275, 9-17.
- Benfenati, F., Valtorta, F., Rubenstein, J. L., Gorelick, F. S., Greengard, P., and Czernik, A. J. (1992). Synaptic vesicle-associated Ca²⁺/calmodulin-dependent protein kinase II is a binding protein for synapsin I. *Nature* 359, 417-420.
- Betz, A., Ashery, U., Rickmann, M., Augustin, I., Neher, E., Sudhof, T. C., Rettig, J., and Brose, N. (1998). Munc13-1 Is a Presynaptic Phorbol Ester Receptor that Enhances Neurotransmitter Release. *Neuron* 21, 123-136.
- Betz, A., Okamoto, M., Benseler, F., and Brose, N. (1997). Direct interaction of the rat unc-13 homologue Munc13-1 with the N terminus of syntaxin. *J Biol Chem* 272, 2520-2526.
- Betz, A., Thakur, P., Junge, H. J., Ashery, U., Rhee, J. S., Scheuss, V., Rosenmund, C., Rettig, J., and Brose, N. (2001). Functional interaction of the active zone proteins Munc13-1 and RIM1 in synaptic vesicle priming. *Neuron* 30, 183-196.
- Brenner, S. (1974). THE GENETICS OF CAENORHABDITIS ELEGANS. *Genetics* 77, 71-94.
- Brose, N., Hofmann, K., Hata, Y., and Sudhof, T. C. (1995a). Mammalian homologues of *Caenorhabditis elegans* unc-13 gene define novel family of C2-domain proteins. *J Biol Chem* 270, 25273-25280.
- Brose, N., Hofmann, K., Hata, Y., and Südhof, T. C. (1995b). Mammalian Homologues of *Caenorhabditis elegans* unc-13 Gene Define Novel Family of C(2)-domain Proteins. *J Biol Chem* 270, 25273-25280.
- Brose, N., Rosenmund, C., and Rettig, J. (2000). Regulation of transmitter release by Unc-13 and its homologues. *Curr Opin Neurobiol* 10, 303-311.

- Brunner, J. (1993). New Photolabeling and Crosslinking Methods
doi:10.1146/annurev.bi.62.070193.002411. Annual Review of Biochemistry 62, 483-514.
- Chin, D., and Means, A. R. (2000). Calmodulin: a prototypical calcium sensor. Trends in Cell Biology 10, 322-328.
- Copley, R. R., Schultz, J., Ponting, C. P., and Bork, P. (1999). Protein families in multicellular organisms. Curr Opin Struct Biol 9, 408-415.
- Crivici, A., and Ikura, M. (1995). Molecular and structural basis of target recognition by calmodulin. Annu Rev Biophys Biomol Struct 24, 85-116.
- Crouch, T. H., Holroyde, M. J., Collins, J. H., Solaro, R. J., and Potter, J. D. (1981). Interaction of calmodulin with skeletal muscle myosin light chain kinase. Biochemistry 20, 6318-6325.
- Deisseroth, K., Heist, E. K., and Tsien, R. W. (1998). Translocation of calmodulin to the nucleus supports CREB phosphorylation in hippocampal neurons. Nature 392, 198-202.
- Dorman, G., and Prestwich, G. D. (1994). Benzophenone Photophores in Biochemistry. Biochemistry 33, 5661-5673.
- Dorman, G., and Prestwich, G. D. (2000). Using photolabile ligands in drug discovery and development. Trends Biotechnol 18, 64-77.
- Elshorst, B., Hennig, M., Forsterling, H., Diener, A., Maurer, M., Schulte, P., Schwalbe, H., Griesinger, C., Krebs, J., Schmid, H., *et al.* (1999). NMR solution structure of a complex of calmodulin with a binding peptide of the Ca²⁺ pump. Biochemistry 38, 12320-12332.
- Falke, J. J., Drake, S. K., Hazard, A. L., and Peersen, O. B. (1994). Molecular tuning of ion binding to calcium signaling proteins. Q Rev Biophys 27, 219-290.
- Fenn, J. B., Mann, M., Meng, C. K., Wong, S. F., and Whitehouse, C. M. (1989). Electrospray ionization for mass spectrometry of large biomolecules. Science 246, 64-71.
- Fitzsimons, D. P., Herring, B. P., Stull, J. T., and Gallagher, P. J. (1992). Identification of basic residues involved in activation and calmodulin binding of rabbit smooth muscle myosin light chain kinase. J Biol Chem 267, 23903-23909.
- Geppert, M., Goda, Y., Hammer, R. E., Li, C., Rosahl, T. W., Stevens, C. F., and Sudhof, T. C. (1994). Synaptotagmin I: a major Ca²⁺ sensor for transmitter release at a central synapse. Cell 79, 717-727.
- Girault, S., Sagan, S., Bolbach, G., Lavielle, S., and Chassaing, G. (1996). The use of photolabelled peptides to localize the substance-P-binding site in the human neurokinin-1 tachykinin receptor. Eur J Biochem 240, 215-222.
- Gracheva, E. O., Burdina, A. O., Holgado, A. M., Berthelot-Grosjean, M., Ackley, B. D., Hadwiger, G., Nonet, M. L., Weimer, R. M., and Richmond, J. E. (2006). Tomosyn inhibits synaptic vesicle priming in *Caenorhabditis elegans*. PLoS Biol 4, e261.
- Haberz, P., Rodriguez-Castaneda, F., Junker, J., Becker, S., Leonov, A., and Griesinger, C. (2006). Two new chiral EDTA-based metal chelates for weak alignment of proteins in solution. Org Lett 8, 1275-1278.
- Hilfiker, S., Pieribone, V. A., Czernik, A. J., Kao, H. T., Augustine, G. J., and Greengard, P. (1999). Synapsins as regulators of neurotransmitter release. Philos Trans R Soc Lond B Biol Sci 354, 269-279.
- Hillenkamp, F., and Peter-Katalinic, J., eds. (2007). MALDI MS. A Practical Guide to Instrumentation, Methods and Applications (Weinheim, WILEY-VCH Verlag GmbH & KGaA).

- Hoeflich, K. P., and Ikura, M. (2002). Calmodulin in Action: Diversity in Target Recognition and Activation Mechanisms. *Cell* 108, 739-742.
- Holmes, D. S., and Quigley, M. (1981). A rapid boiling method for the preparation of bacterial plasmids. *Anal Biochem* 114, 193-197.
- Ikura, M. (1996). Calcium binding and conformational response in EF-hand proteins. *Trends Biochem Sci* 21, 14-17.
- Ikura, M., and Ames, J. B. (2006). Genetic polymorphism and protein conformational plasticity in the calmodulin superfamily: Two ways to promote multifunctionality. *Proceedings of the National Academy of Sciences of the United States of America* 103, 1159-1164.
- Ikura, M., Clore, G. M., Gronenborn, A. M., Zhu, G., Klee, C. B., and Bax, A. (1992). Solution structure of a calmodulin-target peptide complex by multidimensional NMR. *Science* 256, 632-638.
- Jahn, O., Eckart, K., Brauns, O., Tezval, H., and Spiess, J. (2002). The binding protein of corticotropin-releasing factor: ligand-binding site and subunit structure. *Proc Natl Acad Sci U S A* 99, 12055-12060.
- Jahn, O., Hesse, D., Reinelt, M., and Kratzin, H. (2006). Technical innovations for the automated identification of gel-separated proteins by MALDI-TOF mass spectrometry. *Analytical and Bioanalytical Chemistry* 386, 92-103.
- Jahn, O., Tezval, H., Spiess, J., and Eckart, K. (2003). Tandem mass spectrometric characterization of branched peptides derived from photoaffinity labeling. *International Journal of Mass Spectrometry* 228, 527-540.
- Jahn, R., and Südhof, T. C. (1999). MEMBRANE FUSION AND EXOCYTOSIS
doi:10.1146/annurev.biochem.68.1.863. *Annual Review of Biochemistry* 68, 863-911.
- Junge, H. J., Rhee, J.-S., Jahn, O., Varoqueaux, F., Spiess, J., Waxham, M. N., Rosenmund, C., and Brose, N. (2004). Calmodulin and Munc13 Form a Ca^{2+} Sensor/Effector Complex that Controls Short-Term Synaptic Plasticity. *Cell* 118, 389-401.
- Kage, R., Leeman, S. E., Krause, J. E., Costello, C. E., and Boyd, N. D. (1996). Identification of methionine as the site of covalent attachment of a p-benzoyl-phenylalanine-containing analogue of substance P on the substance P (NK-1) receptor. *J Biol Chem* 271, 25797-25800.
- Karas, M., and Hillenkamp, F. (1988). Laser desorption ionization of proteins with molecular masses exceeding 10,000 daltons. *Anal Chem* 60, 2299-2301.
- Katz, B., and Miledi, R. (1968). The role of calcium in neuromuscular facilitation. *J Physiol* 195, 481-492.
- Kauer, J., Erickson-Viitanen, S., Wolfe, H., Jr, and DeGrado, W. (1986). p-Benzoyl-L-phenylalanine, a new photoreactive amino acid. Photolabeling of calmodulin with a synthetic calmodulin-binding peptide. *J Biol Chem* 261, 10695-10700.
- Keen, J. E., Khawaled, R., Farrens, D. L., Neelands, T., Rivard, A., Bond, C. T., Janowsky, A., Fakler, B., Adelman, J. P., and Maylie, J. (1999). Domains responsible for constitutive and Ca^{2+} -dependent interactions between calmodulin and small conductance Ca^{2+} -activated potassium channels. *J Neurosci* 19, 8830-8838.
- Koch, H., Hofmann, K., and Brose, N. (2000). Definition of Munc13-homology-domains and characterization of a novel ubiquitously expressed Munc13 isoform. *Biochem J* 349, 247-253.

- Korogod, N., Lou, X., and Schneggenburger, R. (2005). Presynaptic Ca^{2+} requirements and developmental regulation of posttetanic potentiation at the calyx of Held. *J Neurosci* 25, 5127-5137.
- Lee, A., Wong, S. T., Gallagher, D., Li, B., Storm, D. R., Scheuer, T., and Catterall, W. A. (1999). Ca^{2+} /calmodulin binds to and modulates P/Q-type calcium channels. *Nature* 399, 155-159.
- Leite, J. F., Dougherty, D. A., Lester, H. A., and Shahgholi, M. (2003). Investigation of apparent mass deviations in electrospray ionization tandem mass spectrometry of a benzophenone-labeled peptide. *Rapid Commun Mass Spectrom* 17, 1677-1684.
- Llinás, R., Steinberg, I. Z., and Walton, K. (1981). Relationship between presynaptic calcium current and postsynaptic potential in squid giant synapse. *Biophysical Journal* 33, 323-351.
- Luo, S., Wehr, N. B., and Levine, R. L. (2006). Quantitation of protein on gels and blots by infrared fluorescence of Coomassie blue and Fast Green. *Anal Biochem* 350, 233-238.
- Malenka, R. C., Kauer, J. A., Perkel, D. J., Mauk, M. D., Kelly, P. T., Nicoll, R. A., and Waxham, M. N. (1989). An essential role for postsynaptic calmodulin and protein kinase activity in long-term potentiation. *Nature* 340, 554-557.
- Maruyama, I. N., and Brenner, S. (1991). A phorbol ester/diacylglycerol-binding protein encoded by the unc-13 gene of *Caenorhabditis elegans*. *Proc Natl Acad Sci U S A* 88, 5729-5733.
- McEwen, J. M., Madison, J. M., Dybbs, M., and Kaplan, J. M. (2006). Antagonistic regulation of synaptic vesicle priming by Tomosyn and UNC-13. *Neuron* 51, 303-315.
- Meador, W. E., Means, A. R., and Quirocho, F. A. (1992). Target enzyme recognition by calmodulin: 2.4 Å structure of a calmodulin-peptide complex. *Science* 257, 1251-1255.
- Meador, W. E., Means, A. R., and Quirocho, F. A. (1993). Modulation of calmodulin plasticity in molecular recognition on the basis of x-ray structures. *Science* 262, 1718-1721.
- Miller, W. T., and Kaiser, E. T. (1988). Probing the peptide binding site of the cAMP-dependent protein kinase by using a peptide-based photoaffinity label. *Proc Natl Acad Sci U S A* 85, 5429-5433.
- Mills, J. S., Miettinen, H. M., Barnidge, D., Vlases, M. J., Wimer-Mackin, S., Dratz, E. A., Sunner, J., and Jesaitis, A. J. (1998). Identification of a ligand binding site in the human neutrophil formyl peptide receptor using a site-specific fluorescent photoaffinity label and mass spectrometry. *J Biol Chem* 273, 10428-10435.
- Murase, T., and Iio, T. (2002). Static and kinetic studies of complex formations between calmodulin and mastoparanX. *Biochemistry* 41, 1618-1629.
- Neuhoff, V., Arold, N., Taube, D., and Ehrhardt, W. (1988). Improved staining of proteins in polyacrylamide gels including isoelectric focusing gels with clear background at nanogram sensitivity using Coomassie Brilliant Blue G-250 and R-250. *Electrophoresis* 9, 255-262.
- Olwin, B. B., and Storm, D. R. (1985). Calcium binding to complexes of calmodulin and calmodulin binding proteins. *Biochemistry* 24, 8081-8086.
- O'Neil, K., Erickson-Viitanen, S., and DeGrado, W. (1989). Photolabeling of calmodulin with basic, amphiphilic α -helical peptides containing p-benzoylphenylalanine. *J Biol Chem* 264, 14571-14578.

- O'Neil, K. T., and DeGrado, W. F. (1989). The interaction of calmodulin with fluorescent and photoreactive model peptides: Evidence for a short interdomain separation. *Proteins* 6, 284-293.
- Patton, C., Thompson, S., and Epel, D. (2004). Some precautions in using chelators to buffer metals in biological solutions. *Cell Calcium* 35, 427-431.
- Peersen, O. B., Madsen, T. S., and Falke, J. J. (1997). Intermolecular tuning of calmodulin by target peptides and proteins: Differential effects on Ca^{2+} binding and implications for kinase activation. *Protein Sci* 6, 794-807.
- Peterson, B. Z., DeMaria, C. D., Adelman, J. P., and Yue, D. T. (1999). Calmodulin is the Ca^{2+} sensor for Ca^{2+} -dependent inactivation of L-type calcium channels. *Neuron* 22, 549-558.
- Pettit, D. L., Perlman, S., and Malinow, R. (1994). Potentiated transmission and prevention of further LTP by increased CaMKII activity in postsynaptic hippocampal slice neurons. *Science* 266, 1881-1885.
- Rhoads, A., and Friedberg, F. (1997). Sequence motifs for calmodulin recognition. *FASEB J* 11, 331-340.
- Richmond, J. E., Davis, W. S., and Jorgensen, E. M. (1999). UNC-13 is required for synaptic vesicle fusion in *C. elegans*. *Nat Neurosci* 2, 959-964.
- Richmond, J. E., Weimer, R. M., and Jorgensen, E. M. (2001). An open form of syntaxin bypasses the requirement for UNC-13 in vesicle priming. *Nature* 412, 338-341.
- Rodriguez-Castaneda, F. (2007) NMR Spectroscopic studies of calmodulin plasticity in calcium signalling, PhD, Georg-August-Universitaet, Goettingen, Germany.
- Rosenmund, C., Rettig, J., and Brose, N. (2003). Molecular mechanisms of active zone function. *Current Opinion in Neurobiology* 13, 509-519.
- Rosenmund, C., Sigler, A., Augustin, I., Reim, K., Brose, N., and Rhee, J.-S. (2002). Differential Control of Vesicle Priming and Short-Term Plasticity by Munc13 Isoforms. *Neuron* 33, 411-424.
- Sabatini, B. L., and Regehr, W. G. (1999). TIMING OF SYNAPTIC TRANSMISSION doi:10.1146/annurev.physiol.61.1.521. *Annual Review of Physiology* 61, 521-542.
- Sachon, E., Bolbach, G., Lavielle, S., Karoyan, P., and Sagan, S. (2003). Met174 side chain is the site of photoinsertion of a substance P competitive peptide antagonist photoreactive in position 8. *FEBS Lett* 544, 45-49.
- Singh, A., Thornton, E. R., and Westheimer, F. H. (1962). The Photolysis of Diazoacetylchymotrypsin. *J Biol Chem* 237, PC3006-3008.
- Song, Y., Ailenberg, M., and Silverman, M. (1998). Cloning of a novel gene in the human kidney homologous to rat munc13s: its potential role in diabetic nephropathy. *Kidney Int* 53, 1689-1695.
- Steen, H., and Mann, M. (2004). The ABC's (and XYZ's) of peptide sequencing. *Nat Rev Mol Cell Biol* 5, 699-711.
- Stevens, D. R., Wu, Z. X., Matti, U., Junge, H. J., Schirra, C., Becherer, U., Wojcik, S. M., Brose, N., and Rettig, J. (2005). Identification of the minimal protein domain required for priming activity of Munc13-1. *Curr Biol* 15, 2243-2248.
- Suckau, D., Resemann, A., Schuerenberg, M., Hufnagel, P., Franzen, J., and Holle, A. (2003). A novel MALDI LIFT-TOF/TOF mass spectrometer for proteomics. *Anal Bioanal Chem* 376, 952-965.

- Sudhof, T. C. (1995). The synaptic vesicle cycle: a cascade of protein-protein interactions. *Nature* 375, 645-653.
- Sudhof, T. C. (2004). The synaptic vesicle cycle. *Annu Rev Neurosci* 27, 509-547.
- Sudhof, T. C., and Rizo, J. (1996). Synaptotagmins: C2-domain proteins that regulate membrane traffic. *Neuron* 17, 379-388.
- Swindells, M. B., and Ikura, M. (1996). Pre-formation of the semi-open conformation by the apo-calmodulin C-terminal domain and implications binding IQ-motifs. *Nat Struct Biol* 3, 501-504.
- Thiede, B., Hohenwarter, W., Krah, A., Mattow, J., Schmid, M., Schmidt, F., and Jungblut, P. R. (2005). Peptide mass fingerprinting. *Methods* 35, 237-247.
- Valtorta, F., Benfenati, F., and Greengard, P. (1992). Structure and function of the synapsins. *J Biol Chem* 267, 7195-7198.
- Varoqueaux, F., Sigler, A., Rhee, J. S., Brose, N., Enk, C., Reim, K., and Rosenmund, C. (2002). Total arrest of spontaneous and evoked synaptic transmission but normal synaptogenesis in the absence of Munc13-mediated vesicle priming. *Proc Natl Acad Sci U S A* 99, 9037-9042.
- Vetter, S. W., and Leclerc, E. (2003). Novel aspects of calmodulin target recognition and activation. *European Journal of Biochemistry* 270, 404-414.
- Vodovozova, E. (2007). Photoaffinity labeling and its application in structural biology. *Biochemistry* 72, 1-20.
- Wojcik, S. M., and Brose, N. (2007). Regulation of membrane fusion in synaptic excitation-secretion coupling: speed and accuracy matter. *Neuron* 55, 11-24.
- Xia, X. M., Fakler, B., Rivard, A., Wayman, G., Johnson-Pais, T., Keen, J. E., Ishii, T., Hirschberg, B., Bond, C. T., Lutsenko, S., *et al.* (1998). Mechanism of calcium gating in small-conductance calcium-activated potassium channels. *Nature* 395, 503-507.
- Xia, Z., and Storm, D. R. (2005). The role of calmodulin as a signal integrator for synaptic plasticity. *Nat Rev Neurosci* 6, 267-276.
- Xu, X. Z., Wes, P. D., Chen, H., Li, H. S., Yu, M., Morgan, S., Liu, Y., and Montell, C. (1998). Retinal targets for calmodulin include proteins implicated in synaptic transmission. *J Biol Chem* 273, 31297-31307.
- Yagi, K., Yazawa, M., Ikura, M., and Hikichi, K. (1989). Interaction between calmodulin and target proteins. *Adv Exp Med Biol* 255, 147-154.
- Yamniuk, A., and Vogel, H. (2004). Calmodulin's flexibility allows for promiscuity in its interactions with target proteins and peptides. *Molecular Biotechnology* 27, 33-57.
- Yap, K., Kim, J., Truong, K., Sherman, M., Yuan, T., and Ikura, M. (2000). Calmodulin Target Database. *Journal of Structural and Functional Genomics* 1, 8-14.
- Zikich, D., Mezer, A., Varoqueaux, F., Sheinin, A., Junge, H. J., Nachliel, E., Melamed, R., Brose, N., Gutman, M., and Ashery, U. (2008). Vesicle priming and recruitment by ubMunc13-2 are differentially regulated by calcium and calmodulin. *J Neurosci* 28, 1949-1960.
- Zucker, R. S., and Regehr, W. G. (2002). Short-term synaptic plasticity. *Annu Rev Physiol* 64, 355-405.
- Zuhlke, R. D., Pitt, G. S., Deisseroth, K., Tsien, R. W., and Reuter, H. (1999). Calmodulin supports both inactivation and facilitation of L-type calcium channels. *Nature* 399, 159-162.

7. CURRICULUM VITAE

PERSONAL DATA

Name: Kalina Dimova
Date and place of birth: 02/01/1982 Assenovgrad, Bulgaria
Nationality: Bulgarian
Contact information: Ewaldstrasse 11, 37085 Göttingen, Germany
 Email: dimova@em.mpg.de

EDUCATION

10/2005 – 03/2009 **Ph.D. in Molecular Biology** in the Proteomics Group & Department of Molecular Neurobiology at the Max Planck Institute of Experimental Medicine, Göttingen, Germany. Advisors: Dr. Olaf Jahn and Prof. Nils Brose
 09/2000 – 05/2004 **B.A. *Cum Laude* in Biochemistry and German Studies** at Smith College, Northampton, MA, USA. Highest honors in Biochemistry. Honors Thesis Project: "Exercise-Induced Activation of MAPK Signaling Cascades in Murine Skeletal Muscle" Advisor: Prof. Stylianos Scordilis
 09/1995 – 05/2000 **Secondary Education diploma** at the German Language High School, Sofia. Bulgaria

AWARDS/HONORS

2004 – 2006 International Max Planck Research School Scholarship
 2003 Merck/AAAs Fellowship
 2002 Howard Hughes Medical Institute Fellowship

RELEVANT EXPERIENCE

08/2006 Advanced Methods Course: Summer School in Proteomics Basics – Exploring the Diversity of Proteins. Brixen, Italy.

WORK EXPERIENCE

06/2004 – 08/2004 Research Support Specialist
 SUNY-ESF Department of Polymer Chemistry Syracuse, NY.
 Mycelian production and purification of laccase and its nondestructive regioselective modification by linear-dendritic copolymers. Supervisor: Prof. Ivan Gizov.